NTNU
Norwegian University of
Science and Technology

Modelling of Undrained Clay Subjected to Cyclic Loading

Semi-Explicit Material Model

Aleksander S Gundersen
Jon-Michael Josefsen

Civil and Environmental Engineering
Submission date: June 2016
Supervisor: Gustav Grimstad, BAT

Norwegian University of Science and Technology
Department of Civil and Transport Engineering

NORWEGIAN UNIVERSITY OF SCIENCE AND TECHNOLOGY
DEPARTMENT OF CIVIL AND TRANSPORT ENGINEERING

Report Title:	Date: 10.06.2016			
Modelling of Undrained Clay Subjected to Cyclic Loading:	Number of pages (incl. appendices): 144			
Semi-Ecplicit Material Model	Master Thesis	x	Project Work	

Name: Aleksander S. Gundersen and Jon-Michael Josefsen

Professor in charge/supervisor:
Gustav Grimstad

Other external professional contacts/supervisors:

Abstract:

A material model, based on total stresses, has been developed to represent the undrained cyclic behavior of clay for finite element analyses. The material behavior is split into an average- and a cyclic part, formulated as two material models with a coupling. The cyclic loading is, for the model, assumed to be defined in terms of forces and have a frequency within the "cyclic" range (~ 0.1 Hz), which implies that mass and damping considerations are omitted.

Degradation of the maximum average shear stress and the cyclic shear stiffness is accounted for using the cyclic shear strain accumulation principle. The resulting accumulation of plastic shear strains is a byproduct of the degradation of maximum average shear stress.

The average model and the cyclic model are verified individually by Plaxis simulations with satisfactory results. A bearing capacity problem was simulated with the average model and compared directly to a simulation done by an acknowledged undrained model. The average model exhibited the expected behavior and the authors believe it can be used in similar boundary value problems when used with care.

The cyclic model was used in a cyclic direct simple shear simulation with no average shear stresses. The simulation result was compared directly to a similar calculation and the conclusion is that the cyclic model is able to represent the undrained cyclic behavior in a direct simple shear test. The interaction between the average and the cyclic model was tested in another direct simple shear test. The results obtained was satisfying and prove that the interaction is working as desired.

Another objective was to compare the presented model directly to results from model tests of a gravity base structure. Due to time limitations and the complexity of the problem, only a hypothetical analysis is undertaken. Results indicate further investigation is necessary to confirm the applicability of the soil model on gravity base structures.

Keywords:

1. Soil modell
2. Cyclic soil behavior
3. Cyclic shear strain accumulation principle
4. FEM

Preface

This master's thesis in geotechnics was written at the Norwegian University of Science and Technology (Trondheim) during the spring semester of 2016. It is the final part of a MSc in Civil and Environmental Engineering and was proposed and supervised by Professor Gustav Grimstad.

Trondheim, 2016-06-10

Jon-Michael Josefsen Aleksander S. Gundersen

Acknowledgment

We would like to sincerely thank our supervisor Gustav Grimstad for guidance and discussions throughout this project. Contribution from Jon Rønningen and input from Gudmund Eiksund have also been very much appreciated. Steinar Nordal, Knut H. Andersen, Ana Page and Hans-Petter Jostad have shared their expertise with us, of which we are very grateful. Finally we would like to thank our fellow students for all the good discussions.

A.S.G. & J.M.J.

Summary and Conclusions

A material model, based on total stresses, has been developed to represent the undrained cyclic behavior of clay for finite element analyses. The material behavior is split into an average- and a cyclic part, formulated as two material models with a coupling. The cyclic loading is, for the model, assumed to be defined in terms of forces and have a frequency within the "cyclic" range (≈ 0.1 Hz), which implies that mass and damping considerations are omitted.

Degradation of the maximum average shear stress and the cyclic shear stiffness is accounted for using the cyclic shear strain accumulation principle. The resulting accumulation of plastic shear strains is a byproduct of the degradation of maximum average shear stress.

The average model and the cyclic model are verified individually by Plaxis simulations with satisfactory results. A bearing capacity problem was simulated with the average model and compared directly to a simulation done by an acknowledged undrained model. The average model exhibited the expected behavior and the authors believe it can be used in similar boundary value problems when used with care.

The cyclic model was used in a cyclic direct simple shear simulation with no average shear stresses. The simulation result was compared directly to a similar calculation and the conclusion is that the cyclic model is able to represent the undrained cyclic behavior in a direct simple shear test. The interaction between the average and the cyclic model was tested in another direct simple shear test. The results obtained was satisfying and prove that the interaction is working as desired.

Another objective was to compare the presented model directly to results from model tests of a gravity base structure. Due to time limitations and the complexity of the problem, only a hypothetical analysis is undertaken. Results indicate further investigation is necessary to confirm the applicability of the soil model on gravity base structures.

Sammendrag og konklusjon

En materialmodell for udrenert, syklisk belastning av leire har blitt utviklet med grunnlag i totalspenninger. Materialmodellen er delt i en gjennomsnittsmodell og en syklisk modell, hvor den gjennomsnittlige modellen analyserer den gjennomsnittlige lasten på jordvolumet, mens den sykliske modellen analyserer den sykliske lasten. De er så koblet sammen for å representere den totale oppførselen til leiren. Den sykliske lasthistorien er definert som et antall sykler med en viss kraftamplitude. Det er antatt at frekvensen til de sykliske lastene er tilstrekkelig lav, slik at hensynet til masse eller dempning kan sees bort fra.

Degradaring av den maksimale, gjennomsnittelige skjærspenningen og den sykliske skjærstivheten uttrykkes ved hjelp av "Cyclic Shear Strain Accumulation Principle". Akkumulering av plastiske skjærtøyninger er et resultat av degraderingen av den maksimale, gjennomsnittlige skjærspenningen.

De to delene av materialmodellen er individuelt verifisert gjennom simuleringer i elementmetodeprogrammet, Plaxis. Et bæreevneproblem ble simulert med den gjennomsnittlige modellen og resultatene ble sammenlignet med resultater fra en annerkjent materialmodell. De to modellene viste, som forventet, lignende oppførsel og det konkluderes derfor med at gjennomsnittsmodellen skal kunne brukes med forsiktighet for liknende grenseverdiproblemer når udrenert oppførsel kan antas.

Den sykliske modellen har blitt testet i DSS uten gjennomsnittlig skjærspenninger. Resultatet ble sammenlignet direkte med en tilsvarende beregning og konklusjonen er at den sykliske modellen er i stand til å representere den ønskede oppførselen. Koblingen mellom den gjennomsnittlige- og sykliske modellen ble testet i en annen DSS test. De oppnådde resultatene var tilfredsstillende og indikerer at samspillet fungerer som forventet.

Et annet mål var å sammenligne modellresultater direkte med resultater fra modellforsøk av en gravitasjonsplatform. På grunn av tidsbegrensning og kompleksiteten til problemet, er bare en hypotetisk analyse foretatt. Resultatene indikerer at videre undersøkelser er nødvendig for å bekrefte anvendeligheten av jordmodellen på gravitasjonsplatformer.

Contents

Chapter 1

Introduction

1.1 Background

Offshore wind turbines (OWT) have predominantly been installed in shallow waters and have so far been relatively small. The optimal capacity of future turbines is expected to increase, leading to an increase in structural weight, imposing larger loads on the soil.

Cyclic loading may cause a degradation of soil stiffness and shear strength, and lead to accumulation of permanent displacements. This affects the design of offshore installations, quays, bridges etc. Offshore wind turbines are relatively sensitive to rotation and in design the serviceability limit state is often critical. In design of offshore gravity base structures (GBS) the ultimate limit state is often critical.

Besides the design for the maximum static load, the fatigue design is a very important aspect for offshore structures. The effect of cyclic loading on the soil has to be considered, since the number of load cycles due to wind and waves could exceed 10^8 over the lifetime of the structure.

A standard design procedure for a laterally loaded offshore pile is the p–y curve method, which is described in the guidelines of the American Petroleum Institute (API). The p–y curves formulated for cyclic loading conditions are based on field tests with fewer than 200 cycles. Similarly for other design states there is possible to use hand calculation procedures, however they will all be subject to

some limitations.

Using sophisticated material laws and finite element analysis (FEA), the principle behavior of undrained soil under cyclic loading can be simulated cycle by cycle. However, the accumulation of displacement for every cycle is usually very small, and thus the accumulation of numerical errors could become large in comparison. Implicit calculation concepts are therefore often restricted to design cases with low number of cycles.

The Norwegian Geotechnical Institute (NGI) has developed an explicit finite element soil model to analyse undrained clay subjected to cyclic loading - Undrained Cyclic Accumulation Model (UDCAM). This model is based on contour diagrams from laboratory tests and has been used to design foundations for offshore oil and gas structures, predominantly in the North Sea. The user need extensive schooling in order to use the program. It has been suggested to improve the model by adding mathematical expressions for the soil behavior and make it easier to use.

The problem of this master's thesis is to calculate the accumulated displacements and undrained bearing capacity of offshore foundations on clay when subjected to cyclic loading. The offshore industry is interested in finding the most efficient and correct way to calculate the response due to cyclic loading. A solution may be to use FE analysis with a material model which can account for cyclic behavior. This model should be user friendly and implemented as a User Defined Soil Model (UDSM) in a finite element calculation program.

1.2 Objectives

The main objectives of this master's thesis are as follows:

1. Develop a soil model which can describe the undrained behavior of clay under cyclic loading
2. Implement the soil model into a finite element calculation program
3. Simulate benchmark designs in finite element and compare them to theory

1.3 Limitations and Approach

The soil model is based on average soil parameters e.g. average shear strength of compression- and extension shear strength, and the assumption of isotropic initial stress. The mathematical framework used in the soil model is inspired by contour diagrams e.g. for Drammen Clay. Plaxis is the chosen FEA platform which imposes certain limitations to how the material model is formulated. The model is only capable of representing undrained- and stress controlled behavior. The model is formulated with a von Mises criterion, which results in a higher strength in certain stress states than what is expected from theory.

A literature survey of material modelling and the behavior of undrained clay subjected to cyclic loading is used as a basis for understanding how to construct a cyclic soil model. This includes gathering of articles, selecting the important ones and adopting the knowledge. Analysis and characterisation of existing data sets on undrained cyclic behavior of clay are used to find mathematical relations to be used in the soil model. Numerical calculations of problems where the result is known and a qualitative and quantitative analysis of the results are included.

1.4 Structure of the Report

The rest of the report is structured as follows:

Chapter 2 Literature review of material modelling

Chapter 3 Introduction to cyclic loading characteristics.

Chapter 4 Study of the undrained behavior of clay subjected to cyclic loading.

Chapter 5 Literature review of existing soil models.

Chapter 6 Presentation of the developed soil model.

Chapter 7 Discussion of the simulation results from Plaxis.

Chapter 8 Summarizing of the findings from this master's thesis.

Chapter 2

Preliminaries to Soil Modelling

An important part of a FE analysis is to use a material model which is able to represent the soil behavior with the specific loading scenario and describe parameters of interest properly. FE material models are described by a set of mathematical equations that give a relationship between stresses and strains. These expressions are often on incremental form.

This chapter presents an introduction to stresses and strains as well as basic concepts of the FE theory. There will be shown how material models can be mathematically described from an energy balance point of view and divided in elastic and plastic behavior.

2.1 General Definition of Stress

Stress is a 2^{nd} order tensor defined as force per area. In this paper, extension stress is defined positive, while compression stress is defined negative. The stress tensor can be written in matrix notation as follows:

$$\underline{\underline{\sigma}} = \begin{bmatrix} \sigma_{11} & \sigma_{12} & \sigma_{13} \\ \sigma_{21} & \sigma_{22} & \sigma_{23} \\ \sigma_{31} & \sigma_{32} & \sigma_{33} \end{bmatrix} \tag{2.1}$$

In classical deformation theory a symmetric stress tensor can be derived from Cauchy's tetrahedron (Ottosen and Petersson, 1992). This leads to a simplified and convenient expression for the stress state as the following vector:

$$\underline{\sigma}^T = \begin{bmatrix} \sigma_{11} & \sigma_{22} & \sigma_{33} & \sigma_{12} & \sigma_{23} & \sigma_{31} \end{bmatrix} \tag{2.2}$$

For soils it can be useful to divide the total stress vector into what is known as the effective stress, σ', and the pore pressure, σ_w, such that:

$$\underline{\sigma} = \underline{\sigma}' + \underline{\sigma}_w \tag{2.3}$$

which is known as the Terzaghi's principle, first stated in Terzaghi (1925). The pore pressure is hydrostatic which can be represented by a single value, u (Brinkgreve et al., 2016):

$$\underline{\sigma}_w^T = \begin{bmatrix} u & u & u & 0 & 0 & 0 \end{bmatrix} \tag{2.4}$$

The effective stress is stated as:

$$\underline{\sigma}'^T = \begin{bmatrix} \sigma'_{11} & \sigma'_{22} & \sigma'_{33} & \sigma_{12} & \sigma_{23} & \sigma_{31} \end{bmatrix} \tag{2.5}$$

So far the stresses and strains are dependent on the coordinate system. In soil modelling it is convenient to use stress invariants which is independent of the orientation of the coordinate system. In the geotechnical FEM software Plaxis, the following invariants are used (Brinkgreve et al., 2016). The isotropic effective stress, p', is the mean value of the diagonal axis in the stress matrix.

$$p' = \frac{1}{3}(\sigma'_{11} + \sigma'_{22} + \sigma'_{33}) \tag{2.6}$$

The equivalent shear stress, q, is the deviatoric stress invariant:

$$q = \sqrt{\frac{1}{2}\left[(\sigma_{11} - \sigma_{22})^2 + (\sigma_{22} - \sigma_{33})^2 + (\sigma_{33} - \sigma_{11})^2 + 6(\sigma_{12}^2 + \sigma_{23}^2 + \sigma_{31}^2)\right]} \tag{2.7}$$

This is equivalent to the following expression:

$$q = \sqrt{3J_2} \tag{2.8}$$

where J_2 is the second principal stress invariant. A third invariant used in Plaxis is the Lode angle, θ,

$$\theta = \frac{1}{3} arcsin\left(\frac{27J_3}{2q^3}\right) \tag{2.9}$$

where J_3 is defined as:

$$\begin{aligned} J_3 = (\sigma'_{11} - p')(\sigma'_{22} - p')(\sigma'_{33} - p') - (\sigma'_{11} - p')\sigma^2_{23} \\ - (\sigma'_{22} - p')\sigma^2_{31} - (\sigma'_{33} - p')\sigma^2_{12} + 2\sigma_{12}\sigma_{23}\sigma_{31} \end{aligned} \tag{2.10}$$

2.2 General Definition of Strain

In small deformation theory the definition of strain is the deformation relative to the original geometry. In this paper, positive strain values is defined as extension and negative as compression. The strain state in 3D can be stated as a matrix,

$$\underline{\underline{\varepsilon}} = \begin{bmatrix} \varepsilon_{11} & \varepsilon_{12} & \varepsilon_{13} \\ \varepsilon_{21} & \varepsilon_{22} & \varepsilon_{23} \\ \varepsilon_{31} & \varepsilon_{32} & \varepsilon_{33} \end{bmatrix} \tag{2.11}$$

and similar to the stress, the strain matrix can be simplified to the following strain vector:

$$\underline{\varepsilon}^T = \begin{bmatrix} \varepsilon_{11} & \varepsilon_{22} & \varepsilon_{33} & \gamma_{12} & \gamma_{23} & \gamma_{31} \end{bmatrix} \tag{2.12}$$

where

$$\gamma_{12} = \varepsilon_{12} + \varepsilon_{21}, \qquad \gamma_{23} = \varepsilon_{23} + \varepsilon_{32}, \qquad \gamma_{31} = \varepsilon_{13} + \varepsilon_{31}$$

For strains, it is also useful to define invariants. The following invariants are defined in Brinkgreve et al. (2016). The volumetric strain, ε_V, is defined as:

$$\varepsilon_V = \varepsilon_{11} + \varepsilon_{22} + \varepsilon_{33} \tag{2.13}$$

The deviatoric strain, ε_q, which is energy conjugate to the deviatoric stress invariant q, is defined as:

$$\varepsilon_q = \sqrt{\frac{2}{9}\left[(\varepsilon_{11}-\varepsilon_{22})^2 + (\varepsilon_{22}-\varepsilon_{33})^2 + (\varepsilon_{33}-\varepsilon_{11})^2\right] + \frac{1}{3}(\gamma_{12}^2 + \gamma_{23}^2 + \gamma_{31}^2)} \tag{2.14}$$

which have the following relation to the second principal strain invariant, $J_{2,\varepsilon}$:

$$= \frac{2}{3}\sqrt{3J_{2,\varepsilon}} \tag{2.15}$$

2.3 Deformation Theory

The basics of finite element soil modelling is continuum mechanics. One of the main ideas behind continuum mechanics is that materials are a continuous mass, rather than an assembly of many particles. Another assumption is that deformations applied to a continuum body are infinitely small. This assumption is not required, but it simplifies the expressions.

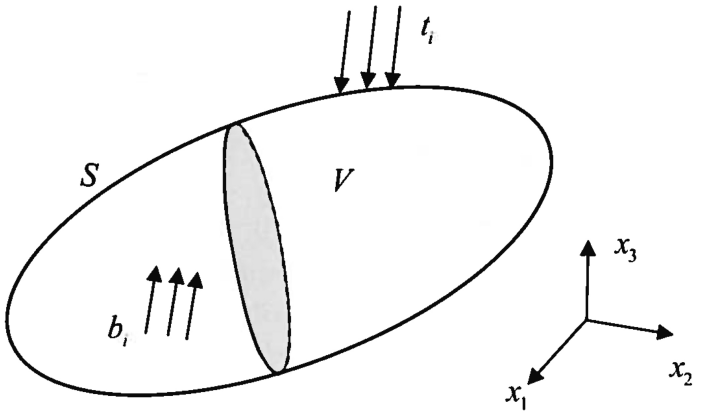

Figure 2.1: Internal forces acting on a continuum body (from Hopperstad and Børvik (2014))

A general problem as seen in figure 2.1 will serve as a basis for derivation of the deformation theory. The body is subjected to external forces, such as gravity and pressure, and the aim is to calculate the static equilibrium. There are two different types of forces, the body forces (b) acting on the volume and the traction forces (t) acting on the surface. These forces all need to be in equilibrium in every direction as well as in moment equilibrium, which leads to the following expression:

$$\int_V \underline{b} dV + \int_S \underline{t} dS = 0 \tag{2.16}$$

$$\int_V \underline{b}\,\underline{x} dV + \int_S \underline{t}\,\underline{x} dS = 0 \tag{2.17}$$

were x is the moment arm.

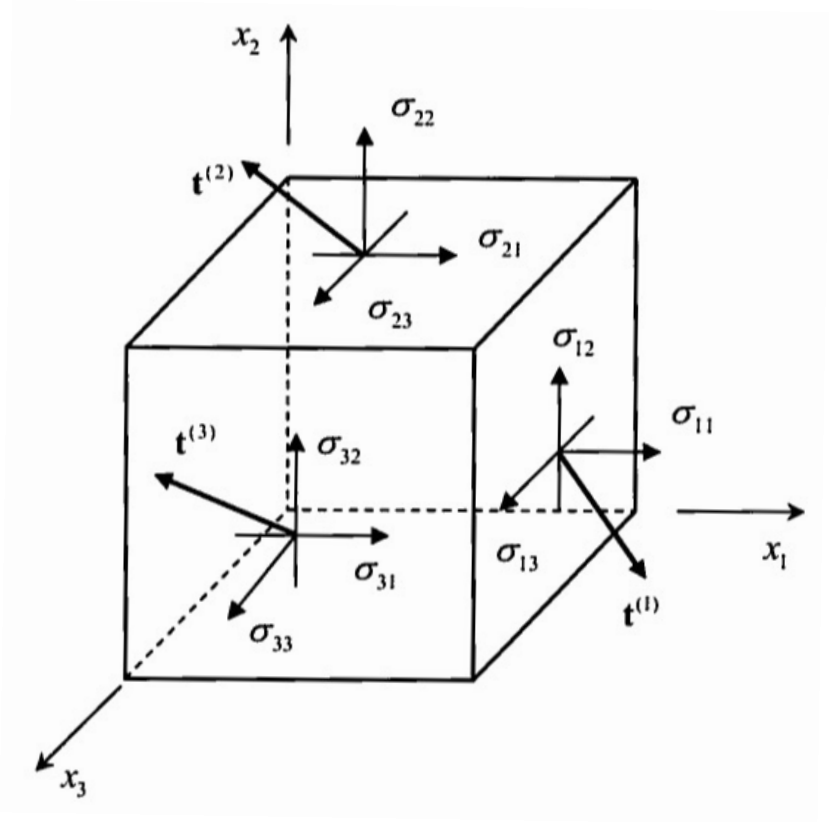

Figure 2.2: Internal forces acting on an infinitesimal continuum body (from Hopperstad and Børvik (2014))

The external forces give rise to internal forces which will be traction forces acting on the surface of every infinitesimal part of the body, as shown in figure 2.2. The infinitesimal elements of the body must also be in static equilibrium according to equations 2.16 and 2.17. For the internal forces the traction vectors are made up of the stresses acting on each plane as shown in figure 2.2. The traction vector will have the following form, were $\underline{e}$ are the unit vectors.

$$\underline{t} = \begin{bmatrix} \underline{t_1} \\ \underline{t_2} \\ \underline{t_3} \end{bmatrix} = \underline{\underline{\sigma}}\,\underline{e} = \begin{bmatrix} \sigma_{11}\underline{e_1} + \sigma_{12}\underline{e_2} + \sigma_{13}\underline{e_3} \\ \sigma_{21}\underline{e_1} + \sigma_{22}\underline{e_2} + \sigma_{23}\underline{e_3} \\ \sigma_{31}\underline{e_1} + \sigma_{32}\underline{e_2} + \sigma_{33}\underline{e_3} \end{bmatrix} \tag{2.18}$$

Inserting equation 2.18 into 2.16 gives the local form of the force equilibrium (Hopperstad and Børvik, 2014) in equation 2.19. The same derivation for the moment equilibrium can readily be done by using equation 2.17.

$$\int_V \underline{b} dV + \int_S \underline{\underline{\sigma}}\,\underline{e} dS = 0 \tag{2.19}$$

In the finite element method the continuum body is split into several finite sized elements. These elements consist of nodes with a certain number of degrees of freedom. The displacement of one node is connected to the displacement of the element through interpolation functions, $\underline{\underline{N}}$. These functions multiplied with the nodal displacement, $\underline{v}$, will give the displacement field, $\underline{u}$, describing the displacement all over the element (Brinkgreve et al., 2016).

$$\underline{u} = \underline{\underline{N}}\,\underline{v} = 0 \tag{2.20}$$

As mentioned in section 2.2 the strain can be expressed as deformation relative to the original geometry. The infinitesimal strain of the element can therefore be found by spatial differentiation of the displacement field such that:

$$\underline{\underline{\varepsilon}} = \underline{\underline{\nabla}}\,\underline{u} = \underline{\underline{\nabla}}\,\underline{\underline{N}}\,\underline{v} \tag{2.21}$$

where $\underline{\underline{\nabla}}$ is the vector differential operator handling the spatial differentiations.

2.4 Elastic Materials

A material is elastic if stresses depend only on strains (Hopperstad and Børvik, 2014). Since the stress-strain dependency do not change from loading to unloading, the material returns to its original configuration when all loading is removed. The internal elastic energy stored within the material can be expressed by the strain energy function, $U_0(\varepsilon)$, as:

$$U_0(\varepsilon) = \int_0^{\varepsilon} \sigma(\varepsilon) d\varepsilon \tag{2.22}$$

The stresses obtained from rearranging equation 2.22 to 2.23 gives a material behavior which is reversible and path independent. This means that strains will be recovered if the material is unloaded and the path of getting to a certain stress state have nothing to say for the further response from the material.

The relation between stresses and strains for an elastic material can be linear or nonlinear. If the material in 1D is simplified by a spring, the linear elastic material will have a constant spring stiffness, E, known as the Young's Modulus. If the material has nonlinear elastic behavior the spring stiffness depends on the strain, $E(\varepsilon)$. This is visualized in figure 2.3.

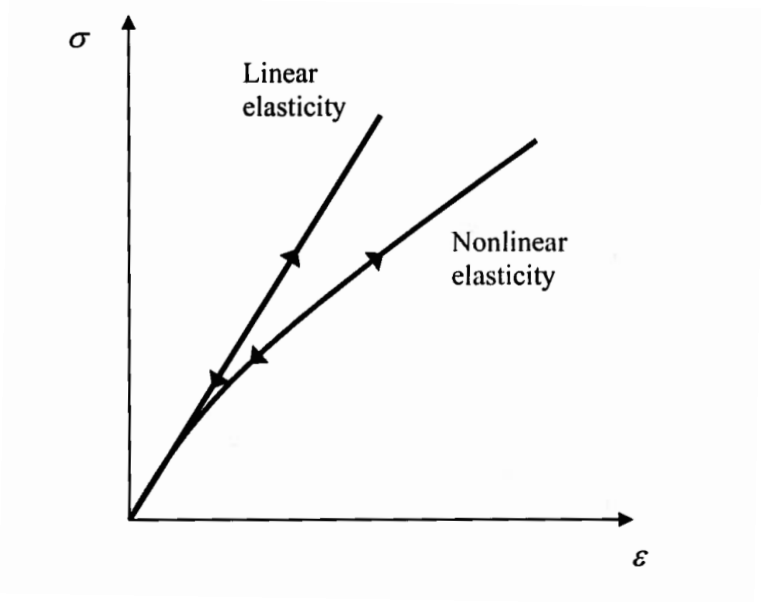

Figure 2.3: Linear and nonlinear elastic behavior (from Hopperstad and Børvik (2014))

The stress-strain relation in elasticity can be described in a 3D space by an elasticity matrix, C, which gives the relation between the stresses and strains in different directions. It leads to the expression known as the generalized hooke's law (Hopperstad and Børvik, 2014).

$$\underline{\sigma} = \underline{\underline{C}}\,\underline{\varepsilon}^{e} \tag{2.23}$$

The elasticity matrix can describe an isotropic or an anisotropic behavior of a material. The elasticity matrix works in the exact same way as for the 1D case which makes an elastic 3D model reversible and path independent in every direction. The generalized Hooke's law for an isotropic material can be described by the poisson's ratio, ν, and the Young's Modulus as follows:

$$\underline{\sigma} = \frac{E}{(1+\nu)(1-2\nu)} \begin{bmatrix} (1-\nu) & \nu & \nu & 0 & 0 & 0 \\ \nu & (1-\nu) & \nu & 0 & 0 & 0 \\ \nu & \nu & (1-\nu) & 0 & 0 & 0 \\ 0 & 0 & 0 & \frac{(1-2\nu)}{2} & 0 & 0 \\ 0 & 0 & 0 & 0 & \frac{(1-2\nu)}{2} & 0 \\ 0 & 0 & 0 & 0 & 0 & \frac{(1-2\nu)}{2} \end{bmatrix} \underline{\varepsilon}^{e} \tag{2.24}$$

2.5 Elastic-Plastic Materials

At a certain point the elastic capacity is reached and the material starts to yield. The yielding introduces irreversible deformations and the total strains can then be separated into two parts, elastic and plastic strains. The elastic strains will act as in a normal elastic material where all the strains will be fully reversible. The plastic strains are irreversible and elastic-plastic materials are therefore path dependent, which means that the path to a certain stress state influence the further material behavior.

To describe an elastic-plastic material, a yield criterion defining the boundary of the purely elastic behavior is necessary. This elastic limit is the capacity if the material is perfectly plastic. Otherwise, the behavior after reaching the elastic

limit is described by a hardening rule (R). The mathematical difference is seen from the following expressions and the visualization can be seen in figure 2.4.

$$f = \sigma_{eq} - \sigma_0 = 0 \tag{2.25}$$

$$f = \sigma_{eq} - \sigma_0 - R = 0 \tag{2.26}$$

where f is called the yield function, σ_0 is called the yield strength and σ_{eq} is the equivalent stress in the spring. Elastic behavior is defined by $f < 0$, plastic behavior by $f = 0$ and $f > 0$ is inadmissible.

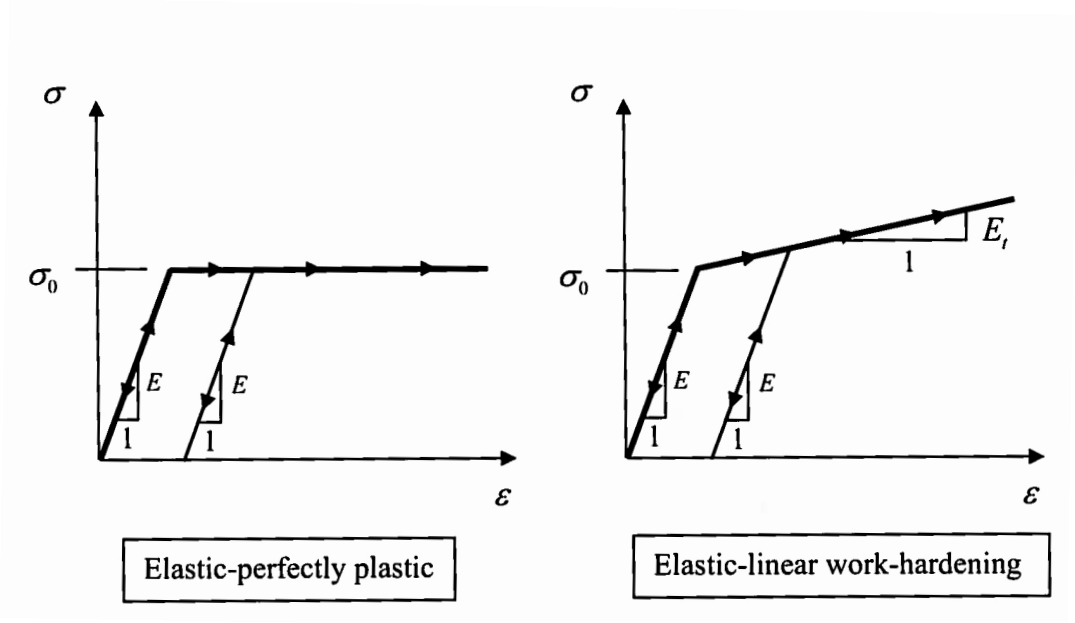

Figure 2.4: Idealized elastic-plastic behavior (from Hopperstad and Børvik (2014))

2.5.1 Yield Criterion

The yield function is a mathematical expression which describes the yield criterion. The Tresca and von Mises criteria are often used to demonstrate the principal of a yield function. They are both pressure independent and are therefore often used for ductile metals. They can also be used for describing the undrained behavior of clay.

The Tresca yield criterion

The Tresca criterion's yielding condition is based on the maximum shear stress reaching a critical shear value, τ_Y. This maximum shear stress, τ_{max}, is described as:

$$\tau_{max} = \frac{1}{2}(\sigma_{max} - \sigma_{min}) \tag{2.27}$$

Extended to 3D and formulated as a yield function, f, the Tresca criterion can be stated in terms of the principal stresses as:

$$f(\sigma_1, \sigma_2, \sigma_3) = \frac{1}{2}(|\sigma_1 - \sigma_2| + |\sigma_2 - \sigma_3| + |\sigma_3 - \sigma_1|) - \sigma_0 \tag{2.28}$$

In order to express the Tresca criterion with the components of the stress vector, $\underline{\sigma}$, the geometry in a Mohr circle can be used to derive the following relation to the principal stresses:

$$\sigma_1 = \frac{1}{2}(\sigma_{11} + \sigma_{22}) + \sqrt{\left[\frac{1}{2}(\sigma_{11} - \sigma_{22})\right]^2 + \sigma_{12}^2}$$

$$\sigma_2 = \frac{1}{2}(\sigma_{22} + \sigma_{33}) + \sqrt{\left[\frac{1}{2}(\sigma_{22} - \sigma_{33})\right]^2 + \sigma_{23}^2}$$

$$\sigma_3 = \frac{1}{2}(\sigma_{11} + \sigma_{33}) - \sqrt{\left[\frac{1}{2}(\sigma_{11} - \sigma_{33})\right]^2 + \sigma_{31}^2}$$

Inserted into the expression for the Tresca yield surface, the result following on the next page can be obtained.

$$
\begin{aligned}
f(\sigma) = &-\sigma_0 + \\
&\frac{1}{2}\left(\left|\frac{1}{2}(\sigma_{11}+\sigma_{33}) + \sqrt{\left[\frac{1}{2}(\sigma_{11}-\sigma_{22})\right]^2+\sigma_{12}^2} - \sqrt{\left[\frac{1}{2}(\sigma_{22}-\sigma_{33})\right]^2+\sigma_{23}^2}\right|\right. \\
&+\left|\frac{1}{2}(\sigma_{22}+\sigma_{33}) + \sqrt{\left[\frac{1}{2}(\sigma_{22}-\sigma_{33})\right]^2+\sigma_{23}^2} + \sqrt{\left[\frac{1}{2}(\sigma_{11}-\sigma_{33})\right]^2+\sigma_{31}^2}\right| \\
&\left.+\left|\frac{1}{2}(\sigma_{22}+\sigma_{33}) - \sqrt{\left[\frac{1}{2}(\sigma_{11}-\sigma_{33})\right]^2+\sigma_{31}^2} - \sqrt{\left[\frac{1}{2}(\sigma_{11}-\sigma_{22})\right]^2+\sigma_{12}^2}\right|\right)
\end{aligned}
$$

A more convenient and compact way to express the Tresca yield function is by using the lode angle (equation 2.9) and the equivalent shear stress (equation 2.8) such that:

$$f(\sigma) = \frac{q}{\sqrt{3}}cos(\theta) - \sigma_0 \tag{2.29}$$

The von Mises yield criterion

The von Mises criterion is based on isotropy and pressure insensitivity of the material. The equivalent stress is described by the second principal invariant of the stress deviator, J_2 (Hopperstad and Børvik, 2014). The second principal stress invariant has the following form:

$$J_2 = \frac{1}{2}(\sigma_{11}^2+\sigma_{22}^2+\sigma_{33}^2+\sigma_{12}^2+\sigma_{21}^2+\sigma_{23}^2+\sigma_{32}^2+\sigma_{13}^2+\sigma_{31}^2) - \frac{1}{6}(\sigma_{11}+\sigma_{22}+\sigma_{33})^2 \tag{2.30}$$

If the yield strength, σ_0, is set to the uniaxial yield stress at failure the value of J_2 is:

$$J_2 = \frac{1}{3}\sigma_0^2 \tag{2.31}$$

This gives the final expression for the von Mises yield function:

$$f = \sqrt{3J_2} - \sigma_0 = 0 \tag{2.32}$$

The difference between the Tresca and von-Mises yield criteria in the π-plane can be seen in figure 2.5. It is evident that the von-Mises criterion overshoots the Tresca criterion. The Tresca criterion is discontinuous around the corners, which may induce numerical problems to a FE simulation. This can be circumvented by using an approximate Tresca criterion after Billington (1988) with rounded corners.

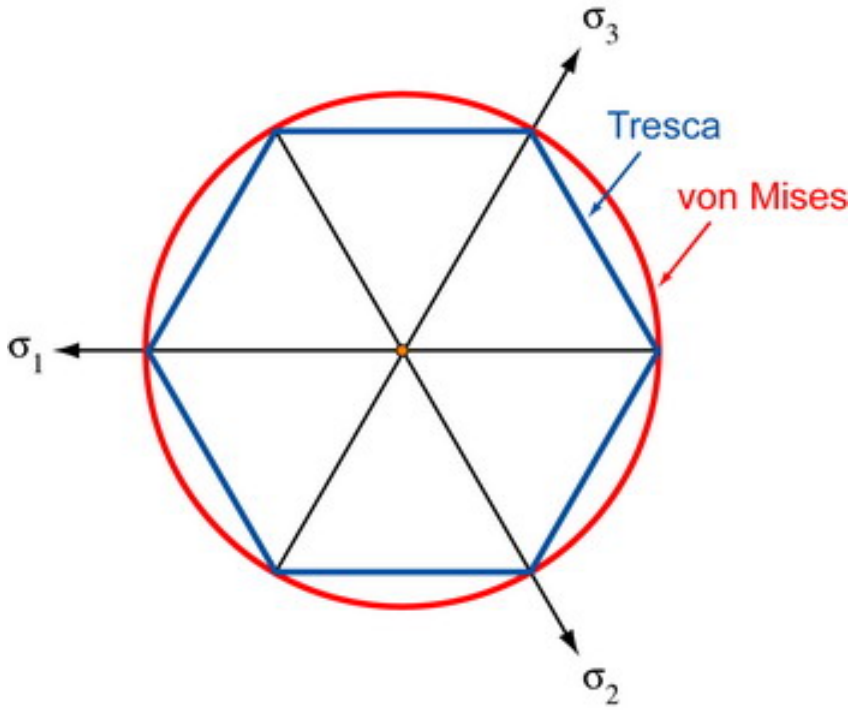

Figure 2.5: Tresca and von-Mises yield criteria in π-plane

2.5.2 Plasticity

To utilize the full capacity of materials, a description of the material behavior in the plastic region is necessary. Soil is a highly nonlinear material where elastic behavior can only be assumed for very small strains. In plasticity the work energy is irreversible and translates to other forms, e.g. heat energy. This leads to permanent (plastic) strains.

Within a yield surface the stress - strain relationship is purely elastic. If the stress state tries to surpass the yield surface the result will be a irreversible plastic response. This response is described by the plastic strain, $\underline{\varepsilon}^p$, while the elastic reversible response is described by the elastic strain, $\underline{\varepsilon}^e$. Summed together they will be the total strain, $\underline{\varepsilon}$.

$$\underline{\varepsilon} = \underline{\varepsilon}^e + \underline{\varepsilon}^p \tag{2.33}$$

The balance of mechanical energy is important for deriving the necessary equations for the framework used in FEM plasticity. The balance can be stated as "... the work per unit time of the external forces equals the work per unit time of the internal forces."(Hopperstad and Børvik, 2014). The work per unit time, known as the power, can be achieved by using the equilibrium equation for forces 2.16 and 2.17. By multiplying them by the velocity and integrating over the volume the following equation can be achieved:

$$\int_V \underline{\sigma}\,\underline{\dot{\varepsilon}}\,dV = \int_V \underline{b}\,\underline{v}\,dV + \int_S \underline{t}\,\underline{v}\,dS \tag{2.34}$$

$$(internal) = (external)$$

where $\underline{\dot{\varepsilon}}$ is the strain rate, $\underline{\mathrm{v}}$ is the velocity, $\underline{\mathrm{b}}$ is the body force and $\underline{\mathrm{t}}$ is the traction force which is integrated over the volume or the surface respectively. Because of the possibility for strain decomposition, the internal work per unit time, called the deformation power (P_d), can be split into an elastic and a plastic part.

$$P_d = \int_V \underline{\sigma}\,\underline{\dot{\varepsilon}}\,dV = \int_V \underline{\sigma}\,\underline{\dot{\varepsilon}}^e\,dV + \int_V \underline{\sigma}\,\underline{\dot{\varepsilon}}^p\,dV \tag{2.35}$$

It is assumed that plastic deformation can not happen without external work and since the energy from the plastic deformation is irreversible, the following restriction applies:

$$\int_V \underline{\sigma}\,\underline{\dot{\varepsilon}}^p\,dV \geq 0$$

Another assumption is that this restriction holds for all parts of the volume. This leads to the expression for the plastic dissipastion, D_p, which will always have to be positive.

$$D_p = \underline{\sigma}\, \underline{\dot{\varepsilon}}^p \geq 0 \tag{2.36}$$

To ensure a non-negative plastic dissipation in a material model, the plastic flow rule is defined as:

$$\underline{\dot{\varepsilon}}^p = \dot{\lambda} \frac{\partial g}{\partial \underline{\sigma}} \tag{2.37}$$

The plastic flow rule consists of the plastic potential function, g, differentiated with respect to the stress vector and the plastic parameter, $\dot{\lambda}$. The plastic parameter is defined to be a non-negative scalar and will be derived in the next section. The plastic potential function is assumed to be a positive homogeneous function of first order and by using Euler's theorem, positive plastic dissipation is achieved (Ottosen and Ristinmaa, 2005):

$$D_p = \dot{\lambda}\, \underline{\sigma} \frac{\partial g}{\partial \underline{\sigma}} = \dot{\lambda} g \geq 0$$

The plastic potential function can for some materials be equal to the yield function, f. When g equals f the flow is said to be associated and when it is not the flow is called non-associated. If the flow is associated and the equivalent stress is a positive homogeneous function, a positive plastic dissipation is assured.

$$D_p = \dot{\lambda}\, \underline{\sigma} \frac{\partial f}{\partial \underline{\sigma}} = \dot{\lambda} \underline{\sigma} \frac{\partial \sigma_{eq}}{\partial \underline{\sigma}} = \dot{\lambda} \sigma_{eq} \geq 0 \tag{2.38}$$

All derivations above are done for rate dependent materials. The same derivations are valid for a rate independent material. The only difference is changing $\dot{\lambda}$ and $\dot{\varepsilon}^p$ with $\Delta\lambda$ and $\Delta\varepsilon^p$. This will also be the case for all the upcoming equations on rate form.

The von Mises flow rule

Based on equation 2.37, the associated von Mises flow rule will get the following form:

$$\underline{\dot{\varepsilon}}^p = \begin{bmatrix} \dot{\varepsilon}^p_{11} \\ \dot{\varepsilon}^p_{22} \\ \dot{\varepsilon}^p_{33} \\ \dot{\varepsilon}^p_{12} \\ \dot{\varepsilon}^p_{23} \\ \dot{\varepsilon}^p_{31} \end{bmatrix} = \dot{\lambda}\frac{\partial f}{\partial \underline{\sigma}} = \frac{\dot{\lambda}}{2\sigma_{eq}} \begin{bmatrix} 2\sigma_{11} - \sigma_{22} - \sigma_{33} \\ 2\sigma_{22} - \sigma_{11} - \sigma_{33} \\ 2\sigma_{33} - \sigma_{22} - \sigma_{11} \\ 3\sigma_{12} \\ 3\sigma_{23} \\ 3\sigma_{31} \end{bmatrix} \tag{2.39}$$

which leads to the following expression for the plastic dissipation:

$$D_p = \underline{\sigma}\,\underline{\dot{\varepsilon}}^p = \underline{\sigma}\dot{\lambda}\frac{\partial f}{\partial \underline{\sigma}} = \underline{\sigma}\frac{\dot{\lambda}}{2\sigma_{eq}} \begin{bmatrix} 2\sigma_{11} - \sigma_{22} - \sigma_{33} \\ 2\sigma_{22} - \sigma_{11} - \sigma_{33} \\ 2\sigma_{33} - \sigma_{22} - \sigma_{11} \\ 6\sigma_{12} \\ 6\sigma_{23} \\ 6\sigma_{31} \end{bmatrix}$$

this is equivalent to:

$$\frac{\dot{\lambda}\sigma^2_{eq}}{\sigma_{eq}} = \dot{\lambda}\sigma_{eq} \geq 0$$

the plastic dissipation is therefore assured to be positive for the associated von Mises flow rule.

2.5.3 Loading/unloading Conditions

An essential part of a material model is to be able to distinguish between elastic loading/unloading and plastic loading. For elastic loading/unloading the stress state will be within the yield surface i.e. $f < 0$ (see figure 2.6). There will be no change in plastic strains during elastic loading/unloading, which means that the plastic parameter, $\dot{\lambda}$, will have to be zero.

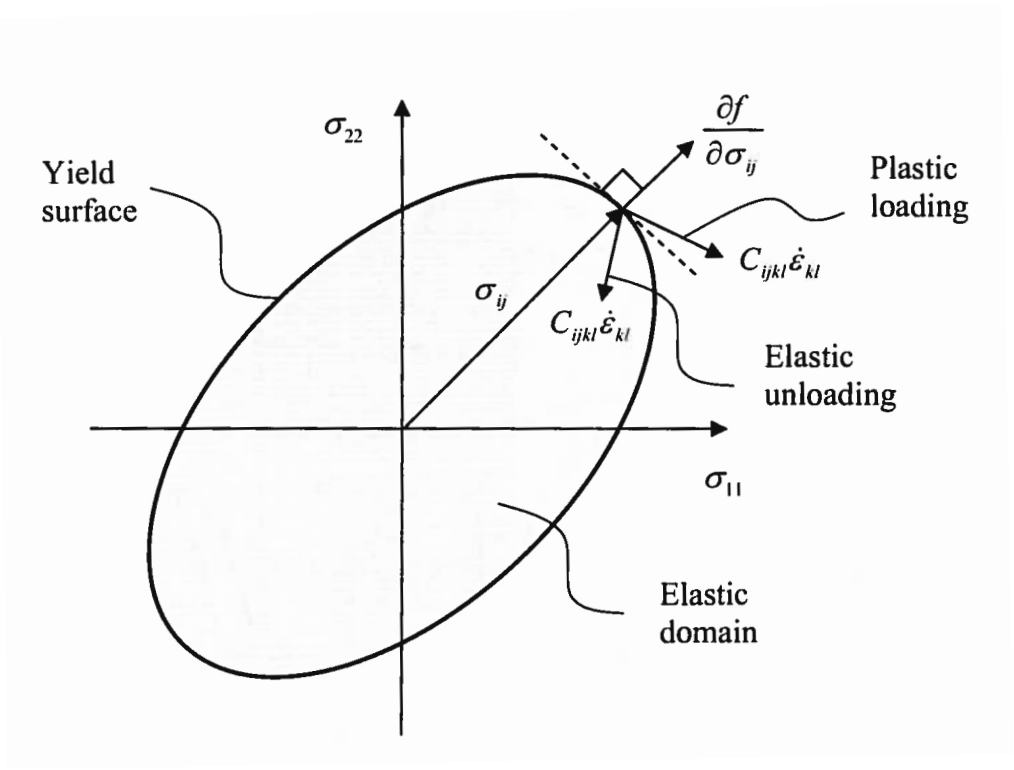

Figure 2.6: Visualization of the loading/unloading conditions (from Hopperstad and Børvik (2014))

For the plastic loading, on the other hand, the stress state will be on the yield surface which means that $f = 0$. The plastic strains will now start to accumulate and the plastic parameter will therefore be greater than zero. These stress states can be expressed by the Kuhn-Tucker conditions, which are:

$$f \leq 0, \qquad \dot{\lambda} \geq 0, \qquad \dot{\lambda} f = 0 \tag{2.40}$$

To be able to solve the plastic behavior of a material model, the plastic parameter needs to be determined. In order to do so the fact that plastic loading require the stress state to be on the yield surface is being used. This means that the change in f will have to be zero for plastic loading and combined with the Kuhn-Tucker conditions the consistency condition in theory of plasticity (Hopperstad and Børvik, 2014) is derived:

$$\dot{\lambda} \dot{f} = 0 \tag{2.41}$$

The plastic parameter can be derived for plastic loading by a first order taylor linearization of $\dot{f}$:

$$\dot{f} = \frac{\partial f}{\partial \underline{\sigma}} \dot{\underline{\sigma}} = 0, \tag{2.42}$$

Then by using Hookes law on rate form and equation 2.33 and 2.37, the following expression for the plastic parameter can be derived for a perfectly plastic material :

$$\dot{\lambda} = \frac{\frac{\partial f}{\partial \underline{\sigma}} \underline{\underline{C}} \, \dot{\underline{\varepsilon}}}{\frac{\partial f}{\partial \underline{\sigma}}^T \underline{\underline{C}} \, \frac{\partial f}{\partial \underline{\sigma}}} > 0 \tag{2.43}$$

2.5.4 Work-hardening

Work-hardening is the phenomena when a material increases its strength when plastic work is done. Mathematically this can be described by work-hardening rules which expand, translate or both expand and translate the material's yield surface.

Isotropic hardening

The yield function can include the work-hardening, R. This work-hardening will together with the initial yield stress, σ_0, form the flow stress, σ_Y ,(Hopperstad and Børvik, 2014). This leads to the following formulation of the yield function:

$$f = \sigma_{eq} - \sigma_0 - R = \sigma_{eq} - \sigma_Y(R)$$

This formulation gives a hardening which expands the yield surface the same amount in every direction i.e. isotropic hardening (see figure 2.7) .

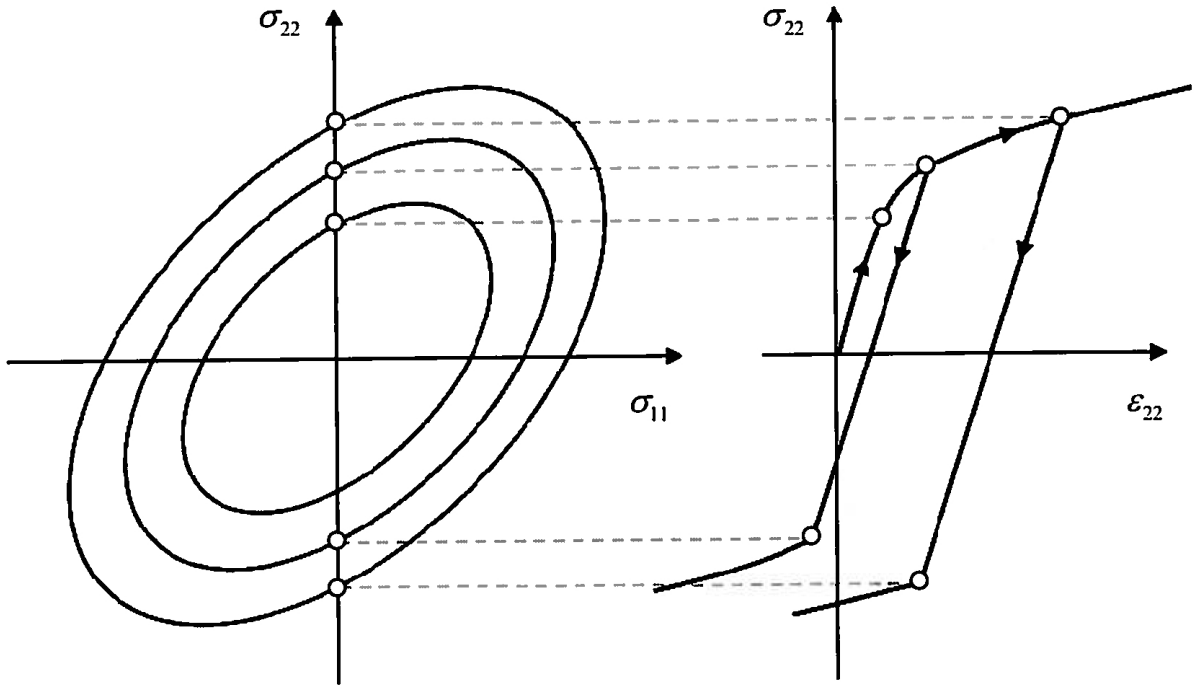

Figure 2.7: Expansion of the yield surface related to the stress path for isotropic hardening (from Hopperstad and Børvik (2014))

Usually the work-hardening is assumed dependent on the equivalent plastic strain, p, which can be found from the equivalent plastic strain rate, $\dot{p}$. The definition of the equivalent plastic strain is the energy conjugate variable to the equivalent stress equal to the plastic dissipation (Hopperstad and Børvik, 2014) such that:

$$D_p = \underline{\sigma}^T \underline{\dot{\varepsilon}}^p = \sigma_{eq} \dot{p} \tag{2.44}$$

Which means that the plastic multiplier for an associated flow rule, as seen in equation 2.38, equals the equivalent plastic strain. For a non-associated flow rule the plastic strain rate can be derived from equation 2.44 as:

$$\dot{p} = \frac{\underline{\sigma}^T \underline{\dot{\varepsilon}}^p}{\sigma_{eq}} \tag{2.45}$$

The equivalent plastic strain is subsequently found by integration of the equivalent plastic strain rate over the time period or by summation of $\Delta\lambda$ if the material is rate independent.

Power law is an example of an isotropic hardening rule which make use of the equivalent plastic strain and is formulated in the following way:

$$R = Kp^n \tag{2.46}$$

where K and n are parameters which can be calibrated from material tests such as an extension test.

The plastic parameter can be derived in a similar manner as before, starting at the following Taylor linearization of $\dot{f}$:

$$\dot{f} = \frac{\partial f}{\partial \underline{\sigma}}\dot{\underline{\sigma}} + \frac{\partial f}{\partial R}\frac{\partial R}{\partial p}\dot{p} = 0 \tag{2.47}$$

and ending up with the following expression for the plastic parameter:

$$\dot{\lambda} = \frac{\frac{\partial f}{\partial \underline{\sigma}}\underline{\underline{C}}\,\dot{\underline{\varepsilon}}}{\frac{\partial f}{\partial \underline{\sigma}}^T \underline{\underline{C}}\,\frac{\partial f}{\partial \underline{\sigma}} - \frac{\partial f}{\partial R}\frac{\partial R}{\partial p}} > 0 \tag{2.48}$$

2.6 Update of Stresses and Stiffness

A material model's purpose is to calculate the proper stresses and stiffness in a node for a FE-program. The FE-program uses the output to solve a global problem existing of multiple nodes. This section describes how the stress and stiffness can be calculated.

2.6.1 Elastic Material

For a purely linear elastic material the stiffness is constant and described by the elasticity matrix, $\underline{\underline{C}}$. The stress can easily be calculated from equation 2.23.

For nonlinear elasticity, stresses can be calculated considering the total strain in each calculation. The global stiffness can be set to a small strain stiffness so that a solution to the global iteration exists.

2.6.2 Elastic-Plastic Material

The FE-program gives strain increments as input and the material model will have to be able to update stresses and stiffness for each increment. Therefore the program provides information from the previous increment, such as the stress, stiffness matrix and state parameters. The state parameters of a certain material model is used to describe the material behavior. The equivalent plastic strain is an example of such a variable.

Elastic or Plastic Increment?

For each strain increment the material model checks violation of the yield surface. This is done by assuming a fully elastic step and calculating the corresponding stresses in the following way:

$$\underline{\sigma}_{tr} = \underline{\sigma}_n + \underline{\underline{C}}_n \Delta\underline{\varepsilon} \tag{2.49}$$

where the subscript n refers to the step number, while subscript tr is short for trial.

If the trial stress, $\underline{\sigma}_{tr}$, do not violate the yield surface, the step is elastic and the trial stress will be the new stress and the stiffness remains unchanged. If the yield surface is violated, the strain increment needs to be split into a purely elastic and an elastic-plastic part. In Cook et al. (2007) the following method is suggested.

The elastic fraction of the strain increment is described by the variable β such that:

$$\underline{\sigma}_C = \underline{\sigma}_n + \beta\, \underline{\underline{C}}_n \Delta\underline{\varepsilon} \tag{2.50}$$

where $\underline{\sigma}_C$ describes the stress at the yield surface.

Equation 2.50 will be a nonlinear set of equations where β and $\underline{\sigma}_C$ are the unknowns. The first approximation of the unkowns will be:

$$\beta_1 = \frac{f(\underline{\sigma}_n)}{f(\underline{\sigma}_n) - f(\underline{\sigma}_{tr})} \tag{2.51}$$

and

$$\underline{\sigma}_{C1} = \underline{\sigma}_n + \beta_1 \underline{\underline{C}}_n \Delta\underline{\varepsilon} \tag{2.52}$$

When the two first points are decided a secant iterations can be used. This type of iteration is a root-finding algorithm. The secant iteration for this specific problem has the following form:

$$\beta_{i+1} = \beta_i - \frac{f(\underline{\sigma}_{Ci})}{\frac{\Delta f(\underline{\sigma}_C)}{\Delta\beta}} \tag{2.53}$$

where

$$\frac{\Delta f(\underline{\sigma}_C)}{\Delta\beta} = \frac{f(\underline{\sigma}_{C(i-1)}) - f(\underline{\sigma}_{Ci})}{\beta_{i-1} - \beta_i} \tag{2.54}$$

The start value for β_0 is set to 0, and the start value for $\underline{\sigma}_{C0}$ equals $\underline{\sigma}_n$.

Plastic Step

The remaining part of the strain increment, $\Delta\underline{\varepsilon}_{ep}$, is described by:

$$\Delta\underline{\varepsilon}_{ep} = (1-\beta)\Delta\underline{\varepsilon} \tag{2.55}$$

If the hardening of the material is linear the solution for the new stress will have the same form as in equation 2.49, with a linear constant plastic stiffness matrix, $\underline{\underline{C}}^t$. If the hardening is nonlinear, the plastic stiffness matrix depends on

the stress state. By using equation 2.23, 2.33, 2.37 and 2.48, the plastic stiffness matrix for an associated, isotropic hardening law can be derived:

$$\underline{\underline{C}}^t = \underline{\underline{C}} - \frac{\left(\underline{\underline{C}}\,\frac{\partial f}{\partial \underline{\sigma}}\right)\left(\frac{\partial f}{\partial \underline{\sigma}}\,\underline{\underline{C}}\right)}{\frac{\partial f}{\partial \underline{\sigma}}^T \underline{\underline{C}}\,\frac{\partial f}{\partial \underline{\sigma}} - \frac{\partial f}{\partial R}\,\frac{\partial R}{\partial p}} > 0 \tag{2.56}$$

The plastic stiffness matrix for a nonlinear hardening can be used to solve the new stress state directly. This is done by forward Euler integration which makes use of the plastic stiffness matrix at $\underline{\sigma}_C$ and smaller increments of the elastoplastic strain increment to calculate a stress increment. The calculation is done by an incremental form of the Hooke's law giving the following expression:

$$\delta\underline{\sigma} = \underline{\underline{C}}\,\delta\underline{\varepsilon} \tag{2.57}$$

This method is explicit because the stresses are found directly. The drawback with such a method is that the calculated stress have the tendency to drift away from the real solution if the increment size is not chosen small enough. Another problem is the calculation cost for the plastic stiffness matrix which can make the procedure time consuming.

A more robust method when it comes to handling larger strain increments $\delta\underline{\varepsilon}$, is the implicit method known as the backward Euler integration. The backward Euler integration is a truncated Taylor series expansion describing the next stress state by the following equation:

$$\underline{\sigma}_{n+1} = \underline{\sigma}_{tr} - \underline{\underline{C}}\Delta\underline{\varepsilon}^p_{n+1} = \underline{\sigma}_{tr} - \underline{\underline{C}}\Delta\lambda_{n+1}\frac{\partial g}{\partial \underline{\sigma}}_{n+1} \tag{2.58}$$

The equation set consists of seven unknown variables and there is a need for another equation to be able to solve the problem. By rearranging the expression to a residual function, and including the yield function as the seventh equation, the system of equations gets the form in equation 2.59.

$$\underline{r}_{n+1} = \begin{bmatrix} \underline{r}_{1,n+1} \\ r_{2,n+1} \end{bmatrix} = \begin{bmatrix} \underline{\sigma}_{n+1} - \underline{\sigma}_{tr} + \underline{\underline{C}}(\lambda_{n+1} - \lambda_n)\frac{\partial g}{\partial \underline{\sigma}}_{n+1} \\ f_{n+1} \end{bmatrix} = \underline{0} \tag{2.59}$$

The system of equations can be solved by a Newton-Raphson iteration. The first step is to linearize the residual function in order to find the roots. The linearization is expressed as:

$$\underline{r}^{i+1}_{n+1} \approx \underline{r}^{i}_{n+1} + \frac{\partial \underline{r}^{i}_{n+1}}{\partial \underline{x}^{i}_{n+1}} \Delta \underline{x}^{i}_{n+1} \approx \underline{0} \tag{2.60}$$

where i refers to the iteration number and the unknown variables are represented by:

$$\underline{x}_{n+1} = \begin{bmatrix} \underline{\sigma}_{n+1} \\ \lambda_{n+1} \end{bmatrix} \tag{2.61}$$

Then by solving for the change in the unknown variables

$$\Delta \underline{x}^{i}_{n+1} = -\frac{\underline{r}^{i}_{n+1}}{\underline{\underline{J}}^{i}_{n+1}} \tag{2.62}$$

The new iteration attempt for the unknown variables can be described by:

$$\underline{x}^{i+1}_{n+1} = \underline{x}^{i}_{n+1} + \Delta \underline{x}^{i}_{n+1} \tag{2.63}$$

The iteration continues until a certain criteria is reached. The criteria can for example be the norm of the residual less than a tolerance, i.e:

$$\left|\left|\underline{r}_{n+1}\right|\right| < tolerance \tag{2.64}$$

The final vector $\underline{x}_{n+1}$ contains the updated stresses and the plastic parameter.

Chapter 3

Cyclic Loading

Knowledge of cyclic loading is important for certain foundation designs of structures offshore, along the coast and on land. Investigations of cyclic loading on soils are often related to foundation design of offshore structures, structures subjected to loading from earthquakes or vibration machinery (Andersen (2015), Kramer (1996), Das and Ramana (2011)). This chapter presents some characteristics of cyclic loading, typical soil reaction for two offshore foundation types i.e. gravity base and monopile and transformation of irregular load history.

3.1 Characteristics of Cyclic Loading

There are many different sources to cyclic loading e.g. waves, wind, drifting ice sheets, earthquakes, tidal variations, traffic, blasting and machine vibrations. Structures experience loads with vastly different amplitudes, periods and durations, and the cyclic load history is irregular with cyclic amplitude varying from one wave to the next. In many cases there can also be an average load component that vary during the storm. Different sources may also generate cyclic loading simultaneously, like wind and wave for an offshore wind power structure. Additionally, resonance of the structure can be a source that generates additional cyclic loading on the soil as a reaction to the primary source. A brief overview of load frequencies for some given situations are summarized in Table 3.1 (developed from Andersen (2015) and Head and Epps (1986)).

Situation	Frequency of load application
Offshore structures:	
- Tidal loading	Usually 2 cycles per day
- Wave loading	≈ 0.1 Hz
- Wind loading	0.01-0.1 Hz
Earthquake on structures	0.1-10 Hz
Subbase for roads and railways	10-100 Hz
Foundations for machinery	Up to 100 Hz

Table 3.1: Load frequencies for given situations

3.2 Soil Reaction to Offshore Cyclic Loading

Offshore foundations are usually fixed to the seafloor by means of gravity only (e.g. GBS) or a combination of soil friction and gravity (e.g. monopiles, skirted foundations). Soil elements beneath offshore foundations experience different stress paths depending on foundation type, type of loading and the geological history. Figure 3.1 shows simplified Ultimate State (US) stress paths beneath a GBS foundation when subjected to cyclic horizontal forces.

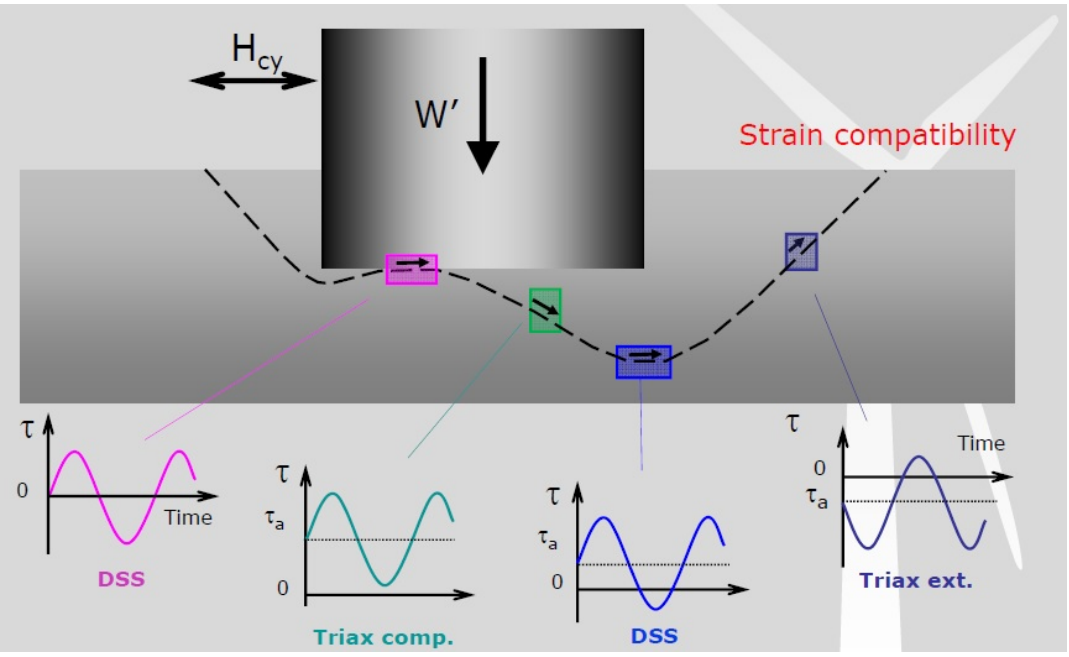

Figure 3.1: Simplified stress paths beneath offshore GBS (from Andersen and Lauritzsen (1988))

Stress paths along potential failure surfaces beneath GBS foundations may be related to stress paths in triaxial compression- and extension, and direct simple shear tests according to figure 3.1. The assumption of strain compatibility along the failure surface may be applied to calculate bearing capacity using the limit equilibrium framework established by NGI (Andersen and Lauritzsen, 1988). Cyclic loading may lead to permanent foundation displacements in a Serviceability State (SS) for the soil, which may induce stresses in structural elements resulting in an US for the structural components.

Figure 3.2 displays simplified stress paths around a monopile foundation. Similar to figure 3.1, the stress paths around a monopile can be related to stress paths found in laboratory testing, however no strain compatibility in US can be assumed and the degree of soil strength mobilization varies throughout the soil volume.

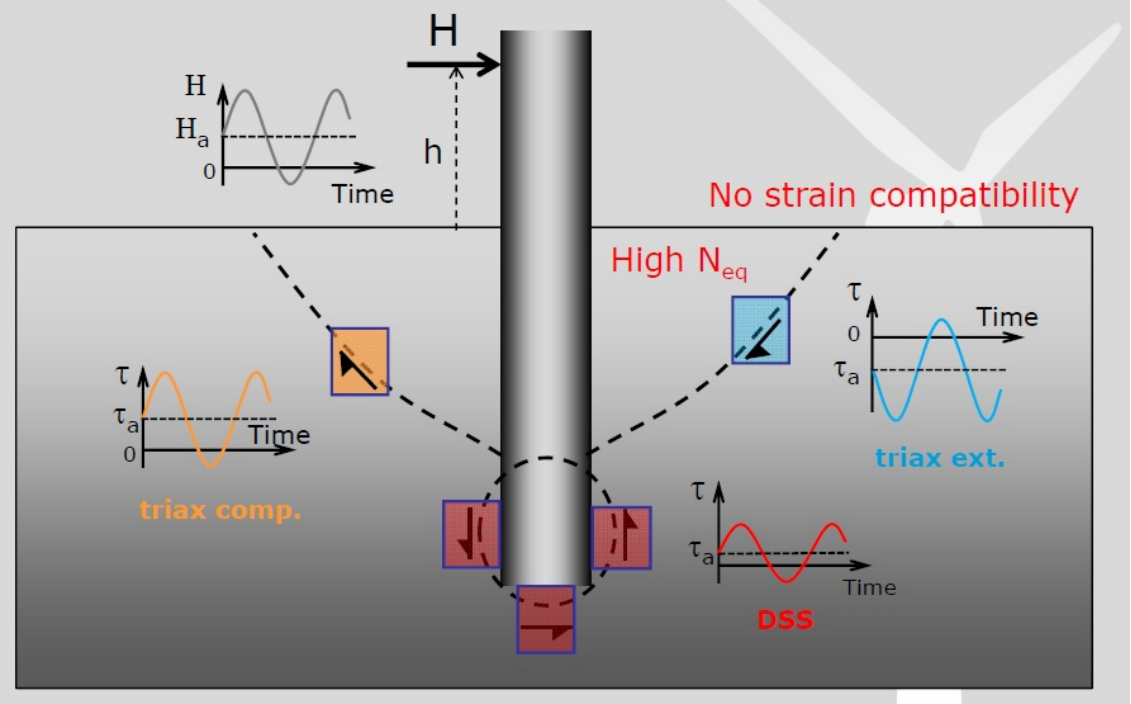

Figure 3.2: Simplified stress paths around offshore monopiles (from (Andersen, 2015))

Monopiles are often used as foundation for Offshore Wind Turbines (OWT). Low turbine efficiency due to tilting leads to strict criterion for acceptable displacements and the design state is often in SS.

3.3 Transformation of Irregular Load History

For design purposes it may be convenient to transform the real, irregular load history to an idealized load history. A Rain Flow Method or other methods may be used (Amzallag et al., 1994). An example is taken from Andersen (2015) and presented in figure 3.3 to demonstrate the principle. This load history yields eleven load parcels which become input to FE calculations. In the figure, maximum load is only repeated once and the other load parcels are defined as fractions of the maximum load.

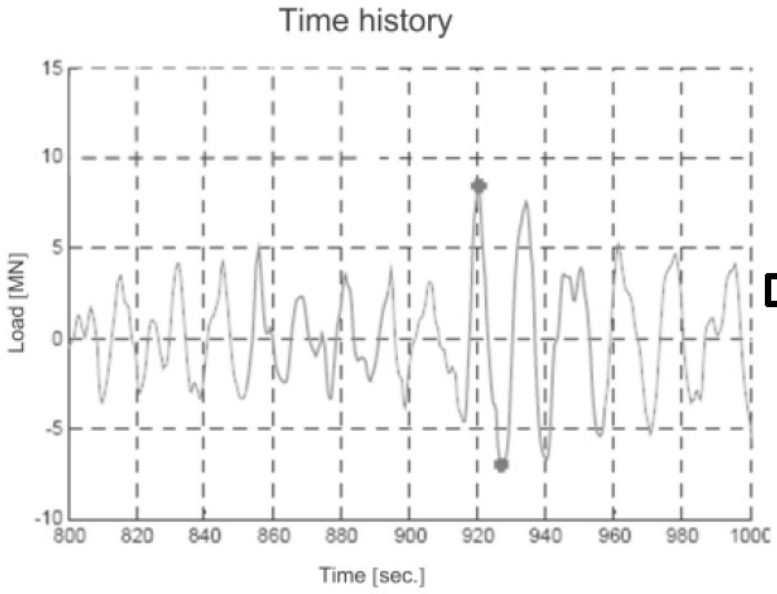

Load parcels

Number of cycles, N	Load in % of max. load
1	100
2	96
4	89
8	83
15	77
30	70
50	64
90	58
200	49
500	37
900	20

Figure 3.3: Transformation from real load history to idealized load history.

Chapter 4

Undrained Behavior of Clay Subjected to Cyclic Loading

Soils are classified as undrained if significant pore pressure dissipation is prevented within a specific time of interest. This applies to design situations in which soil permeability is low and/or the rate of loading is such that significant pore pressure dissipation does not occur. In this case an undrained shear strength approach may be adopted (Grimstad et al., 2012).

Cyclic loading tends to break down the soil structure i.e. change the properties of the soil (Andersen (2015), Kramer (1996)). The strength and stiffness of the soil is, for instance, expected to decrease due to cyclic loading. The ability to describe the cyclic soil behavior is therefore highly dependent on the ability to describe this change in soil properties. This chapter presents the basic theory of undrained cyclic behavior of clay. The first section introduces some parameters which are important in describing the cyclic soil behavior. Subsequently an overview of the most frequently used laboratory tests to obtain cyclic soil properties and typical laboratory test results are presented. Finally, the degradation of soil strength and stiffness, as well as the shear strain accumulation principle are discussed.

4.1 Introduction to Important Parameters

Shear Stresses- and Strains

Shear stress beneath offshore foundations can be divided into initial shear stress (τ_0), additional shear stress due to the structure (τ^s) and additional shear stress induced by environmental loads (τ^{env}). Both additional shear stresses are assumed to act undrained herein. Shear stress beneath offshore foundations can be related to shear stress in different laboratory tests. In a triaxial test, the initial shear stress can be expressed as $\tau_0 = 0.5(1-K_0')\,p_0'$, while $\tau_0 = 0$ in a direct simple shear (DSS) test. p_0' is the effective vertical overburden pressure while K_0' is the coefficient of earth pressure at rest (Andersen, 2015).

The shear stress induced by environmental loads can be divided into an average part (τ_a^{env}) and a cyclic part ($\tau_{cy}^{env} = \tau_{cy}$). From figure 4.1, the cyclic shear stress τ_{cy} can be regarded as the shear stress amplitude. This shear stress amplitude is further referred to as the "cyclic shear stress". The subdivision of shear stress finally gives the expression for the total average shear stress beneath offshore foundations.

$$\tau_a = \tau_0 + \tau^s + \tau_a^{env} \tag{4.1}$$

Similarly, the shear strain can be described by average, cyclic and permanent shear strain (γ_a, γ_{cy} and γ_p) according to figure 4.1. γ_a can be regarded as the mean value of the peak shear strains within a cycle and γ_{cy} as the cyclic shear strain amplitude i.e. half the peak to peak value within a cycle. The cyclic shear strain amplitude is further referred to as the "cyclic shear strain".

γ_p is the shear strain at the end of each cycle, but is often assumed equal to the average shear strain, $\gamma_p = \gamma_a$. This can be a good approximation when there is no shear stress reversal. The difference is greater when the cyclic shear strain is predominant, but the difference between the permanent and the average shear strains will be less than the cyclic shear strain, i.e. $|\gamma_p\text{-}\gamma_a| < \gamma_{cy}$.

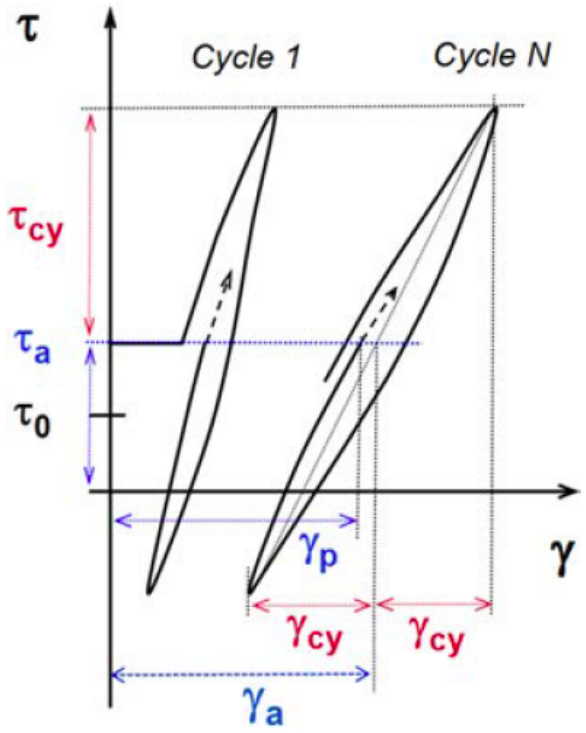

Figure 4.1: Shear stress- and strain induced by cyclic loading (from Andersen (2015))

Many laboratory tests on clay with undrained cyclic loading have been conducted to study the behavior. The undrained cyclic loading can be imposed as a number of harmonic stress- or strain cycles (N) with specific values of the average shear stress (τ_a) and cyclic shear stress (τ_{cy}), or a specific value for the cyclic shear strain (γ_{cy}), respectively. The number of harmonic cycles is therefore an important parameter in order to describe the material behavior.

Pore Water Pressure

Soft clays may have very low permeability i.e. during rapid loading or unloading of saturated clays, the pore water cannot dissipate, which leads to an increase in pore pressure. As for the shear strain, the pore pressure can be described by average (u_a), permanent (u_p) and cyclic pore pressure (u_{cy}), all defined in the same way as for the shear strains (see figure 4.2).

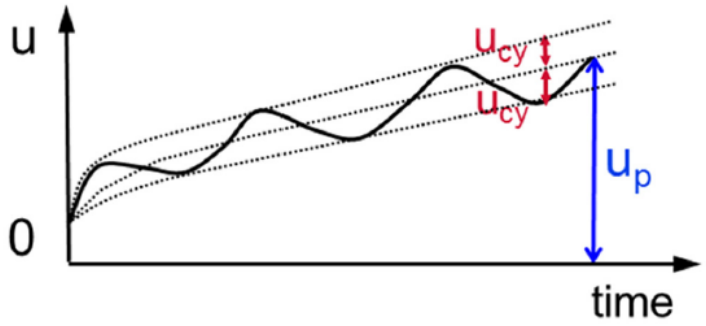

Figure 4.2: Development of excess pore pressure with time (from Andersen (2015))

The permanent pore pressure (u_p) is the preferred measure of the accumulated effect of a previous cyclic load history within a cyclic event (Andersen, 2015). If no pore pressure dissipation occurs during the cyclic event, only negligible volumetric strains develop due to the high bulk stiffness of pore water. From this, it has been assumed that also the cyclic shear strain (γ_{cy}) uniquely represents the accumulated effect. The cyclic shear strain is used to quantify this accumulated effect on soil properties in the Undrained Cyclic Clay Model presented in chapter 6. Andersen (2015) presents how to calculate this accumulated effect and a further demonstration is given in section 4.5. If dissipation of pore pressure do occur during the cyclic event, only the permanent pore pressure can be used.

Shear Modulus

The shear modulus is an important parameter in geotechnical engineering. Laboratory tests have shown that the shear stiffness is influenced by cyclic strain amplitude, void ratio, mean principal effective stress, plasticity index, overconsolidation ratio and number of cycles (Kramer, 1996). A linear relationship between shear stress- and strain is described by the secant shear modulus and can be used in both static and dynamic soil modelling :

$$G_{sec} = \frac{\tau_{cy}}{\gamma_{cy}} \tag{4.2}$$

Since soil behavior is highly nonlinear this approach can only seek to estimate two shear stress-strain points within each cycle, except at very low strains where $G_{sec} \rightarrow G_{max}$.

Undrained Shear Strength

The peak shear stress that can be mobilized during undrained cyclic loading is defined by Andersen and Lauritzsen (1988).

$$\tau_{f,cy} = (\tau_a + \tau_{cy})_f \tag{4.3}$$

$\tau_{f,cy}$ is referred to as the cyclic shear strength and depends on inherent soil properties, loading characteristics (τ_a, τ_{cy}, N) and the stress path. Cyclic failure can occur either as large cyclic shear strains, large average shear strains, or a combination of the two. Cyclic shear strength can be both higher and lower than the undrained static shear strength due to rate effects and degradation respectively (Åhnberg et al.). Figure 4.3 illustrates undrained cyclic shear strength compared to undrained static shear strength in a triaxial compression test. It can be seen that the cyclic shear strength is degraded to a lower value than the static shear strength.

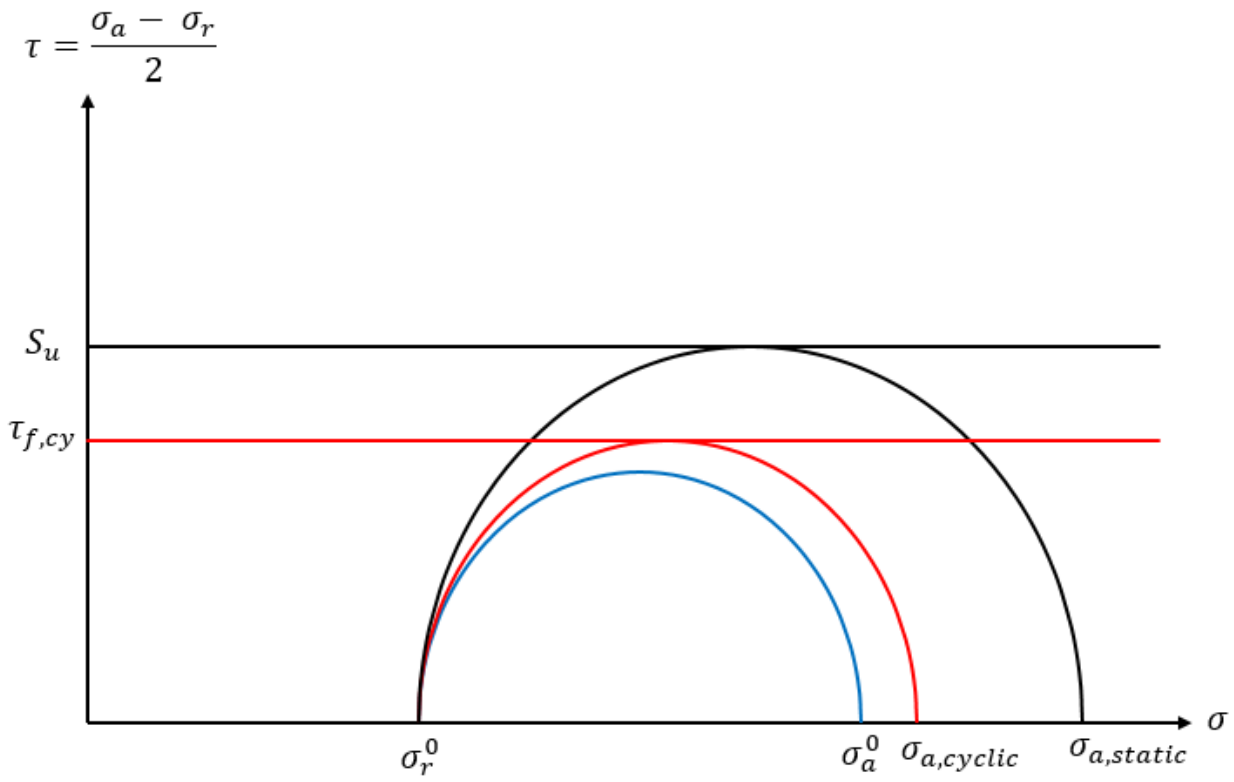

Figure 4.3: Undrained static and cyclic shear strengths of triaxial compression test

Static soil parameters can be used as reference for cyclic soil parameters. It is in particular convenient to normalize shear stress by the static undrained shear strength ($S_u = c_u$). The static undrained shear strength is the highest possible stress that can be mobilized during static loading (see fig. 4.3). Similar to the undrained cyclic shear strength, the undrained static shear strength has different magnitude depending on the stress path. Static shear strengths normally obtained from laboratory tests are compression-, direct- and extension shear strength (S_u^C, S_u^{DSS}, S_u^E respectively).

4.2 Important Laboratory Tests

Triaxial Test

A commonly used test for measuring dynamic- and cyclic soil properties at high strain levels is the cyclic triaxial test (Kramer (1996), Andersen (2015)). A cylindrical specimen is surrounded by a thin rubber membrane and placed between top and bottom loading plates (see fig. 4.4). The specimen is subjected to radial and axial stress. Given the boundary conditions, the principal stresses in the specimen are always vertical and horizontal.

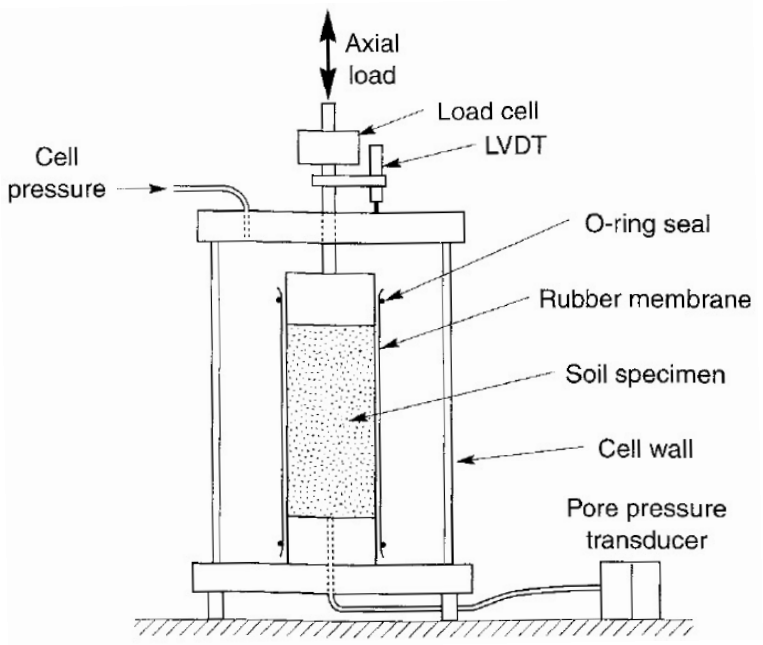

Figure 4.4: Typical triaxial apparatus (from Kramer (1996))

In an undrained triaxial test, the difference between the axial and radial stress is the *deviator* stress (q), while the shear strain is defined as:

$$\gamma = \varepsilon_a - \varepsilon_r = \frac{3}{2}\varepsilon_a \tag{4.4}$$

The deviator stress will have the same value as the equivalent shear stress defined in section 2.2. In a cyclic triaxial test the deviator stress is applied cyclically, either under stress- or strain-controlled conditions. Stress-controlled testing is considered the best representation for cyclic events defined in terms of forces (GBS), while soil elements reaching the same deformation configuration after each cycle is best represented by strain-controlled tests. Stress-controlled testing is preferred by some researchers to keep control of the average- and cyclic shear stress. Cyclic triaxial tests are most commonly performed with the radial stress held constant and the axial stress cycled at a frequency in the range of 0.1 to 1 Hz (Åhnberg et al.).

As seen in section 4.1, the permanent pore pressure is the preferred measure of the accumulated cyclic effect on soils. For clays, it should be noted that it is challenging to measure the cyclic pore pressure reliably in the laboratory (Andersen (2015), Åhnberg et al.). Due to rapid stress changes and short testing durations the requirement to the system compliance can be difficult to fulfill

Both static and cyclic triaxial tests can be performed under isotropically or anisotropically consolidated conditions. Isotropically consolidated tests are performed on soil elements where K_0' is close to 1. Anisotropically consolidated tests are used for K_0' values between 0.5-1 and is most commonly used in Norway.

Direct Simple Shear Test

The cyclic direct simple shear (DSS) test is capable of reproducing certain stress states as shown in section 3.2. A short, cylindrical specimen is restrained against lateral expansion by for instance rigid boundary plates, a wire-reinforced membrane or a series of stacked rings. Cyclic horizontal shear stresses are applied to the top or the bottom of the specimen (see figure 4.5).

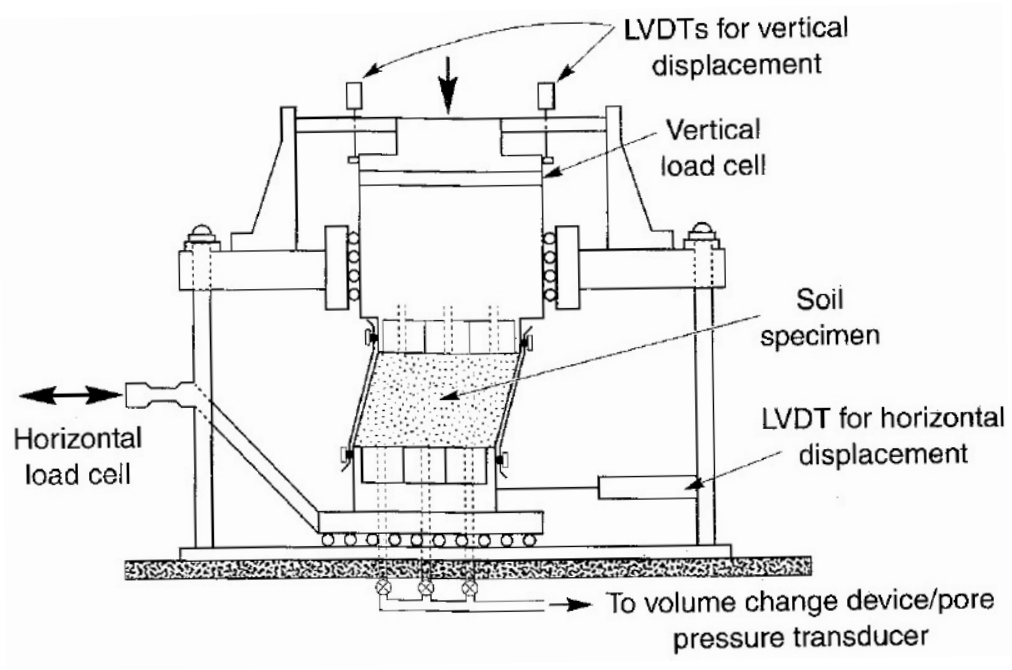

Figure 4.5: NGI cyclic simple shear apparatus (from Kramer (1996))

In this configuration no complimentary shear stresses are imposed on the vertical sides. Moment caused by the horizontal shear stresses at top and bottom must be balanced by non-uniformly distributed shear and normal stresses within the soil specimen. The effects of non-uniformity of stresses can be reduced by increasing the diameter/height ratio of the specimen. Conventional simple shear apparatuses are limited by their inability to impose initial stresses other than those corresponding to K_0 conditions (Kramer, 1996).

4.3 Typical Laboratory Test Results

Stress-controlled Tests

Figure 4.6 shows the undrained stress-strain response to cyclic loading (1 Hz) in stress-controlled, active triaxial testing (Åhnberg et al.). After the accumulated deformations reach the failure deformation in the undrained static test, the cyclic deformation accelerates until cyclic failure occurs. The stress-strain response after cyclic failure approaches the stress-strain response obtained in the static test past failure. In tests where no failure occur, the stress-strain curves

in static tests, after a rest period, closely follow those in the ordinary static test (see figure 4.7). Results from the same study suggests that the accumulated excess pore pressure accelerates after passing the static failure deformation.

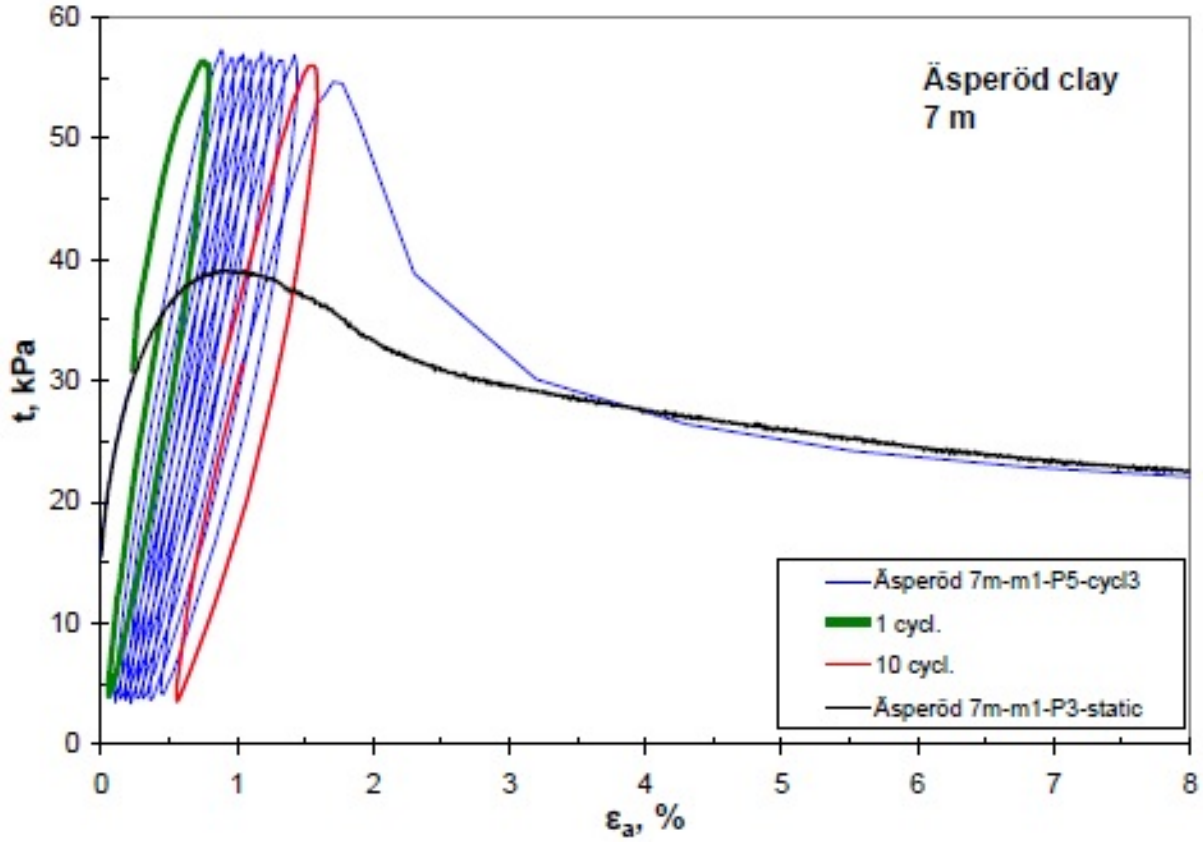

Figure 4.6: Stress-strain response to cyclic and static loading on Äsperöd clay (from Åhnberg et al.)

Figure 4.8 illustrates typical cyclic triaxial- and direct simple shear test results from Andersen (2015). The two leftmost tests in figure 4.8 have symmetrical cyclic loading with approximately the same cyclic shear stress. Their behavior is different and shows that the response to symmetrical cyclic loading is different in DSS and triaxial tests. In DSS tests, the shear strain develops relatively symmetrically. In the triaxial test, the shear strain development is unsymmetrical. This is due to the strength anisotropy under triaxial loading, with an extension strength that is smaller than the compression strength. The triaxial test develops larger shear strains at a lower number of cycles than the DSS test.

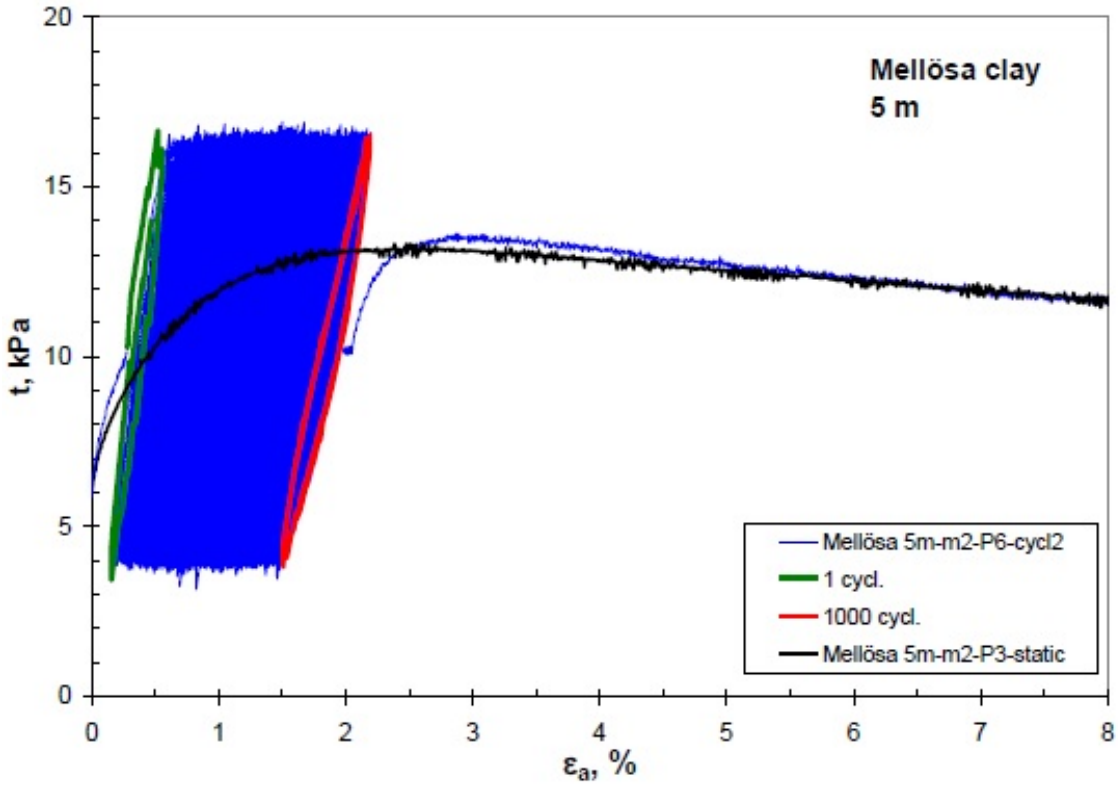

Figure 4.7: Stress-strain response to cyclic and static loading on Mellösa clay (from Åhnberg et al.)

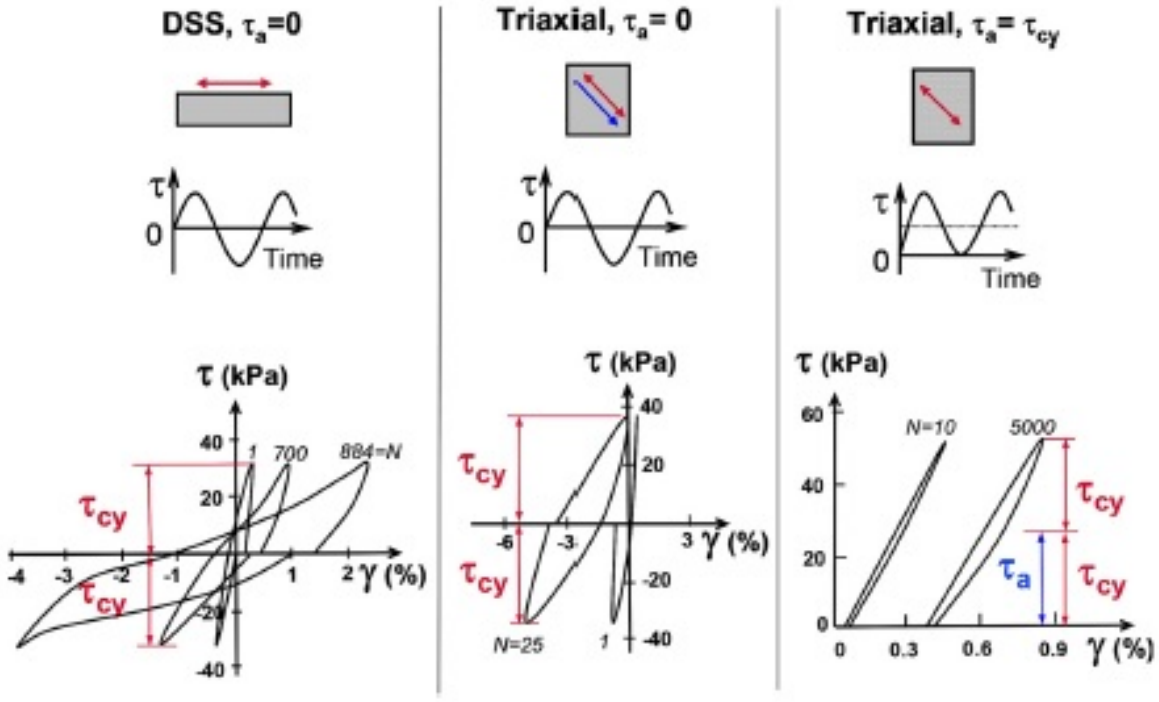

Figure 4.8: Typical laboratory test results (from Andersen (2015))

The rightmost test result in figure 4.8 has a shear stress with equal average and cyclic components. The result is a shear strain development where the average and permanent shear strains dominate and increase with number of cycles. The small cyclic shear strain does not increase significantly with number of cycles.

The three tests in figure 4.9 have the same maximum shear stress, but different average and cyclic shear stress components. The test with $\tau_a = 0$ fails after 10 cycles, whereas the tests with $\tau_a = 0.5\tau_{max}$ and $\tau_a = 0.85\tau_{max}$ have developed only small shear strains after 2500 cycles, and the test with the highest τ_a has the smallest shear strains. Hence figure 4.9 shows that the cyclic behavior is not governed by the maximum shear stress alone and the strain development under cyclic loading cannot be explained by creep.

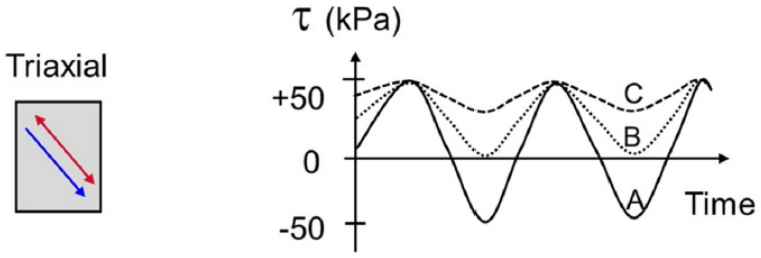

Test	τ_{max}	τ_a	τ_{cy}	Result
A	50	0	50	Failure (γ=15%) 10 cycles
B	50	25	25	γ_p=0.8%, γ_{cy}=0.3% 2500 cycles
C	50	42.5	7.5	γ_p=0.03%, γ_{cy}=0.02% 2500 cycles

Figure 4.9: Typical laboratory results (from Andersen (2015))

Results from laboratory tests can be organized in contour diagrams (Andersen, 2015). γ_{cy} and γ_a can be recorded and illustrated, as in figure 4.10, for specific values of N, τ_{cy} and τ_a. Figure 4.10 shows a contour diagram of the first loading cycle ($N = 1$) for NC Drammen Clay. If τ_a is constant throughout the soil testing, results can be illustrated in a N-τ_{cy} diagram as illustrated in figure 4.11. Here each line represents a cyclic shear strain level which is given in percent in the figure.

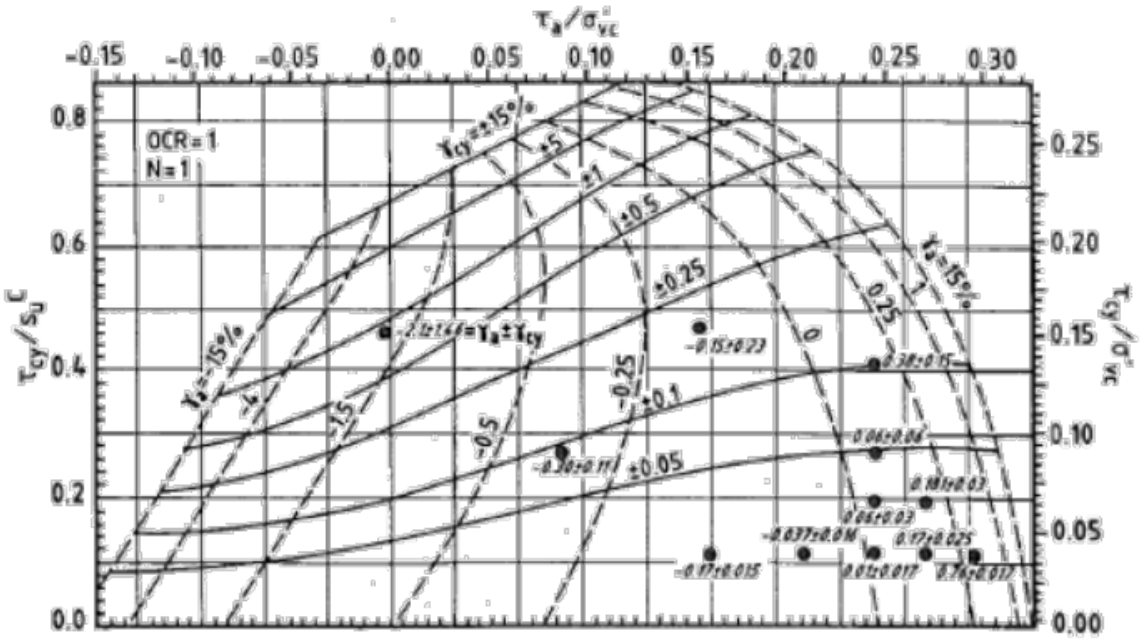

Figure 4.10: Laboratory test results Drammen Clay $OCR = 1$ (from Gustav Grimstad (2012))

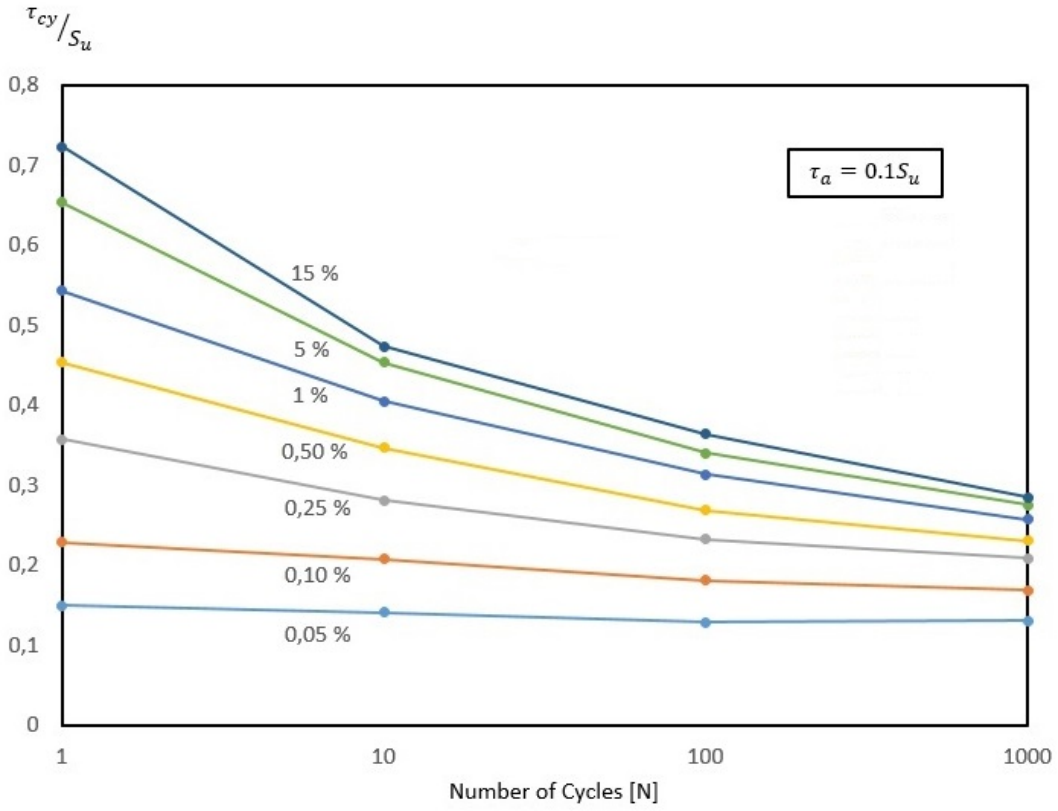

Figure 4.11: N-τ_{cy} diagram for Drammen Clay $OCR = 1$ (developed from Gustav Grimstad (2012))

Strain-Controlled Tests

Strain controlled cyclic triaxial tests were performed at Statens Geotekniska Institut (SGI) with 100 cycles (Åhnberg et al.). Two cyclic strain amplitudes were tested:

1. Axial failure strain in static triaxial test
2. Two times the axial failure strain in static triaxial test

At the first strain level, the cyclic shear stress decreased gradually from values considerably above the shear strength to values below the shear strength in static tests. (see fig. 4.12).

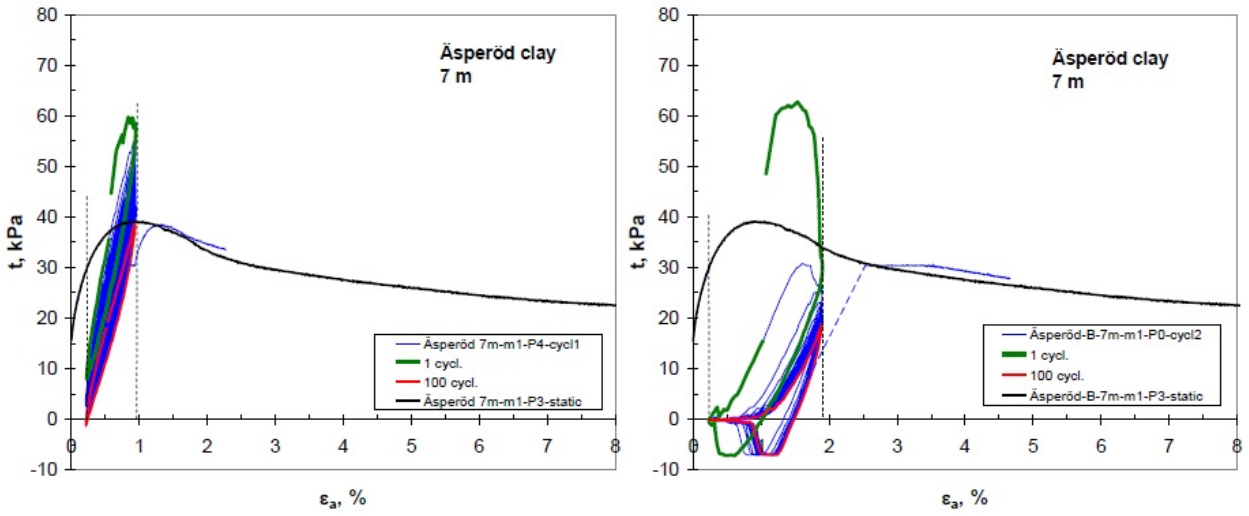

Figure 4.12: Stress-strain response to strain-controlled cyclic loading (from Åhnberg et al.)

The specimens were then subjected to further deformation at the normal rate of strain and the stress-strain curves rapidly adhered to those obtained in the normal static tests.

A reduction in maximum shear stress with increasing number of cycles was observed as seen in figure 4.13. At the first strain level, the stress generally decreased to values close to the undrained shear strength. The decrease was largest during the first cycles and almost evened out towards the end of the cycling. At the second cyclic strain level, the shear stresses decreased more rapidly.

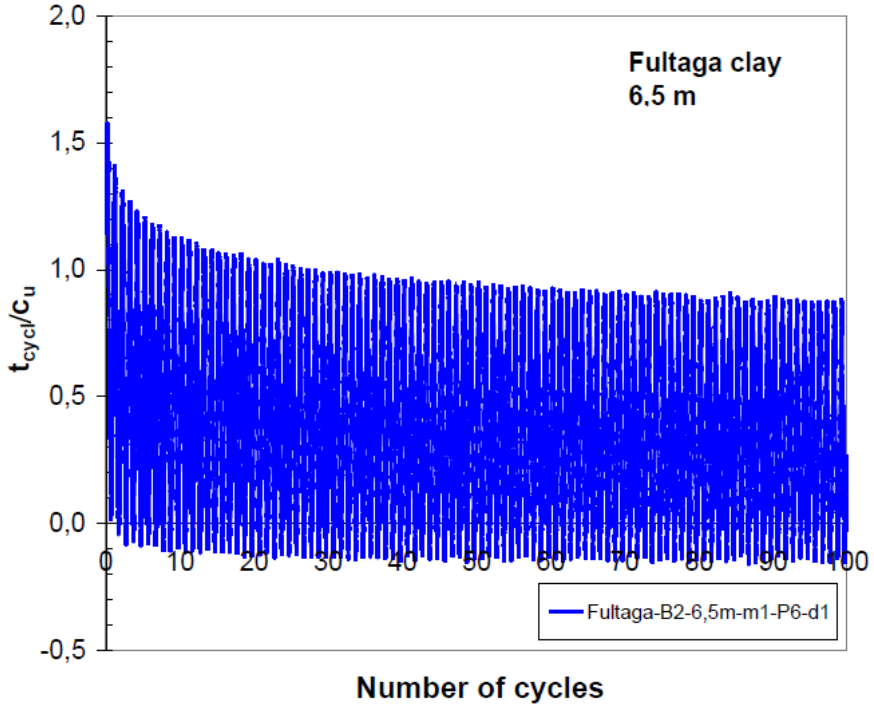

Figure 4.13: N-τ_{cy} diagram for strain-controlled Fultaga clay ($\gamma_{cy} \simeq 1.4$ %) (from Åhnberg et al.)

4.4 Stiffness and Strength

Two principal mechanical properties of all materials are required for engineering design - strength and stiffness. These properties inspired, and essentially form the basis of, the limit state design approach including *ultimate limit state* (ULS) and *serviceability limit state* (SLS) respectively (Wood, 1990). This section presents the undrained strength- and stiffness of clays subjected to both static and cyclic loading.

Undrained Static Stiffness

Soil reaction to loading is in general nonlinear (strain dependent), but in many cases a linear elastic approach is adopted. The soil stiffness is an important parameter in defining the behavior in this assumed elastic- or serviceability-state zone. In soil mechanics, a distinction is often made between *bulk* stiffness and *shear* stiffness. The bulk stiffness defines the volumetric change in geometry, while the shear stiffness represents the material reaction to shear loading or de-

formation.

$$\begin{bmatrix} \Delta p \\ \Delta q \end{bmatrix} = \begin{bmatrix} K & 0 \\ 0 & 3G \end{bmatrix} \begin{bmatrix} \Delta \varepsilon_v \\ \Delta \varepsilon_q \end{bmatrix} \tag{4.5}$$

Water is close to volumetrically incompressible and unable to take shear forces, i.e. the bulk stiffness is high and shear stiffness is zero. Bulk stiffness of the soil skeleton is low compared to the bulk stiffness of water ($K_s << K_w$). Hence, in undrained saturated soils, the volumetric stresses are mostly carried by the pore water, while shear forces must be taken by the soil skeleton. Since the volumetric change in geometry is prevented by the incompressible water, shear stiffness plays an important role in describing the undrained soil behavior (Nordal, 2014).

A typical stress-strain curve from a triaxial test is presented in figure 4.14. The stress-strain response is nonlinear, but the shear modulus can be interpreted as a secant modulus (linear) or a tangent modulus (nonlinear). If the shear modulus is approximated to a secant value, it is common practice to approximate with the value G_u^{50} (Brinkgreve et al., 2016). This value describes a straight line that intersects the stress-strain curve at $\tau = 0.5c_u$, as seen in figure 4.14.

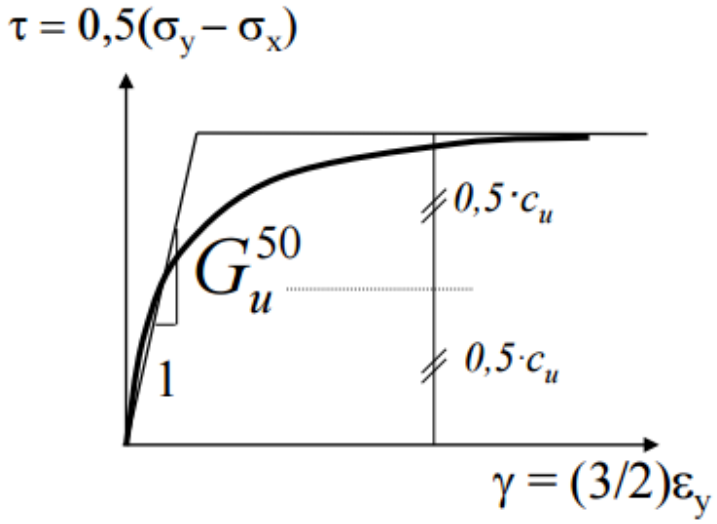

Figure 4.14: Typical stress-strain response from triaxial test (from Nordal (2014))

A tangent shear stiffness describes the real stress-strain curve, which may be convenient in incremental analyses:

$$\Delta\tau = G\Delta\gamma \tag{4.6}$$

Along the stress-strain curve in figure 4.14, both the tangent- and secant shear modulus decreases with increasing shear strain level. This is normally referred to as modulus reduction, which is frequently used in geotechnical earthquake engineering, as well as in some Plaxis soil models.

Figure 4.15 shows typical stress-strain response in undrained triaxial compression- and extension tests for soft clays. The response is clearly different and the material is said to show anisotropic behavior. Hence, the static shear stiffness can be assumed to depend on both the shear strain level and the soil element stress path.

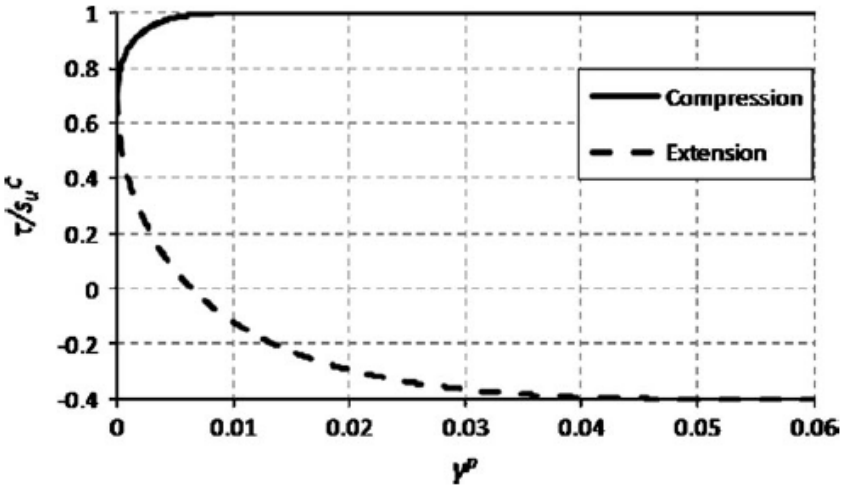

Figure 4.15: Typical stress-strain response from triaxial test (from Grimstad et al. (2012))

Undrained Cyclic Stiffness

Undrained cyclic loading can generate permanent pore pressure and structural changes of a soil element. Under stress-controlled harmonic loading this leads to an increased shear strain amplitude with increasing number of cycles. Under strain-controlled undrained conditions, the shear stress amplitude decreases with increasing number of cycles, as observed from laboratory tests in section

4.3. Both conditions illustrate the tendency of repeated cyclic loading to degrade the shear stiffness of the specimen.

It has been suggested that the cyclic soil stiffness is influence by the cyclic strain amplitude, void ratio, mean principal effective stress, plasticity index, overconsolidation ratio and number of loading cycles (Kramer, 1996). For cohesive soils the following equation for the shear stiffness with number of cycles was proposed by Idriss et al. (1978):

$$G_N = G_1 N^{-t} \tag{4.7}$$

Here, G_1 is the shear modulus in the first stress-strain cycle, N is the number of harmonic loading cycles and t is a degradation parameter. The degradation parameter has been shown to decrease with increasing plasticity index (PI) and overconsolidation ratio (OCR), and to increase with increasing cyclic strain amplitude (γ_{cy}) (Kramer, 1996). Figure 4.16 shows the effect of cyclic degradation on the shear modulus reduction behavior.

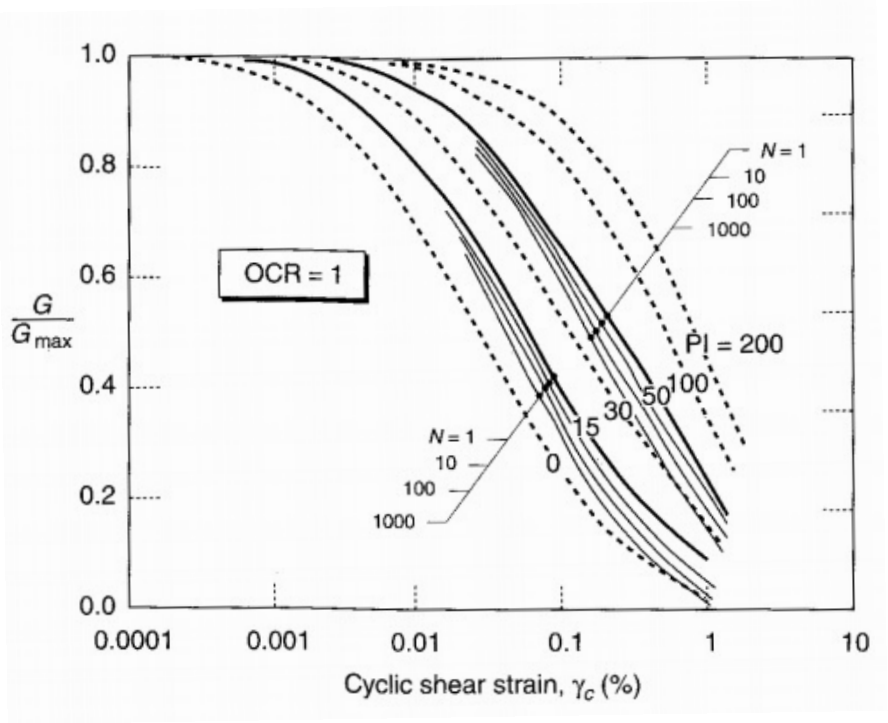

Figure 4.16: Effect of cyclic degradation on shear modulus (from Kramer (1996))

Undrained Static Shear Strength

The undrained static shear strength (S_u) can be used in engineering practice for the short-term condition in clay. If the soil is fully saturated and the pore water (and minerals) are assumed incompressible the volume of a soil element will be constant for undrained conditions (Nordal, 2014):

$$\Delta\varepsilon_v = \Delta p' - D\Delta q = 0 \tag{4.8}$$

If Janbu's dilatancy parameter $D > 0$, the soil is said to dilate. This means more normal forces are taken by the soil skeleton compared to the undrained purely elastic condition, $D = 0$ (see equation 4.9). If $D < 0$, which is normal for NC clay and loose sands, more normal forces must be taken by the pore pressure according to equation 4.9.

$$\Delta u = \Delta p - D\Delta q \tag{4.9}$$

The static strength can be derived from an effective stress based consideration combining Coulomb's law and the undrained condition $\Delta\varepsilon_v = 0$. Given the initial stress state and the dilatancy parameter (D), the effective stress path (ESP) can be determined. Failure is reached when the ESP reach the Coulomb-line (see figure 4.17).

The critical state line, CSL, presented in figure 4.17 depends on the friction angle and the stress path parameter (b). The failure line for a triaxial compression test where $\phi = 30°$ has $M = 6/5$, while in extension the inclination is $M = 6/7$. This will lead to an anisotropic value of the undrained shear strength as observed in laboratory test results for undrained clays.

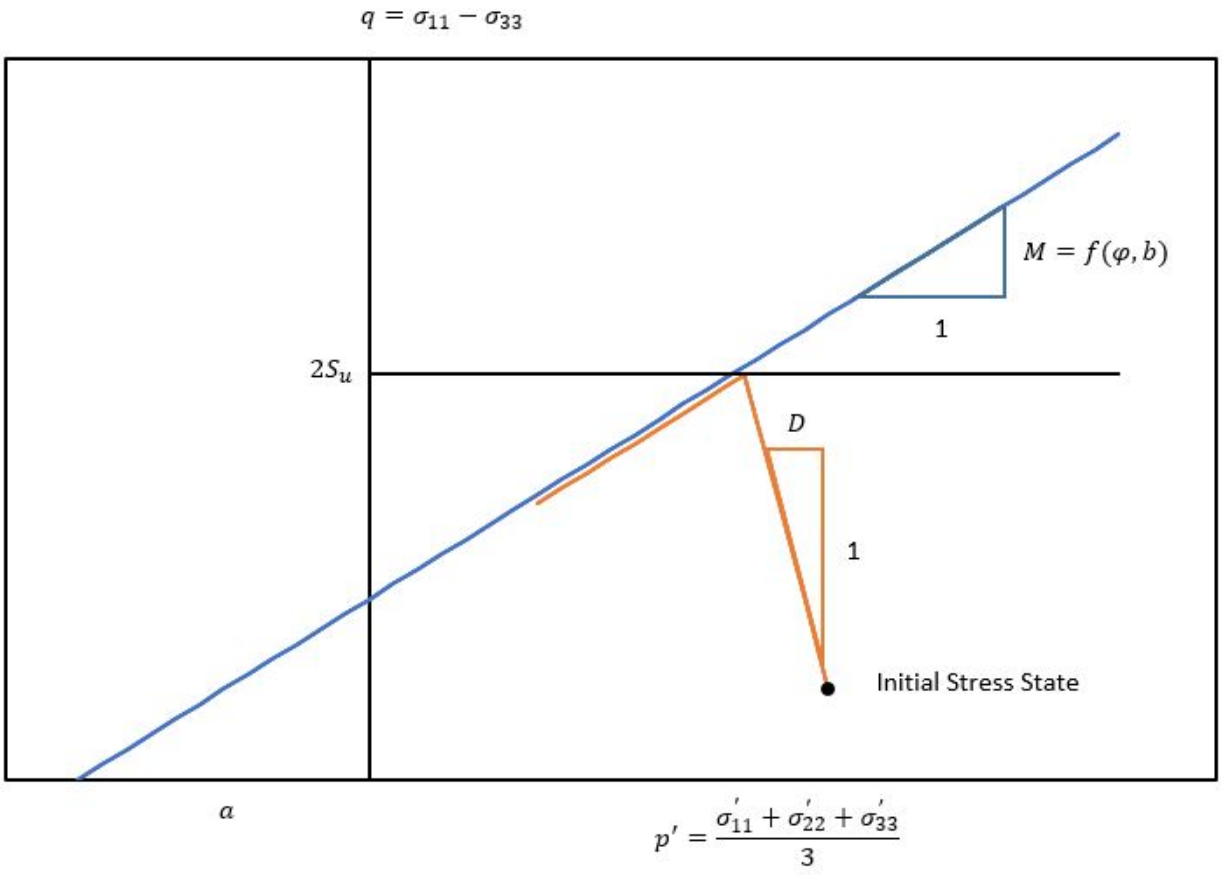

Figure 4.17: Undrained triaxial stress path in p'-q plot (developed from Nordal (2014))

Undrained Cyclic Shear Strength

Cyclic loading will generally tend to break down the structure of the soil skeleton and cause a tendency for volumetric compression (Andersen, 2015). With repeated cycles of loading where the soil dilates and contracts, a permanent excess pore pressure may develop. The development of permanent excess pore pressure with number of cycles may be similar to figure 4.2 (Åhnberg et al.).

The accumulation of excess pore pressure leads to a decrease in effective stresses in the soil, and the stress state moves towards the critical state line seen in figure 4.18-4.20. Figure 4.18 shows a NTNU-plot for an undrained cyclic triaxial test as well as a monotonic triaxial test. In the monotonic test the soil exhibits a peak shear stress, softens and follows the critical state line.

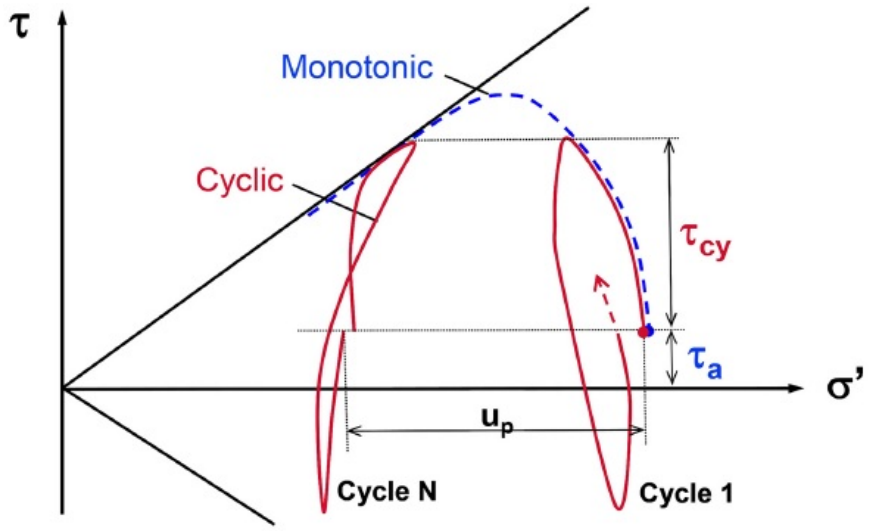

Figure 4.18: NTNU plot of undrained static and cyclic triaxial test (from Andersen (2015))

In the cyclic test, the soil is loaded with a maximum shear stress lower than the undrained static shear strength. During the first cycle the stress path forms a loop that ends up to the left of the initial effective stress. This corresponds to a permanent pore pressure, u_p. Each cycle gives an additional increment in permanent pore pressure as seen in figure 4.2, and after some cycles the effective stress path reaches the critical state line. The shear strains may not necessarily become excessive once the failure line is reached, as the soil may dilate and follow the CSL.

Results from different studies indicate there exist a lower limit for cyclic actions. Cyclic loading below this limit only results in temporary elastic strains and no accumulation of permanent pore pressure. This limit has been reported to be about 20 to 40% of the undrained shear strength in both triaxial and direct simple shear tests. These results were obtained in tests where no static shear stress were imposed before, during or after the cyclic loading (Thiers and Seed (1969), Ansal and Erken (1989)).

The undrained stiffness of the soil skeleton depends on the stress path as seen above. The stiffness is usually lower in extension compared to compression. This indicates more normal forces must be taken by the pore water if stress reversal takes place in a triaxial test as seen in figure 4.19 and 4.20. The excess pore pressure will therefore accumulate more rapidly compared to triaxial tests where no shear stress reversal takes place. This is illustrated in figure 4.19 and

4.20 where the stress path with two-ways loading reaches the critical state line after a lower number of loading cycles compared to the test with one-way loading.

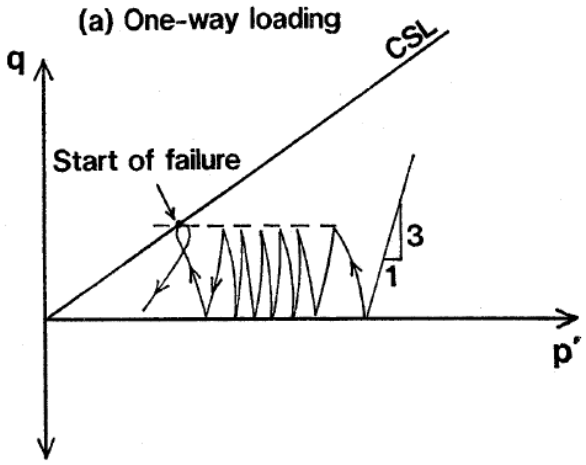

Figure 4.19: Triaxial test with one-way loading (from Yasuhara et al. (1992))

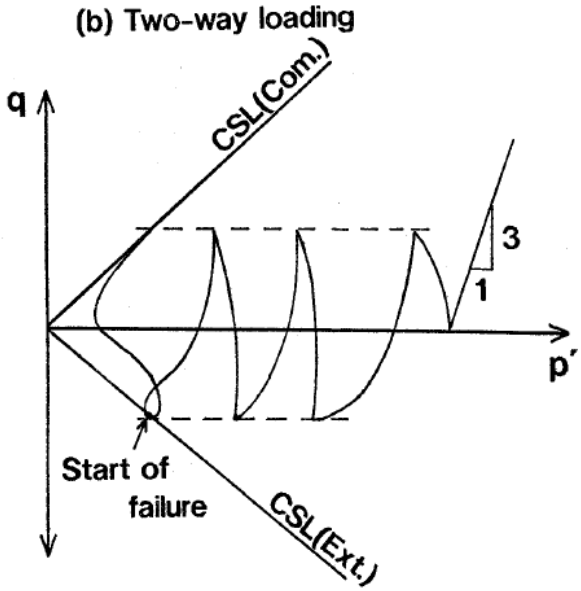

Figure 4.20: Triaxial test with two-way loading (from Yasuhara et al. (1992))

4.5 Cyclic Shear Strain Accumulation Principle

As introduced in section 4.1, the cyclic shear strain (γ_{cy}) can be used to quantify the accumulated effect of a cyclic load history if only negligible pore water dissipation takes place during the cyclic event (Andersen, 2015). Figure 4.21 illustrates the cyclic stress-strain behavior of NC Drammen Clay in the first cycle and the development of cyclic shear strain with number of shear stress cycles. The cyclic shear strain is constant along the yellow- and green line, 0.5% and 5% respectively. No average shear stress ($\tau_a = 0$) is present in the soil element for the material behavior presented in figure 4.21.

There must be compatibility between the current and previous cyclic load histories in order to add them, i.e. they must have the same cyclic shear stress ($\tau_{cy}^{n+1} = \tau_{cy}^{n}$). The index n refers to the parcel number defined in section 3.3. If the current and previous load histories are not compatible, the cyclic shear strain accumulation principle enables a transformation of the previous load history to an *intermediate, equivalent* load history. The intermediate, equivalent cyclic load history has the same cyclic shear stress as the current load history ($\tau_{cy}^{intm} = \tau_{cy}^{n+1}$). It is referred to as intermediate equivalent because, according to the principle, it represents the same state of material degradation as the previous load history. The cyclic shear strain accumulation principle can be stated as:

$$\gamma_{cy,eq}^{intm} = \gamma_{cy,eq}^{n} + \Delta\gamma_{cy}^{inst} \tag{4.10}$$

$\gamma_{cy,eq}^{intm}$ is the cyclic shear strain as result of the intermediate equivalent load history and $\gamma_{cy,eq}^{n}$ is the cyclic shear strain due to the previous cyclic load history. $\Delta\gamma_{cy}^{inst}$ is an instantaneous change in the cyclic shear strain due to the change in cyclic shear stress, and is defined as:

$$\Delta\gamma_{cy}^{inst} = \gamma_{cy,\psi} - \gamma_{cy,\phi} \tag{4.11}$$

where $\gamma_{cy,\psi}$ is the cyclic shear strain in the first loading cycle corresponding to the current cyclic shear stress (see figure 4.21). $\gamma_{cy,\phi}$ is the cyclic shear strain in the first loading cycle corresponding to the previous cyclic shear stress.

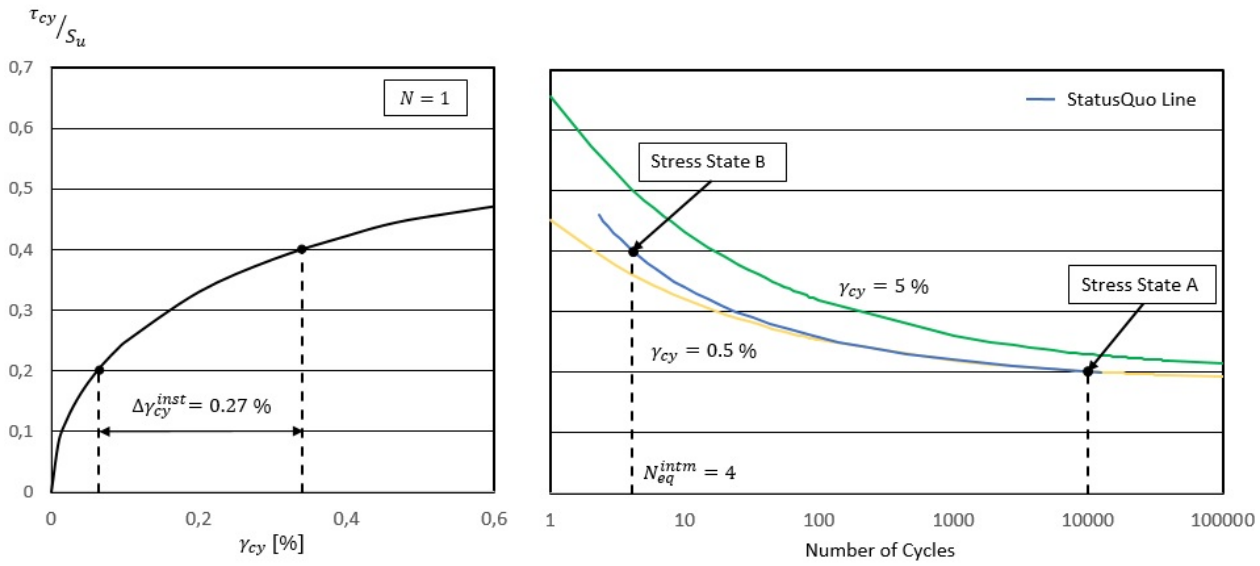

Figure 4.21: Undrained triaxial test results, NC Drammen Clay (developed from Gustav Grimstad (2012))

For instance, a previous cyclic load history of $N_{eq}^{n} = 10^4$ and $\tau_{cy}^{n} = 0.2S_u$ yields a previous cyclic shear strain of $\gamma_{cy,eq}^{n} = 0.5\%$ (stress state A in figure 4.21). For a change in cyclic shear stress of $\Delta\tau_{cy} = 0.2S_u$, the intermediate equivalent cyclic shear strain would be $\gamma_{cy,eq}^{intm} = 0.77\%$. The intermediate equivalent number of cycles is then, from figure 4.21, $N_{eq}^{intm} = 4$. Stress state B is defined by $N_{eq}^{intm} = 4$, $\gamma_{cy,eq}^{intm} = 0.77\%$ and $\tau_{cy}^{intm} = 0.4S_u$. The current cyclic load history, given by ΔN_{eq}^{n+1} and a cyclic shear stress of $\tau_{cy}^{n+1} = 0.4S_u$, can be added from this stress state.

From the cyclic shear strain accumulation principle, the blue line in figure 4.21 can be defined. This line represents loading histories leading to the same amount of material degradation as the previous load history (StatusQuo-line). Stress state A and B are clearly on the line. All stress states (load histories) above the line represent a more degraded material compared to the stress states below.

Chapter 5

Existing Cyclic Soil Models

A variety of models have been proposed to describe the cyclic behavior of soils. In this chapter, a distinction is made between implicit- and explicit soil models. Implicit models follow the stress path within every loading cycle, while explicit models describe the cyclic behavior in terms of the number of loading cycles. Implicit models tend to accumulate errors for every cycle and is time consuming. If the number of cycles is high, the accumulated error may be significant and the computational time increases in order to decrease the error. Explicit models tend to give more accurate results for cyclic load histories with a large number of loading cycles and is more time efficient. The implicit models have the advantage of describing the complete stress path and have a physical behavior related to energy considerations.

Some approaches to implicit representation of cyclic soil behavior are multi-surface plasticity models, nonlinear kinematic- and isotropic hardening rules or a bounding surface. Approaches for the explicit methods are based on empirical laws relating the soil behavior to the number of cycles. Many empirical laws have been proposed based on ideas like stiffness degradation, accumulated strains or accumulated pore pressure.

In the following sections a presentation of the implicit models Extended Masing Model, IWAN model and the coupled NGI-ADP model is given. The explicit models presented in this chapter are Undrained Cyclic Accumlation Model (UDCAM), High-Cycle Accumulation Model (HCAM) and Stiffness Degradation Model (SDM).

5.1 Extended Masing Models

Extended Masing Models are described by a backbone curve depending on the low-strain stiffness (G_{max}) and the high-strain shear strength (τ_{max}), and different rules for the unloading-reloading behavior (Kramer, 1996). The backbone curve can be described as:

$$\tau = \frac{G_{max}\gamma}{1 + \left(\frac{G_{max}}{\tau_{max}}\right)|\gamma|} \tag{5.1}$$

The quantities G_{max} and τ_{max} may be measured directly, computed, or obtained by empirical correlation. The response of the soil to cyclic loading is governed by the following 4 rules:

1. The stress-strain response follows the backbone curve in initial loading as seen in figure 5.1:

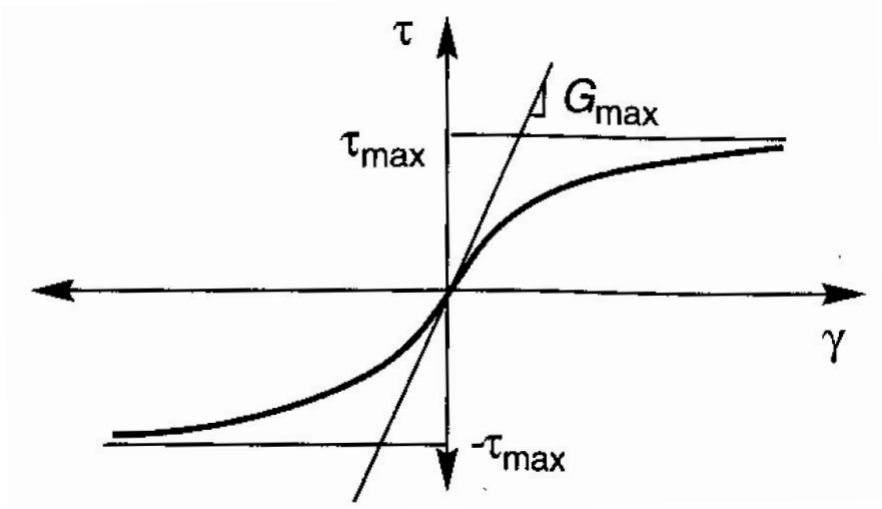

Figure 5.1: Backbone curve extended Masing Models (from Kramer (1996))

2. If a stress reversal occurs at a point defined by (γ_r, τ_r), the stress-strain curve follows a path given by:

$$\tau = \tau_r - \frac{G_{max}(\gamma_r - \gamma)}{1 + \left(\frac{G_{max}}{2\tau_{max}}\right)|\gamma_r - \gamma|} \tag{5.2}$$

3. If the unloading or reloading curve exceeds the maximum past strain and intersects the backbone curve, it follows the backbone curve until the next stress reversal.

4. If an unloading or reloading curve crosses another unloading or reloading curve from the previous cycle, the stress-strain curve follows that of the previous cycle.

This model does not account for pore pressure development in undrained conditions. As pore pressures increase, effective stresses decrease, and consequently the values of G_{max} and τ_{max} decrease. Since the shape and position of the backbone curve depends on G_{max} and τ_{max}, the backbone curve degrades with increasing pores pressure. Using constant values for G_{max} and τ_{max} will therefore have limited possibility of representing the degradation of strength and stiffness.

5.2 IWAN Model

Iwan proposed a mathematically tractable model in order to study the effect of hysteretic behavior on a general system (Iwan, 1966). The general hysteretic system is regarded as a high number of ideal elasto-plastic elements. Each element, originally called Jenkin's elements, have different stiffness and yield level. The configuration of this system could either be series-parallel or parallel-series. The first term refers to the coupling of the Jenkin's elements, and the second term refers to the coupling between the linear elastic- and rigid plastic part of the Jenkin's element. For simplicity, this presentation will focus only on the parallel-series system as presented in figure 5.2.

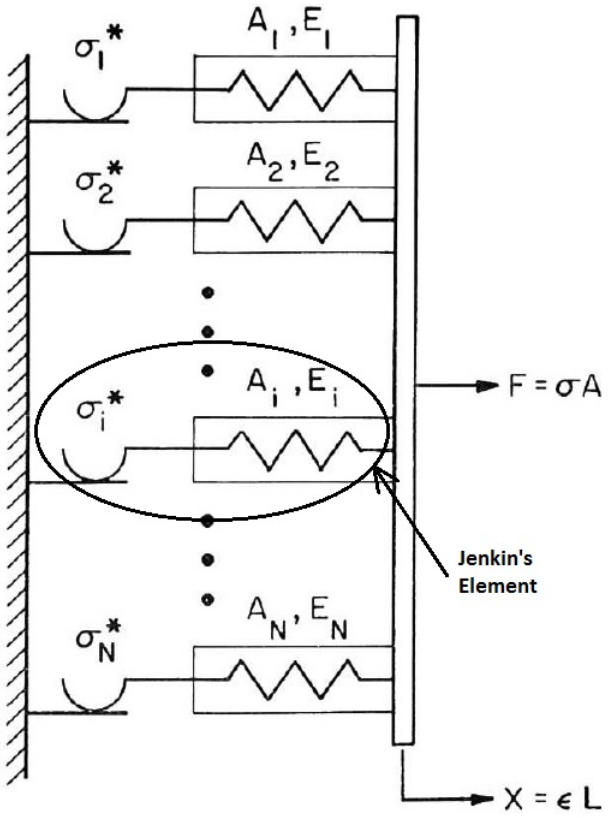

Figure 5.2: Parallel-series system (from Iwan (1967))

In figure 5.2, all Jenkin's elements consist of a linear spring in series with a slip element. The linear spring and the slip element is defined by the stiffness (E_i) and the critical slipping stress (σ_i^*) respectively. If N is the number of elements, the initial loading behavior is described by:

$$\sigma = \frac{F}{A} = \sum_{i=1}^{n} \frac{E_i}{N} \varepsilon + \sum_{i=n+1}^{N} \frac{\sigma_i^*}{N} \tag{5.3}$$

where the summation from 1 to n includes all elements which remain elastic after loading to a strain ε, and the summation from $n+1$ to N includes all elements which have yielded.

An example with three Jenkin's elements is used to demonstrate the principle of this model. The characteristic parameters of the system are summarised in table 5.1 and the resulting stress-strain curve is presented in figure 5.3.

Index (i)	σ_i [kPa]	E_i [MPa]
1	40	9
2	50	10
3	60	11

Table 5.1: Example demonstrating the principle of the IWAN model

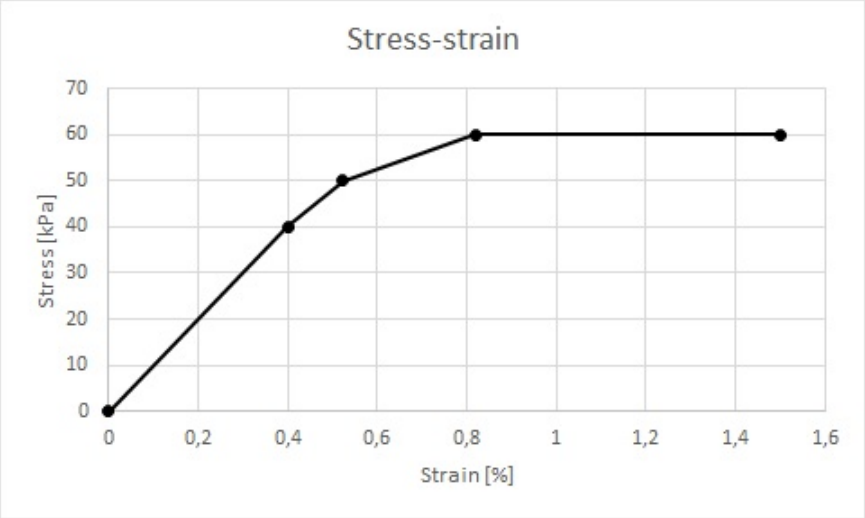

Figure 5.3: Initial loading with 3 elements

If the total number of elements becomes very large the backbone curve of the system will have a similar shape as presented in figure 5.4. In unloading, three different groups of elements contribute to the relationship between stresses and strains. One group of elements reach positive yielding during initial loading and are in a state of negative yielding. Other elements reached positive yielding, but has not yet reached negative yielding, and some elements have not reached yielding at all.

The model was proposed for general hysteretic systems and is limited to undrained situations. It predicts an isotropic shear strength and cannot model cyclic degradation, which can be seen as a drawback with this model. In order to include shear strength anisotropy, a coupled NGI-ADP has been suggested (Grimstad et al. (2014)).

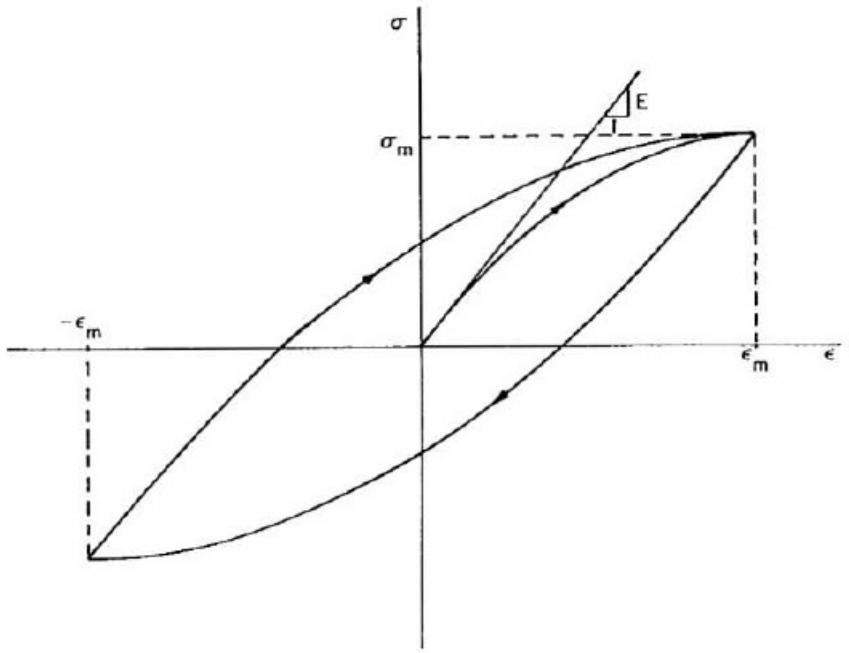

Figure 5.4: General hysteresis response (from Iwan (1967))

5.3 Coupled NGI-ADP Model

Although analysis of undrained behavior of clay is of interest in many geotechnical problems, most of the material models are effective stress based, and the undrained shear strength (S_u) is therefore a prediction. The NGI-ADP material model is based on total stresses and consequently undrained shear strengths are direct input to the model (Grimstad et al. (2012)).

Soft clays normally exhibit anisotropic behavior i.e. strength and stiffness characteristics depend on the stress path. The NGI-ADP model accounts for anisotropy in shear strength and stiffness by a modified Tresca criterion after Billington (1988) and an elliptical interpolation between failure strains. The initial stress state is included in the modified deviatoric stress vector used in the yield criterion. The general 3D yield criterion is defined as:

$$F = \sqrt{H(\omega)\hat{J}_2} - \kappa\frac{S_u^A + S_u^P}{2} \tag{5.4}$$

where ω and $\hat{J}_2$ depend on the modified deviatoric stress vector and κ is the hardening function which is an elliptical interpolation between the failure strains from laboratory tests, within the 3D stress space.

The model itself has limited possibility of reproducing the behavior seen in figure 5.4 due to its linear elastic behavior in stress reversal. To improve the ability to represent cyclically loaded soils, a coupling of several NGI-ADP models has been suggested by Grimstad et al. (2014).

The elements with NGI-ADP properties can either be coupled in parallel or series as described in section 5.2. The basic assumption for the parallel coupling is that strain is compatible (figure 5.5). For the series coupling, it is assumed that stresses are in equilibrium (figure 5.6). Different coupling algorithms are used and can be found in Grimstad et al. (2014).

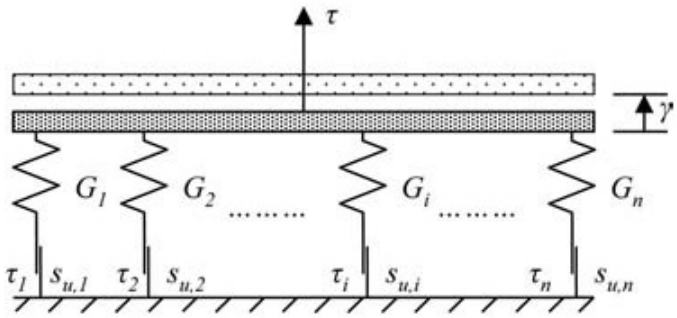

Figure 5.5: Parallel-series coupling of NGI ADP elements (from Grimstad et al. (2014)).

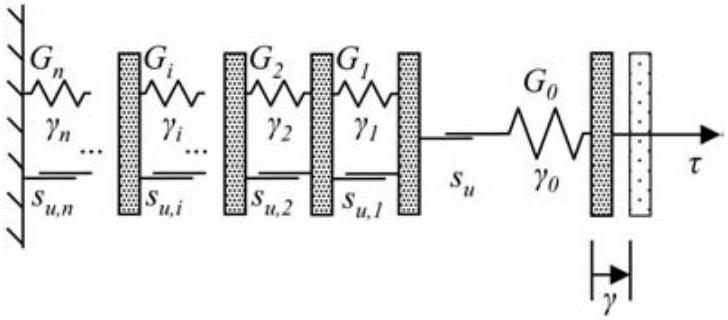

Figure 5.6: Series-parallel coupling of NGI ADP models (from Grimstad et al. (2014)).

A major drawback with this model is that it cannot predict cyclic degradation unless a softening term is included. This model is additionally limited to undrained situations only.

5.4 Undrained Cyclic Accumulation Model

A framework, based on contour diagrams from laboratory testing, has been developed at NGI for the design of offshore structures. The framework has been verified by several model tests and used in the design of a large number of offshore structures with satisfactory results. UDCAM is the FE version of this framework and is implemented as a user-defined soil model in Plaxis (Jostad et al., 2014).

Contour diagrams and the load history are input to the model. The load history is idealized as a number of load parcels, in which average- and cyclic loads are constant, as described in section 3.3. The contour diagrams are contained inside tables $(\tau_a, \tau_{cy}, \gamma_a, \gamma_{cy}, N)$ and interpolation methods are used for intermediate points.

UDCAM analyzes the soil behavior when subjected to load parcels. It accounts for the soil degradation using the *strain accumulation principle* described in Andersen (2015) and in section 4.5. From this principle the equivalent number of cycles (N_{eq}) is calculated in each integration point.

Interpolation between the specific laboratory stress states in the contour diagrams is used to make a complete soil model. The contribution of triaxial behavior is indicated by the ratio between a vertical deviatoric strain and the deviatoric strain invariant:

$$X = \frac{\sqrt{3}e_y}{2\sqrt{J_{2\varepsilon}}} \tag{5.5}$$

The shear stress for a general principal stress orientation is then found by an elliptic interpolation between the triaxial- and DSS stress state:

$$\tau = \frac{1}{2}\sqrt{(\tau_{TXC} - \tau_{TXE})^2 X^2 + 4\tau_{DSS}^2(1 - X^2)} \tag{5.6}$$

The principal deviatoric stress can be calculated from the assumption of coaxiality between strains and stresses.

A cyclic DSS example taken from Jostad et al. (2014) is reproduced here to demonstrate the principle of this model. The idealized load history and the calculation result is summarised in table 5.2.

Load History & Calculation Results					
Parcel	1	2	3	4	5
τ_{cy}/s_u^C	0.458	0.498	0.531	0.571	0.598
ΔN	15	8	4	2	1
Calculated N_{eq}	15	15	13	10	8

Table 5.2: Load history and calculation results DSS example (from Jostad et al. (2014))

Contour diagrams defining the material behavior are presented in figure 5.7 and the resulting cyclic shear stress-strain relationship is illustrated in figure 5.8. The calculation history of N_{eq} is illustrated to the left in figure 5.9.

In order to use the material model, the user needs extensive understanding of how the model works and access to a large amount of laboratory test results. This is the major limitation of this model. It has been suggested to replace the laboratory test results with a mathematical description of the contour diagrams.

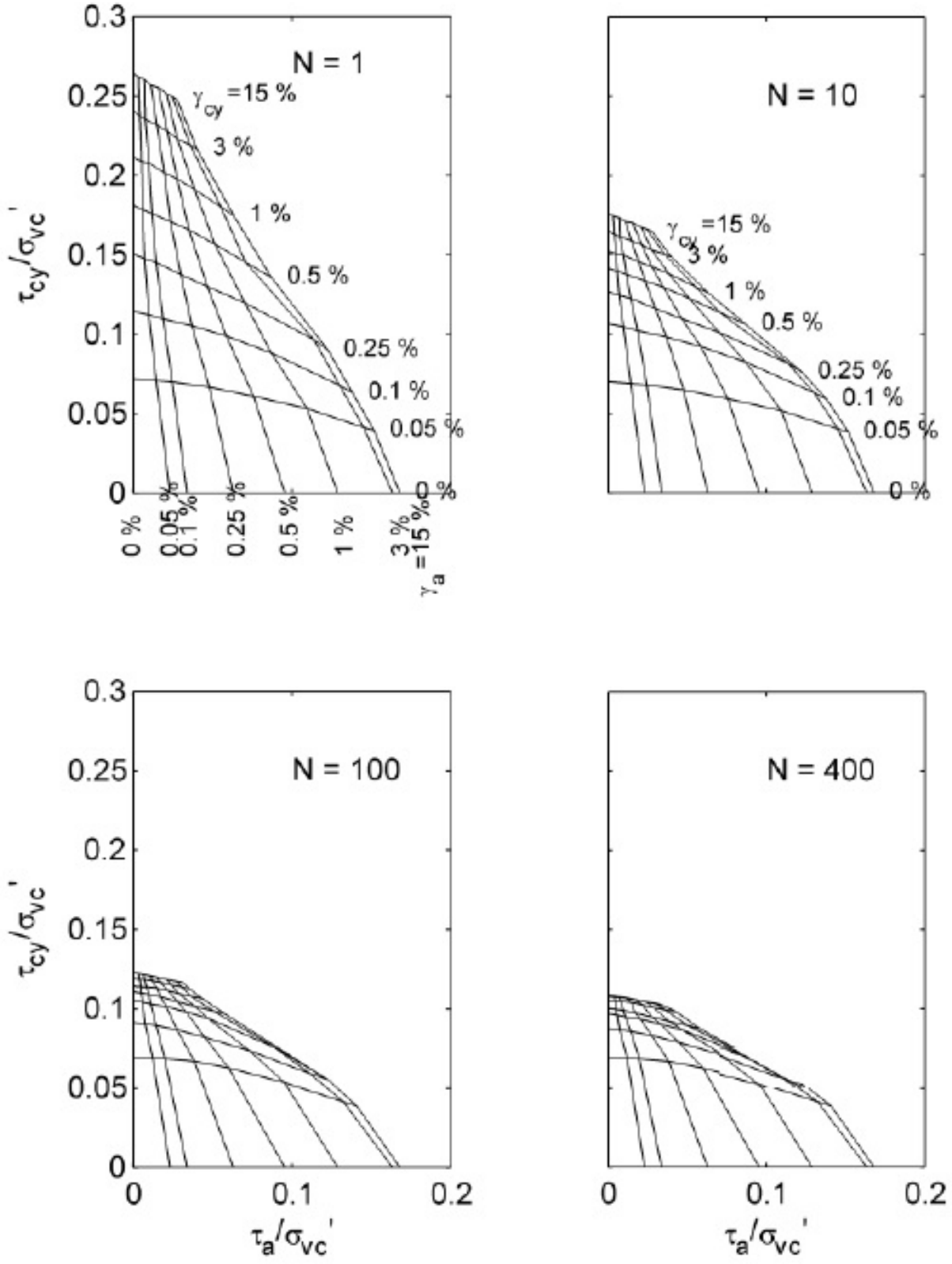

Figure 5.7: Soil behavior in DSS stress state (from Jostad et al. (2014))

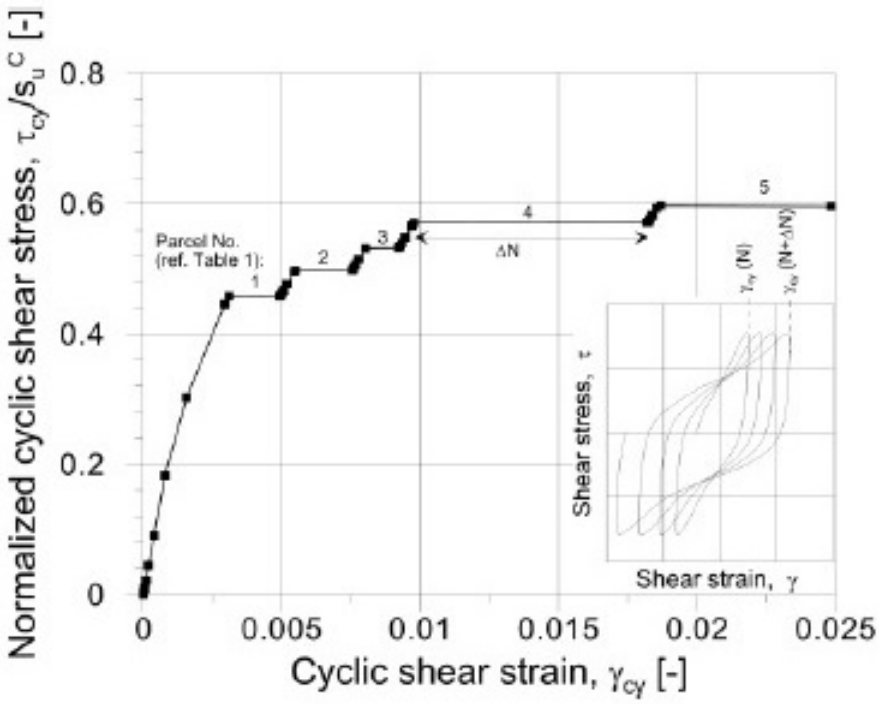

Figure 5.8: Stress-strain response (from Jostad et al. (2014))

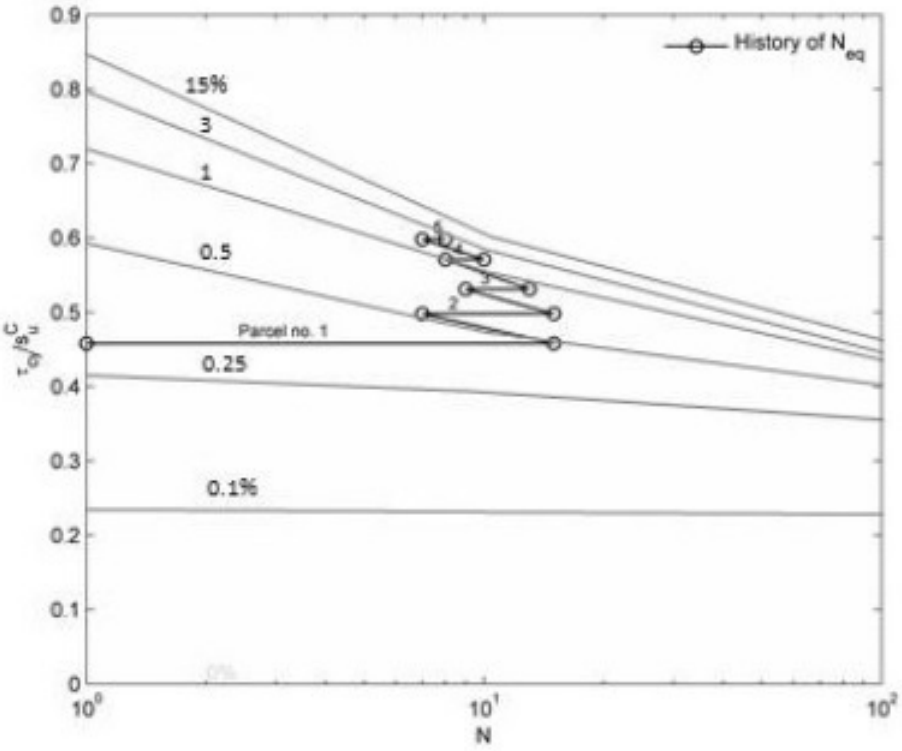

Figure 5.9: Calculation of N_{eq} (from Jostad et al. (2014))

5.5 High-Cycle Accumulation Model

This section gives a brief introduction to the High-Cycle Accumulation Model as presented in Niemunis et al. (2005). The model is based on an explicit formulation where time is replaced by the number of cycles, N. This formulation gives a framework which requires less computational time and gives a lower accumulation of numerical errors compared to implicit formulations. The model is suitable for sand and other granular soils.

Even though this model is considered explicit, it makes use of an implicit calculation for a first set of cycles. The strain amplitude is found in these steps and used for the explicit calculations. Since the strain amplitude can change during cycling, there is occasionally done a control cycle to update the strain amplitude. In addition, the control cycle is used to check whether the stress state violates the yield criteria.

When the strain amplitude is known, the explicit calculation can be done in order to describe the accumulation of the average strain with number of cycles. Niemunis et al. (2005) proposed the following equation for the rate of strain accumulation:

$$\underline{D}^{acc} = \underline{m}\, f_{ampl}\, \dot{f}_N\, f_p\, f_Y\, f_e\, f_\pi \tag{5.7}$$

The parameters f_{ampl}, $\dot{f}_N$, f_p, f_Y, f_e and f_π are functions relating different variables to the rate of strain accumulation, $\underline{D}^{acc}$. The function f_{ampl} gives the effect of the strain amplitude, ε^{ampl} and f_N relates to the number of cycles, N. f_e is relatet to void ratio, f_p to the average mean pressure, f_Y to the average stress ratio and f_π to the change of the polarization of the strain loop. All these functions are proposed in Niemunis et al. (2005).

$\underline{m}$ is a unit tensor which points in the direction of the accumulation in strain space. The unit tensor can according to Niemunis et al. (2005) be well approximated by the associated flow rule:

$$\underline{m} \sim -\frac{1}{3}(p - \frac{q^2}{M^2 p})\underline{1} + \frac{3}{M^2}\underline{T}^* \tag{5.8}$$

where M is the inclination of the critical state line in the p-q plot, $\underline{T}^*$ is the stress state and $\underline{1}$ is a 6×6 identity matrix.

The rate of strain accumulation, $\underline{D}^{acc}$, will produce the path of the accumulated average strain, ε^{av}, as shown in figure 5.10.

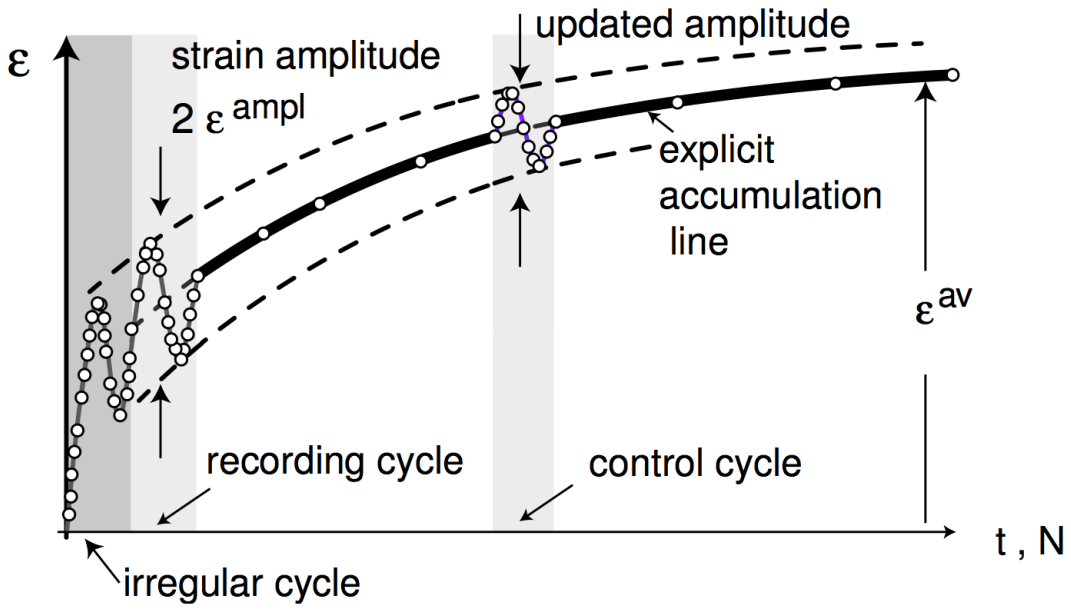

Figure 5.10: The basic idea of explicit calculation of the cumulative deformation (from Niemunis et al. (2005))

The rate of Cauchy stress ($\dot{\underline{T}}$) can be found from the following equation:

$$\dot{\underline{T}} = E : (\underline{D} - \underline{D}^{acc} - \underline{D}^{pl}) \tag{5.9}$$

where the plastic strain rate, D^{pl}, describes the plastic strain related to monotonic loading. The monotonic loading uses the Matsuoka and Nakai yield condition (Niemunis et al., 2005).

5.6 Stiffness Degradation Model

The Stiffness Degradation Model was proposed by Achmus et al. (2009) to describe the behavior of sand subjected to cyclic loading with purpose of analyzing pile–soil systems. The underlying concept is that the stiffness of the finite elements depends on the number of cycles, the stress state and the material parameters determined in cyclic triaxial tests.

Figure 5.11 shows typical results from stress-controlled cyclic triaxial tests under drained conditions. Results indicate an increase in plastic axial strain (ε_p^a) with the number of load cycles (N). The quantity of the plastic strain increase is mainly dependent on the initial stress state (confining stress) and on the magnitude of the cyclic load portion, similar to Andersen (2015).

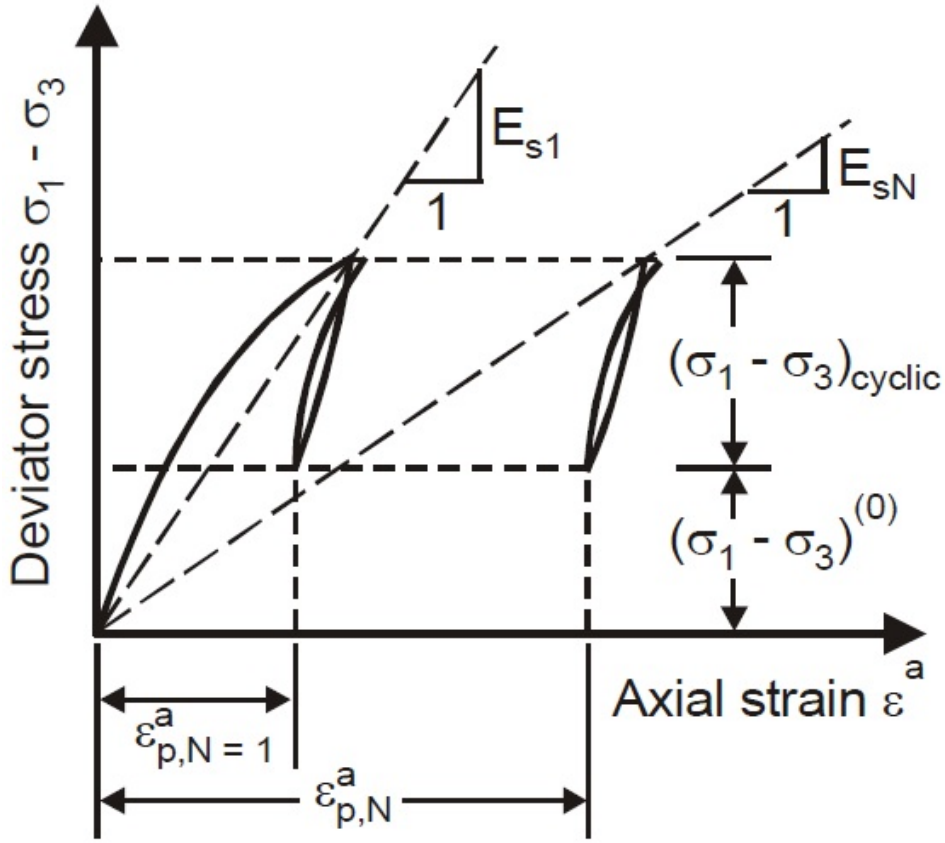

Figure 5.11: Cyclic behavior of sand in triaxial tests (from Achmus et al. (2009))

The increase in strain is interpreted as a decrease of the secant stiffness modulus (E_{sN}). If the elastic strain is negligible, the degradation of the secant stiffness modulus can be formulated in the following way:

$$\frac{E_{sN}}{E_{s1}} \cong \frac{\varepsilon^a_{p,N=1}}{\varepsilon^a_{p,N}} \tag{5.10}$$

Here, $\varepsilon^a_{p,N=1}$ and $\varepsilon^a_{p,N}$ are the plastic strains in the first and the N^{th} cycle respectively. E_{s1} is the secant stiffness modulus for N equals 1.

Huurman (1996) proposed a semi-empirical equation describing the development of plastic strains in a cyclic triaxial test. It is used in the stiffness degradation model and reads as follow:

$$\frac{E_{sN}}{E_{s1}} = \frac{\varepsilon^a_{p,N=1}}{\varepsilon^a_{p,N}} = N^{-b_1(X)^{b_2}} \tag{5.11}$$

where N is the number of cycles, X is the cyclic stress ratio, and b_i are regression parameters determined from triaxial tests. The cyclic stress ratio is defined as:

$$X = \frac{\sigma_{1,cyc}}{\sigma_{1,sf}} \tag{5.12}$$

where $\sigma_{1,sf}$ is the major principal stress at failure in a monotonic test and $\sigma_{1,cyc}$ is the major principal stress for the actual cyclic stress state. In other words, the stress ratio depends on the initial stress state (confining stress) and the cyclic loading.

Equation 5.11 and 5.12 were derived from triaxial tests with isotropic confining pressure and constant radial stress during the application of cyclic loading. In a pile–soil system, the initial stress condition is anisotropic. Additionally, the minor principal stress and the direction of the principal stresses change with the application of loads. Hence equation 5.11 and 5.12 are not valid. To overcome this problem, a characteristic cyclic stress ratio X_C is suggested by Achmus et al. (2009).

$$X_C = \frac{X^{(1)} - X^{(0)}}{1 - X^{(0)}} \tag{5.13}$$

where $X^{(1)}$ and $X^{(0)}$ represent the cyclic stress ratio in the loading and unloading phase respectively. X_C varies from 0 to 1 due to the denominator. The accumulation of plastic strain and the degradation of stiffness can be obtained from equation 5.11 by replacing X by X_C.

Chapter 6

Undrained Cyclic Clay Model

The idea of splitting external and internal forces into cyclic and average parts has been explored at NGI (Andersen, 2015). This has resulted in the finite element material model UDCAM presented in (Gustav Grimstad, 2012) and in section 5.4.

The material model presented in this paper is referred to as Undrained Cyclic Clay Model (UCCM). To represent the behavior of undrained clay, a coupling of an average model (UCCM-Average) and a cyclic model (UCCM-Cyclic) has been chosen, inspired by UDCAM. The reaction to the cyclic part of the loading is determined by UCCM-Cyclic, while UCCM-Average finds equilibrium between average external- and internal forces. An explicit formulation is chosen for UCCM-Cyclic where the cyclic loading is imposed as load parcels, as defined in section 3.3. This chapter presents the details of UCCM-Average and UCCM-Cyclic, and some important aspects of UCCM.

6.1 UCCM-Average

Both drained and undrained soil behavior can be described, based on effective stresses, however the undrained behavior may also be described in terms of total stresses. UCCM-Average is described in terms of total stresses and effective stresses are therefore unknown. One of the features is direct input of the undrained shear strength (S_u), which is readily obtained from laboratory tests. The first section presents UCCM-Average in a general 3D stress state. A presentation of the response in triaxial stress state and plane strain is also included.

UCCM-Average in 3D

A yield criterion, which is modified from the von-Mises yield criterion presented in section 2.5.1, is used in UCCM-Average. The criterion is isotropic and based on a single deviatoric strength, $2S_u$.

$$f = 0.5q - \kappa S_u \delta = 0 \tag{6.1}$$

S_u is the average of the undrained shear strength in triaxial compression- and extension testing, and herein referred to as the undrained shear strength.

$$S_u = \frac{S_u^C + S_u^E}{2} \tag{6.2}$$

The deviatoric stress invariant, q, is defined in section 2.1 and δ is a shear strength degradation parameter defined in section 6.2 due to cyclic loading. κ is an isotropic hardening parameter developed from Vermeer and De Borst (1984):

$$\kappa = \begin{cases} 2\frac{\sqrt{\gamma_a^p/\gamma_{a,f}^p}}{1+\gamma_a^p/\gamma_{a,f}^p}, & \gamma_a^p < \gamma_{a,f}^p \\ 1, & \gamma_a^p \geq \gamma_{a,f}^p \end{cases} \tag{6.3}$$

Here, $\gamma_a^p/\gamma_{a,f}^p$ is a deviatoric, plastic strain invariant indicating the degree of mobilization of the ultimate shear strength, S_u. If $\gamma_a^p/\gamma_{a,f}^p$ is equal to one, the shear strength is fully mobilized and further deviatoric loading leads to large plastic shear strains. γ_a^p and $\gamma_{a,f}^p$ are defined in equations 6.4 and 6.5 respectively.

$$\gamma_a^p = \frac{3}{2}\varepsilon_q^p \tag{6.4}$$
$$= \sqrt{\frac{1}{2}\left[(\varepsilon_{11}^p - \varepsilon_{22}^p)^2 + (\varepsilon_{22}^p - \varepsilon_{33}^p)^2 + (\varepsilon_{33}^p - \varepsilon_{11}^p)^2\right] + \frac{3}{4}\left[(\gamma_{12}^p)^2 + (\gamma_{23}^p)^2 + (\gamma_{31}^p)^2\right]}$$

$$\gamma_{a,f}^p = \frac{\gamma_{fC}^p + \gamma_{fE}^p}{2} \tag{6.5}$$

γ^p_{fC} and γ^p_{fE} are obtained from triaxial compression- and extension tests as the plastic shear strain when the maximum shear stress, S^C_u and S^E_u, is reached. An associated flow rule is chosen such that the principle of maximum plastic dissipation is fulfilled and thereby the increment in plastic strain is assured normal to the failure surface.

$$d\underline{\varepsilon}^p = d\lambda \frac{\partial F}{\partial \underline{\sigma}} \tag{6.6}$$

The internal response of the soil volume when subjected to cyclic forces is dependent on the average shear stress level of the cyclic loading (Andersen, 2015). A deviatoric shear stress from UCCM-Average is therefore input to UCCM-Cyclic, as illustrated in section 6.3, and defined as:

$$\tau_a = 0.5q \tag{6.7}$$

UCCM-Average in Triaxial Test with $\delta = 1$

In a triaxial test, no shear stresses are imposed directly ($\tau_{12} = \tau_{23} = \tau_{31} = 0$), but invoked through deviatoric compression or extension i.e. $\sigma_{11} \neq \sigma_{33}$. If the shear strength degradation parameter is equal to one, $\delta = 1$, equation 6.1 reduces to the following expression for the triaxial stress state:

$$f = \left| \frac{\sigma_{11} - \sigma_{33}}{2} \right| - \kappa S_u = 0 \tag{6.8}$$

The expected triaxial test results for normally consolidated Drammen Clay, and from simulations with UCCM-Average are illustrated in figure 6.1. The shear stress is normalized by the shear strength in compression S^C_u.

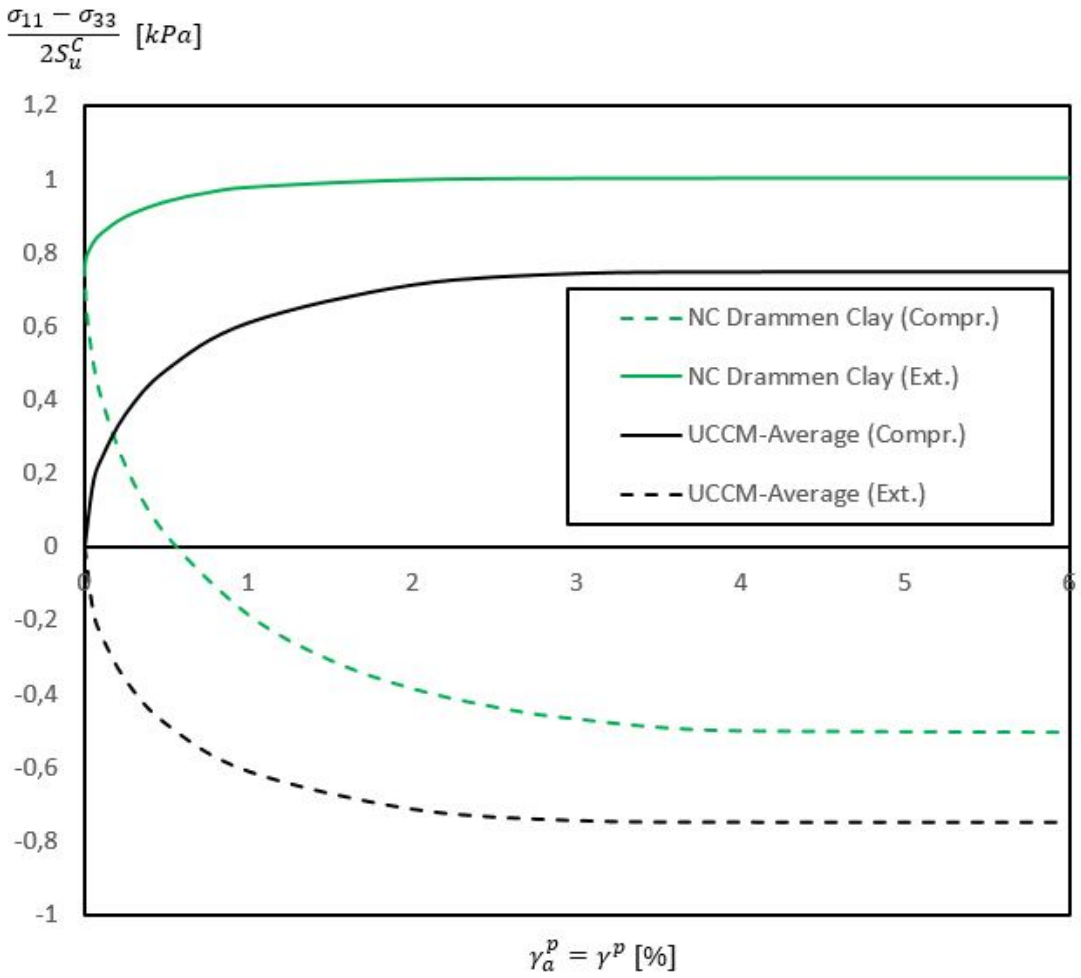

Figure 6.1: Expected hardening response for NC Drammen Clay and simulation results for UCCM-Average

Figure 6.1 illustrates how UCCM-Average tends to underestimate the shear strength in compression, and overestimate the capacity in extension.

UCCM-Average in Plane Strain with $\delta = 1$

The plane strain yield surface of UCCM-Average can be illustrated in a deviatoric plot as in figure 6.2 with $\delta = 1$. The yield surface can either be an ellipse or a circle depending on the second principle stress ($\sigma_2 = \sigma_{22}$). A plane strain state is subject to the following constraint:

$$d\varepsilon_{22} = d\varepsilon_{22}^e + d\varepsilon_{22}^p = 0 \tag{6.9}$$

If the undrained shear strength is fully mobilized, no further elastic strains can develop. A von Mises associated flow (section 2.5.2) and the plane strain constraint then leads to:

$$d\varepsilon_{22}^{e} = -d\varepsilon_{22}^{p} = 0 = \frac{\Delta\lambda}{2\sigma_{eq}}\left(2\sigma_{22} - \sigma_{11} - \sigma_{33}\right) \Rightarrow \sigma_{22} = \frac{\sigma_{11} + \sigma_{33}}{2} \tag{6.10}$$

The plane strain yield criterion can therefore be written in the following way, when the shear strength is fully mobilized ($\kappa = 1$):

$$f = \sqrt{\left(\frac{\sigma_{11} - \sigma_{33}}{2}\right)^2 + \tau_{13}^2} = \frac{2S_u^{2D}}{\sqrt{3}} = S_u^* \tag{6.11}$$

The resulting yield surface is illustrated in a deviatoric stress space in figure 6.2.

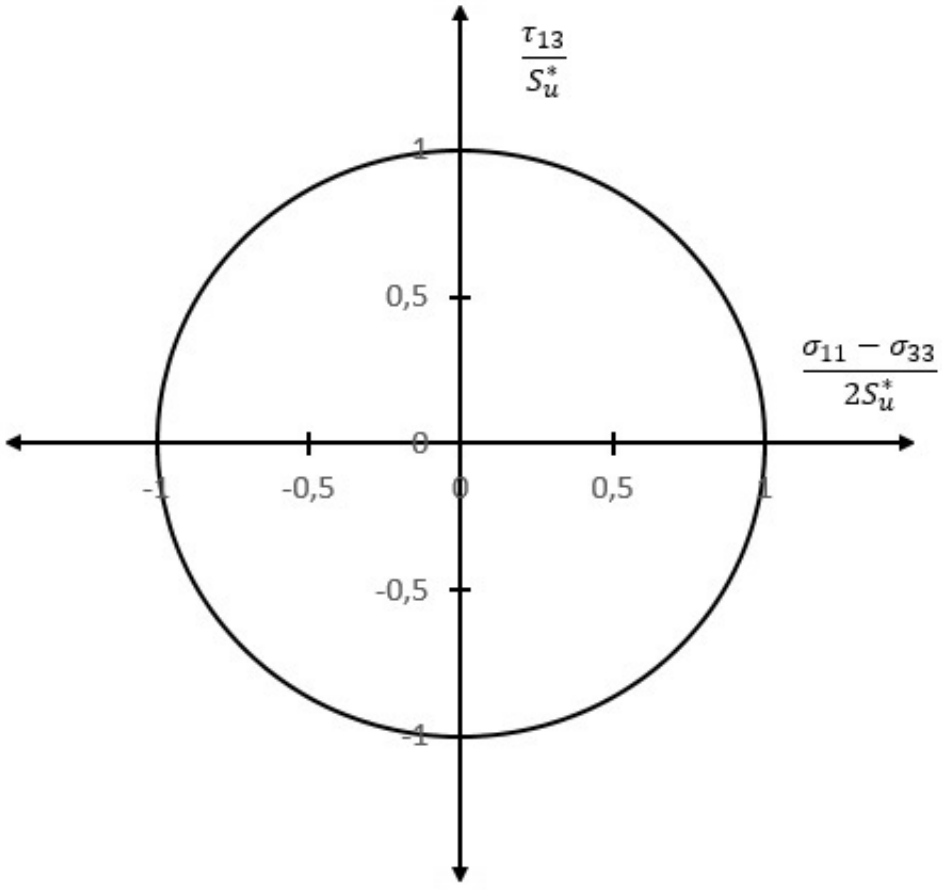

Figure 6.2: Yield surface of Average Model in plain strain

The failure shear strain (γ_f^p) is taken as the values obtained in triaxial testing according to equation 6.5. The deviatoric strength in $2D$ (S_u^{2D}) is defined as:

$$S_u^{2D} = \frac{\sqrt{3}}{2} S_u = \frac{\sqrt{3}\left(S_u^C + S_u^E\right)}{4} \tag{6.12}$$

Stress Integration Procedure

UCCM-Average is implemented as a user defined soil model in Plaxis (UDSM). An implicit stress integration scheme, explained in section 2.6, is used and presented in the following. The principle of the integration scheme is illustrated in figure 6.3.

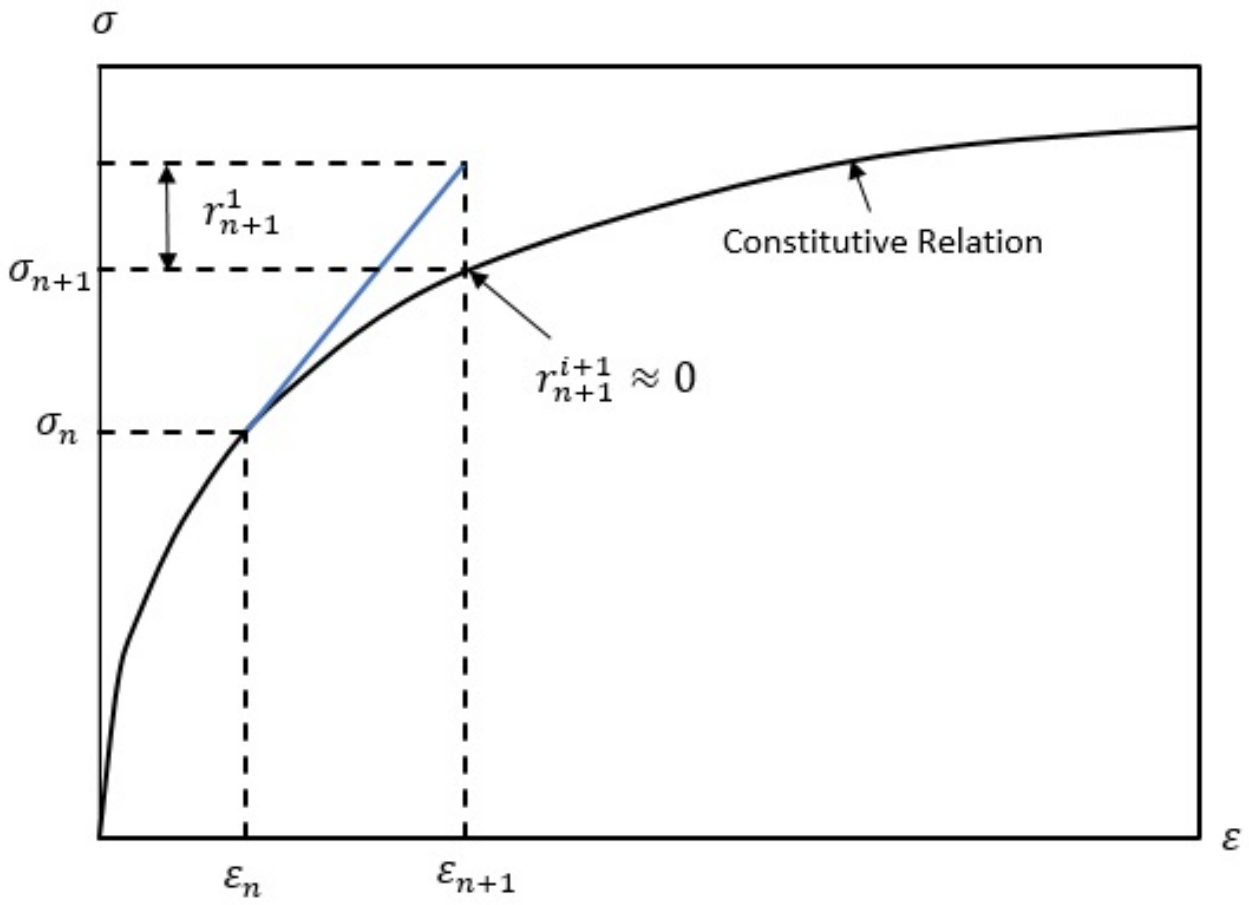

Figure 6.3: Principle of integration scheme

A residual vector for the current step $n+1$, $\underline{r}_{n+1}$, can be developed from the flow rule and the consistency condition as follows:

$$\underline{r}_{n+1} = \begin{bmatrix} \underline{r}_{1,n+1} \\ r_{2,n+1} \end{bmatrix} = \begin{bmatrix} \underline{\sigma}_{n+1} - \underline{\sigma}_n + \underline{\underline{D}}\left[\left\{\frac{\partial f}{\partial \underline{\sigma}}\right\}_{n+1}(\lambda_{n+1} - \lambda_n) - (\underline{\varepsilon}_{n+1} - \underline{\varepsilon}_n)\right] \\ f_{n+1} \end{bmatrix} = \underline{0} \quad (6.13)$$

Here $\underline{\underline{D}}$ is the stress independent elastic stiffness matrix and $\underline{\sigma}_{n+1}$ is the unknown stress at this step. f_{n+1} is the value of the yield function at the current step and $(\lambda_{n+1} - \lambda_n)$ is the unknown finite increment of the plastic multiplier. A vector with the unknown variables can be established as:

$$\underline{x}_{n+1} = \begin{bmatrix} \underline{\sigma}_{n+1} \\ \lambda_{n+1} \end{bmatrix} \quad (6.14)$$

The elastoplastic finite step is solved with a Newton-Raphson iteration method when $\underline{r}_{n+1} \approx \underline{0}$. This is achieved by setting a tolerance for the norm of $\underline{r}_{n+1}$ as described in section 2.6. The vector of unknowns, $\underline{x}_{n+1}$, which contains the current stress state and the updated plastic multiplier can be determined from equation 6.15.

$$\underline{r}^{i+1}_{n+1} \approx \underline{r}^{i}_{n+1} + \frac{\partial \underline{r}^{i}_{n+1}}{\partial \underline{x}^{i}_{n+1}} \Delta \underline{x}^{i}_{n+1} \approx \underline{0}$$

$$\Rightarrow \underline{x}^{i+1}_{n+1} = \underline{x}^{i}_{n+1} - \left\{\underline{\underline{J}}^{i}_{n+1}\right\}^{-1} \underline{r}^{i}_{n+1} = \underline{x}_{n+1} \quad (6.15)$$

The derivatives are as follows:

$$\frac{\partial \underline{r}_1}{\partial \underline{\sigma}_{n+1}} = \underline{\underline{1}} + \Delta\lambda \, \underline{\underline{D}} \left\{\frac{\partial^2 f}{\partial \underline{\sigma}^2}\right\}_{n+1} \quad (6.16)$$

$$\frac{\partial \underline{r}_1}{\partial \lambda_{n+1}} = \underline{\underline{D}} \left\{\frac{\partial f}{\partial \underline{\sigma}}\right\}_{n+1} \quad (6.17)$$

$$\frac{\partial r_2}{\partial \underline{\sigma}_{n+1}} = \left\{ \frac{\partial f}{\partial \underline{\sigma}} \right\}_{n+1} \tag{6.18}$$

$$\frac{\partial r_2}{\partial \lambda_{n+1}} = \frac{\partial f}{\partial \kappa} \frac{d\kappa}{d\gamma_a^p} \frac{d\gamma_a^p}{d\lambda} \tag{6.19}$$

where $\underline{\underline{1}}$ is a 6×6 identity matrix, and the full expressions for the derivatives are presented in appendix B.

6.2 UCCM-Cyclic

UCCM-Average obtains equilibrium between average external and internal forces in a FE calculation. In order to be in equilibrium with the cyclic external forces, a nonlinear elastic cyclic model is developed. The assumption of no volumetric changes during the cyclic event and a description based on total stresses is chosen. Isotropic contour diagrams define the material behavior in which the cyclic shear strain accumulation principle describes the degradation of cyclic shear stiffness and average shear strength (S_u) (see Andersen (2015) and section 4.5). This section presents UCCM-Cyclic, starting with the mathematical description of the isotropic contour diagrams. The degradation of cyclic shear stiffness and undrained shear strength in UCCM-Average (equation 6.1) is also described.

Mathematical Description of Contour Diagrams

As stated in section 4.4, a simple equation for the degradation of secant shear modulus is given by Idriss et al. (1978):

$$G_N = G_1 N^{-t} \tag{6.20}$$

G_1 is the shear modulus in the first stress-strain cycle, N is the number of harmonic loading cycles and t is a degradation parameter. The equation can be further developed, assuming the soil has an undrained residual strength- ($S_{u,\infty}$) and stiffness (G_∞). This leads to equation 6.21 and 6.22.

$$G_N = (G_1 - G_\infty)N^{-t} + G_\infty \tag{6.21}$$

$$\frac{\tau_{cy,N}}{\gamma_{cy,N}} = \left(\frac{\tau_{cy,1}}{\gamma_{cy,1}} - \frac{\tau_{cy,\infty}}{\gamma_{cy,\infty}}\right)N^{-t} + \frac{\tau_{cy,\infty}}{\gamma_{cy,\infty}} \tag{6.22}$$

where $\tau_{cy,\#}$ represents the cyclic shear stress during a specific number of cycles (#). In a N-τ_{cy} contour diagram, a constant γ_{cy} defines a continuous line which indicates the degradation of the material (see figure 4.11 and 4.21).

$$\gamma_{cy,N} = \gamma_{cy,1} = \gamma_{cy,\infty} = \gamma_{cy} \tag{6.23}$$

Normalizing with respect to the undrained shear strength, S_u, equation 6.22 can be expressed as:

$$\frac{\tau_{cy,N}}{S_u} = \frac{\tau_{cy,1}}{S_u}N^{-t} + \frac{\tau_{cy,\infty}}{S_u}(1 - N^{-t}) \tag{6.24}$$

Equation 6.24 describes the isotropic contour diagram used to calculate the internal response to external cyclic forces in UCCM-Cyclic. $\tau_{cy,\#}$ can be estimated from laboratory tests using a *maximum* cyclic shear stress, $\tau^{max}_{cy,\#}$, and a specific cyclic shear strain $\gamma_{cy,\#}$ as follows:

$$\tau_{cy,\#} = \tau^{max}_{cy,\#}\sqrt{\frac{\gamma_{cy}}{\gamma_{cy,\#} + \gamma_{cy}}} \tag{6.25}$$

γ_{cy} is a cyclic deviatoric strain invariant defined as:

$$\gamma_{cy} = \sqrt{3J_{2,\varepsilon}} \tag{6.26}$$

$$= \sqrt{\frac{1}{2}[(\varepsilon_{11} - \varepsilon_{22})^2 + (\varepsilon_{22} - \varepsilon_{33})^2 + (\varepsilon_{33} - \varepsilon_{11})^2] + \frac{3}{4}[(\gamma_{12})^2 + (\gamma_{23})^2 + (\gamma_{31})^2]}$$

Figure 6.4 illustrates results developed from contour diagrams in Gustav Grimstad (2012), for $\tau_a = 0$. The estimated values for equation 6.25 is included in the figure. The contour diagrams represent results from undrained cyclic triaxial tests on NC Drammen Clay. According to figure 6.4, an element subjected to $N = 10^3$ cycles with a cyclic shear stress of $\tau_{cy} = 0.23 S_u$ has a cyclic shear strain of $\gamma_{cy} = 1\%$. NC Drammen Clay parameters, for the first stress-strain cycle, can be estimated to: $\tau_{cy,1}^{max} = 0.67 S_u$ and $\gamma_{cy,1} = 0.9\%$. Parameters for a high number of cycles can be delimited to; $\tau_{cy,\infty}^{max} < 0.26 S_u$ and $\gamma_{cy,\infty} < 0.15\%$. $\tau_{cy,\infty}^{max}$ is further referred to as the cyclic fatigue shear strength and the authors believe the remolded undrained shear strength provides a conservative value for this parameter, $\tau_{cy,\infty}^{max} \geq S_{u,rem}$.

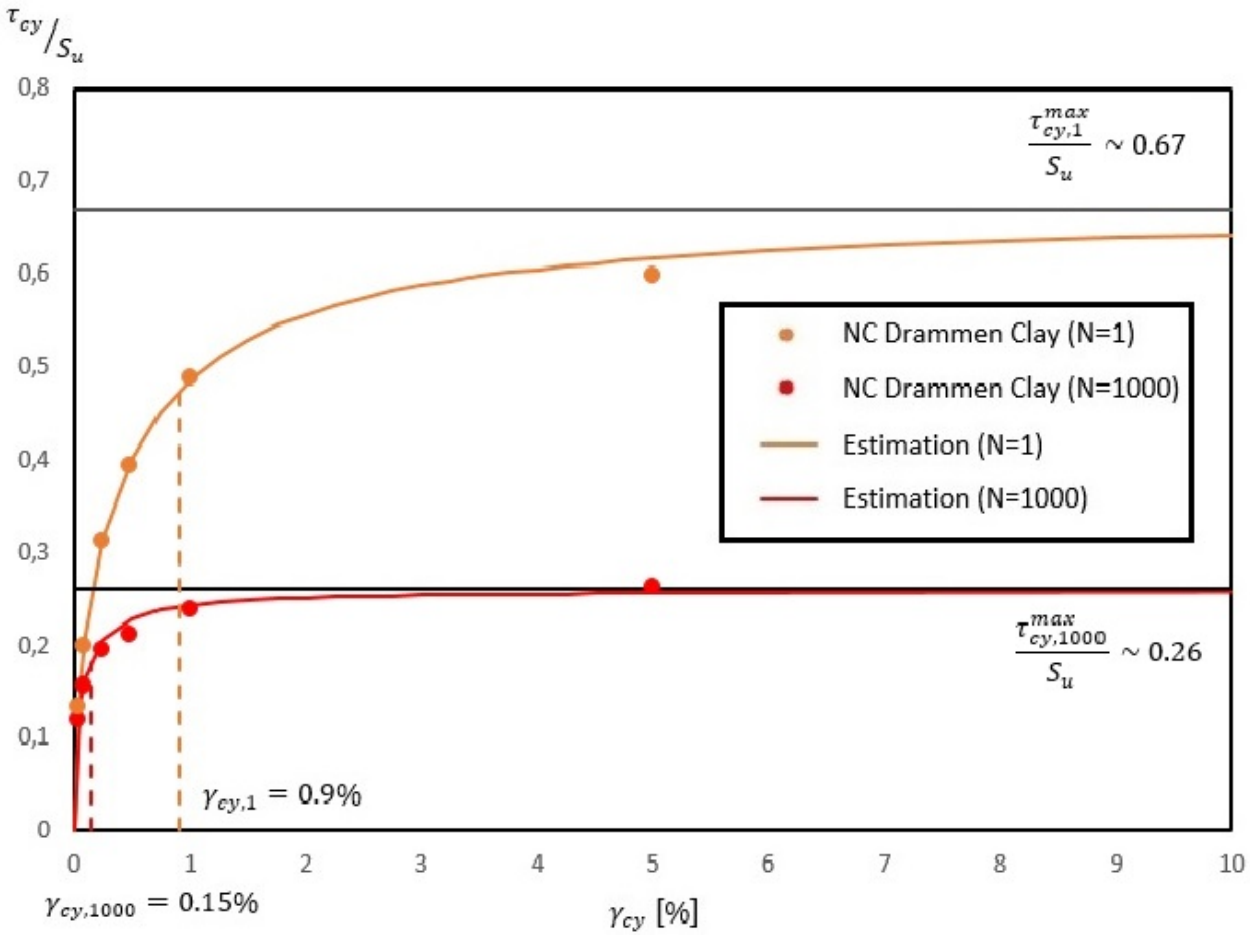

Figure 6.4: Estimation of $\tau_{cy,\#}^{max}$ and $\gamma_{cy,\#}$ for NC Drammen Clay

The cyclic response of clay is expected to depend on the average shear stress level (Andersen, 2015). The results presented in figure 6.4 are only valid for $\tau_a = 0$. A simplification of this dependency can be described by a constant, $\beta_\#$, with the same dependency to the cyclic shear strain as the cyclic shear stress:

$$\beta_\# = \frac{d\tau_{cy,\#}^{max}}{d\tau_a} \tag{6.27}$$

This leads to the final expression for the maximum cyclic shear stress:

$$\tau_{cy,\#}^{max} = \tau_{cy,\#}^{max}\Big|_{\tau_a=0} - \beta_\# \tau_a \tag{6.28}$$

τ_a represents the average shear stress level from UCCM-Average, presented in equation 6.7.

Degradation of Cyclic Shear Stiffness

The degradation of secant shear stiffness is regarded as equivalent to the decrease in cyclic shear strain for a constant cyclic shear stress. The mathematical expressions used to calculate the cyclic shear strain is closely connected to the concept of the StatusQuo-line presented in section 4.5. The equivalent number of load cycles at any stress state (γ_{cy}, τ_{cy}) is given as:

$$N_{eq} = \left(\frac{\tau_{cy,1} - \tau_{cy,\infty}}{\tau_{cy} - \tau_{cy,\infty}}\right)^{1/t} \tag{6.29}$$

where $\tau_{cy,\#}$ can be described by equation 6.25. The condition $\gamma_{cy} = \gamma_{cy,eq}^{intm}$ defines the StatusQuo-line introduced in section 4.5 and $\gamma_{cy} = \gamma_{cy,eq}^{n+1}$ defines the current equivalent number of cycles, N_{eq}^{n+1}. The index n refers to the parcel number defined in section 3.3. In a finite element analysis, $\gamma_{cy,eq}^{n+1}$ is input to the material model. Adding the intermediate equivalent number of cycles to the current change in number of cycles, yields the current equivalent number of cycles:

$$N_{eq}^{n+1} = N_{eq}^{intm} + \Delta N_{eq}^{n+1} \tag{6.30}$$

While both N_{eq}^{n+1} and N_{eq}^{intm} depend on the current cyclic shear stress, ΔN_{eq}^{n+1} is input to the material model. $\gamma_{cy,eq}^{intm}$ must be calculated according to the mathematical expressions for the contour diagrams and the cyclic shear strain accumulation principle:

$$\gamma_{cy,eq}^{intm} = \gamma_{cy,eq}^{n} + \Delta\gamma_{cy}^{inst}$$

$$\Delta\gamma_{cy}^{inst} = \gamma_{cy,\psi} - \gamma_{cy,\phi}$$

$\gamma_{cy,\phi}$ is known from the previous cyclic loading historie, while the expression for $\gamma_{cy,\psi}$ is developed from equation 6.25 as:

$$\gamma_{cy,\psi} = \frac{\gamma_{cy,1}}{\left(\frac{\tau_{cy,1}^{max}}{\tau_{cy}^{n+1}}\right)^2 - 1} \tag{6.31}$$

where τ_{cy}^{n+1} is the current cyclic shear stress defined by the contour diagrams. Finally, equation 6.30 is solved using an implicit Newton-Raphson iteration procedure. The residual function can be defined as:

$$r = N_{eq}^{n+1} - N_{eq}^{intm} - \Delta N_{eq}^{n+1} \tag{6.32}$$

The nonlinear elastic finite step is solved when $r \approx 0$. This is achieved by setting a tolerance for the norm of r as described in section 2.6

$$r_{i+1} = r_i + \left\{\frac{dr}{d\tau_{cy}^{n+1}}\right\}_i \Delta\tau_{cy}^{n+1} \approx 0 \tag{6.33}$$

where the index i is the iteration number. The derivatives are presented in appendix B and the current cyclic shear stress, τ_{cy}^{n+1}, can then be solved for using the following equation:

$$\tau_{cy}^{n+1} = \tau_{cy,i+1}^{n+1} = \tau_{cy,i}^{n+1} - \left\{\frac{dr}{d\tau_{cy}^{n+1}}\right\}_i^{-1} r_i \tag{6.34}$$

The secant, cyclic shear stiffness, G_{cy}^{n+1} is then defined as:

$$G_{cy}^{n+1} = \frac{\tau_{cy}^{n+1}}{\gamma_{cy,eq}^{n+1}} \tag{6.35}$$

Degradation of Maximum Average Shear Stress

The maximum average shear stress the material can sustain, when subjected to N number of loading cycles, is called $\tau_{a,N}^{max}$. This strength is assumed to decrease with increasing cyclic shear stress (τ_{cy}) and/or equivalent number of loading cycles (N_{eq}). The strength degradation parameter, δ, is input to UCCM-Average. UCCM-Cyclic uses the following expression to determine the degradation parameter:

$$\delta = \frac{\tau_{a,N}^{max}}{S_u} = 1 - \frac{d\tau_{a,N}^{max}}{d\tau_{cy,N}} \frac{\Delta\tau_{cy,N}}{S_u} = 1 - \alpha N_{eq}^{t} \frac{\tau_{cy,N}}{S_u} \tag{6.36}$$

α is a constant value defining the slope in the contour diagram for $N = 1$. N_{eq} is the equivalent number of cycles and t is the degradation parameter. A typical α-value for NC Drammen Clay in a DSS stress state is $\alpha = 0.375$.

The set of equations presented in this chapter define isotropic contour diagrams similar to figure 6.5. The details of the contour diagrams depend on the parameters $\tau_{cy,\#}^{max}\big|_{\tau_a=0}$, $\beta_\#$, α, $\gamma_{cy,\#}$ and t. The definition of β_1 and α can be seen in figure 6.5 and the isotropy is evident.

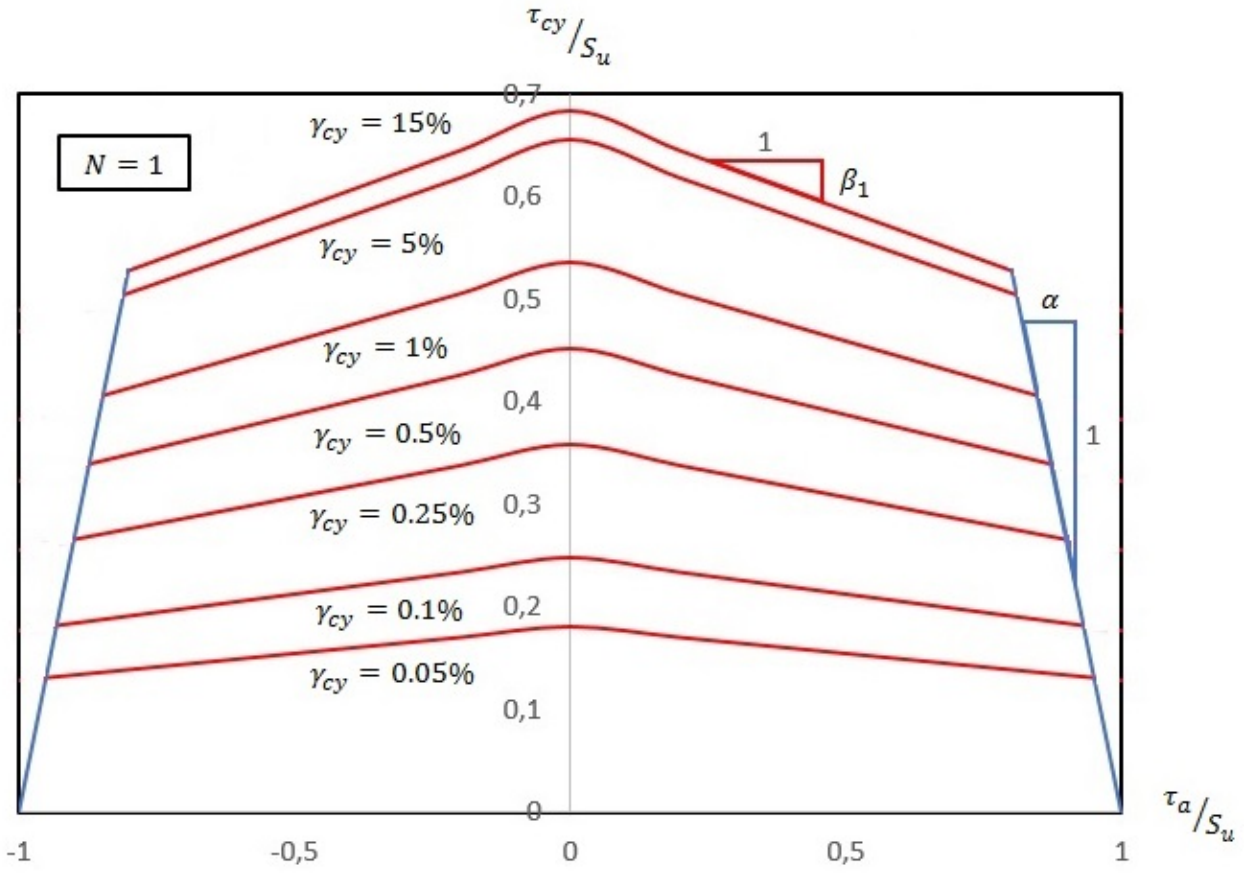

Figure 6.5: Typical contour diagram produced by UCCM

6.3 Aspects of UCCM

In order to use the model correctly, some important aspects must be considered. This section presents aspects of UCCM, including how calculations should be executed, how loads should be applied and the limitations of the material model.

Global Iteration

Plaxis works well for different *global* iteration schemes using the arc-length method as default. Most material models are implemented with the initial stiffness method (Brinkgreve et al., 2016). UCCM-Average uses a modified Newton-Raphson procedure to find global equilibrium between average internal and external forces. UCCM-Cyclic uses the initial stiffness method.

Calculation

Total Stresses
UCCM is defined in terms of total stress and cannot give information about effective stresses. For simplicity the model is implemented into drained settings in Plaxis. A calculation must therefore be executed as drained and the resulting effective stresses are, in reality, the undrained stresses. If an undrained calculation is executed, Plaxis will add a large bulk stiffness to the global stiffness matrix, and the calculation will be more time consuming.

Initial Phases
Due to the semi-explicit formulation of UCCCM, a Plaxis calculation must follow a certain setup. Two initial phases are needed, one for UCCM-Cyclic, and one for UCCM-Average. The weight of the soil is regarded as an average action and is considered in the average calculation only. An average initial phase is therefore needed to initialize the weight of the soil. In the cyclic initial phase, the soil weight is set equal to zero. The average initial phase must set the initial effective stress state in the material. The isotropic nature of UCCM requires a coefficient of earth pressure at rest equal to one ($K_0 = 1$) imposing no initial shear stresses in the soil volume.

Application of Loads
UCCM-Average has a linear elastic behavior in unloading. It is therefore recommended to impose average forces in ascending order. For most purposes, the average load component can be assumed constant throughout the calculation (Gustav Grimstad, 2012).

In UCCM-Cyclic, the cyclic loads are imposed as a number of loading cycles with a specific cyclic load magnitude, as opposed to specific displacement magnitude. This is referred to as a cyclic load *history* or a cyclic load parcel. A total cyclic load history normally contains several cyclic load parcels as seen in section 3.3. It is further assumed that the frequency of the cyclic loads are within the "cyclic" range ($\approx$ 0.1Hz) i.e. mass and damping considerations can be omitted. In UCCM-Cyclic, there are in principal three different cyclic load case scenarios:

Case:

1. Current cyclic load is higher than the previous, $F_{cy}^{n+1} > F_{cy}^{n}$
2. Current cyclic load is lower than the previous, $F_{cy}^{n+1} < F_{cy}^{n}$
3. Current cyclic load is much lower than the previous, $F_{cy}^{n+1} << F_{cy}^{n}$

It is generally recommended to apply cyclic loads in ascending order, i.e. load case 1. In this way the cyclic shear strain accumulation principle is used throughout the full calculation. This is regarded as the most severe total cyclic load history, giving a conservative design. For unloading, the cyclic shear strain accumulation principle is used to some degree, depending on the magnitude of the cyclic loading. If the magnitude of the cyclic loading is below a certain limit, the degradation will be negligible and the material will be linear elastic. This limit separates load case scenario 2 and 3, where 3 is linear elastic with no cyclic degradation.

Interaction Between UCCM-Average & UCCM-Cyclic

The two material models are mutually dependent and their interaction imposes certain restrictions on the setup of the calculation phases. As stated in section 6.2, δ is input to UCCM-Average and τ_a is input to UCCM-Cyclic. An iteration between average- and cyclic phases can be executed until two consecutive average- and cyclic phases obtain the same results. For practical purposes, it is chosen to only do two iterations on phase level and according to Gustav Grimstad (2012) this should be sufficient. Table 6.1 presents the information flow between UCCM-Average and UCCM-Cyclic for every integration point.

Parcel No.	Phase No.	Average/Cyclic	Applied Load	Input	Output
1	1	UCCM-Average	$F_{a,1}$	$\delta_0 = 1$	$\tau_{a,1}$
1	2	UCCM-Cyclic	$F_{cy,1}$	$\tau_{a,1}$	δ_1
1	3	UCCM-Average	$F_{a,1}$	δ_1	$\tau_{a,2}$
1	4	UCCM-Cyclic	$F_{cy,1}$	$\tau_{a,2}$	δ_2
2	5	UCCM-Average	$F_{a,2}$	δ_2	$\tau_{a,3}$
2	6	UCCM-Cyclic	$F_{cy,2}$	$\tau_{a,3}$	δ_3
2	7	UCCM-Average	$F_{a,2}$	δ_3	$\tau_{a,4}$
2	8	UCCM-Cyclic	$F_{cy,2}$	$\tau_{a,4}$	δ_4

Table 6.1: Interaction between UCCM-Average and UCCM-Cyclic

Applicability

UCCM is an isotropic model based on the mean value of active and passive parameters. Hence, it is first and foremost applicable for scenarios where active and passive stress states contribute equally to the equilibrium. It is therefore believed that symmetric boundary value problems can be solved satisfactorily. Bearing capacity and monopiles are examples of such symmetric problems, while special considerations are needed before modelling excavations and supporting sheet piles etc.

The concept of the NGI-ADP model was introduced in section 5.3. The model uses the undrained shear strength approach, similar to the UCCM-Average, and is assumed to represent the behavior of undrained clays in a precise way. Any deviation between the two models can be regarded as a limitation for the UCCM-Average model.

In a general 3D stress state, UCCM-Average overestimates the DSS shear strength compared to the default value used in NGI-ADP by 15%. In a plane strain stress state the DSS shear strength will coincide between NGI-ADP and UCCM-average as long as S_u^{2D} described in section 6.1 is used.

The isotropic contour diagrams define the material behavior when subjected to stress controlled loading cycles. Strain controlled loading cycles, above a certain magnitude, leads to faster degradation of shear strength and stiffness. The cyclic fatigue shear strength, $\tau_{cy,\infty}^{max}$, also tends to approach a lower value for strain controlled tests, as shown in figure 6.6. The current formulation of the UCCM-Cyclic model is therefore not applicable for strain controlled loading scenarios. Pile foundations is one type of design which often tends to show strain controlled behavior.

Strain controlled cycles can be regarded as stress controlled cycles where the cyclic shear stress changes for each stress-strain cycle (see figure 4.12). A solution to the limitation above, is therefore to utilize the cyclic shear strain accumulation principle to create the strain controlled behavior from stress controlled contour diagrams (Andersen, 2015). This feature is so far not incorporated in UCCM, but could readily be done.

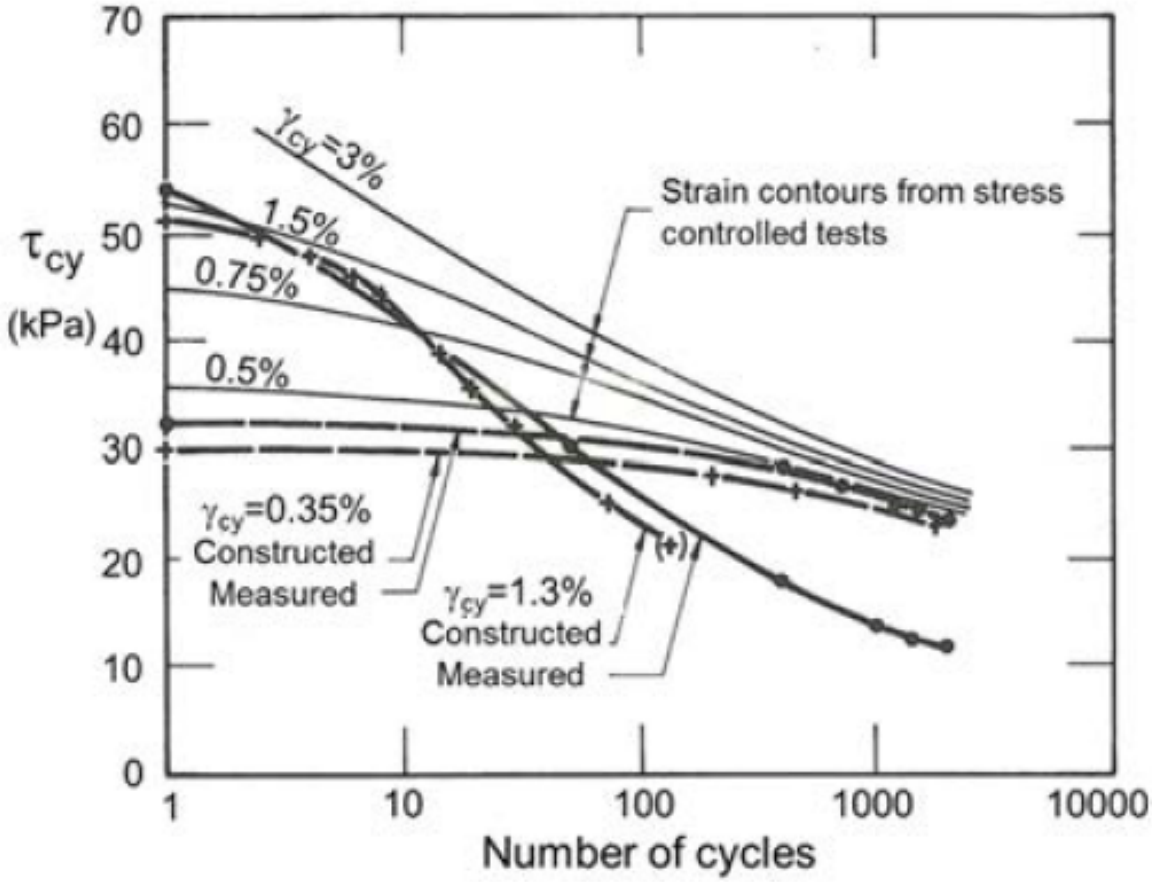

Figure 6.6: Results from strain-controlled cyclic tests plotted in diagram with strain contours from stress-controlled cyclic tests (from Andersen (2015))

Accumulation of Plastic Strains

UCCM consists of an elastic-plastic average model (UCCM-Average) and a non-linear elastic cyclic model (UCCM-Cyclic). Undrained cyclic loading above a specific magnitude is expected to lead to an accumulation of plastic shear strains. In UCCM, no explicit formulation of the plastic strain accumulation is included. The increase in plastic strains is implemented through the factor δ. A decrease in δ is equivalent to a decrease in maximum average shear stress. To still obtain equilibrium in the average phase, an increase in plastic strains must take place.

δ is therefore an important parameter for the estimation of accumulated plastic shear strains. The current formulation of the contour diagrams in UCCM-

Cyclic is expected to be able to represent the plastic strains developed in a DSS stress state (see figure 6.5). From laboratory results, the accumulation of plastic strains is faster in extension compared to compression. The model only seek to estimate the average plastic shear strains in these stress states (see figure 4.8).

Chapter 7

Simulation Results and Discussion

This chapter verifies and demonstrates the applicability of the Undrained Cyclic Clay Model (UCCM) in Plaxis. The first sections are individual verifications of the UCCM-Average and UCCM-Cyclic. This is demonstrated through the soil test facility in Plaxis. Results from a bearing capacity problem using UCCM-Average is included in addition to a cyclic DSS simulated with UCCM-Cyclic. Finally, the results from an analysis of a gravity base foundation with UCCM is presented.

7.1 Soil Tests

Plaxis provides the possibility of performing soil tests with all material models, either they are default or user defined. This feature is a convenient tool to calibrate a Plaxis material model to results from laboratory tests, field tests etc. It is also convenient to confirm that a UDSM works as expected. In this section, some results from Plaxis Soil Test are presented.

UCCM-Average

Soil test results for UCCM-Average are illustrated in figure 7.1 and 7.2. Input parameters and an overview of the tests are presented in table 7.1. Figure 7.1 illustrates the stress-strain response in a triaxial stress state and figure 7.2 presents the behavior in a DSS stress state. Results from soil tests using the Plaxis default material model, NGI-ADP, are included in the figures for direct comparison.

Input Parameters:
$S_u^C = 10$ kPa, $S_u^E = 4$ kPa, i.e. $S_u^{DSS} = 7$ kPa
$\gamma_f^C = 0.015$, $\gamma_f^E = 0.05$, i.e. $\gamma_f^{DSS} = 0.03$
$S_u = 7$ kPa, $\gamma_{a,f}^p = 0.03$

Type of Test	Soil Model	Curve
Triax. Compression	UCCM-Average	A
Triax. Compression	NGI-ADP	B
Triax. Extension	NGI-ADP	C
DSS	UCCM-Average	D
DSS	NGI-ADP	E

Table 7.1: Summary of soil tests UCCM-Average and NGI-ADP

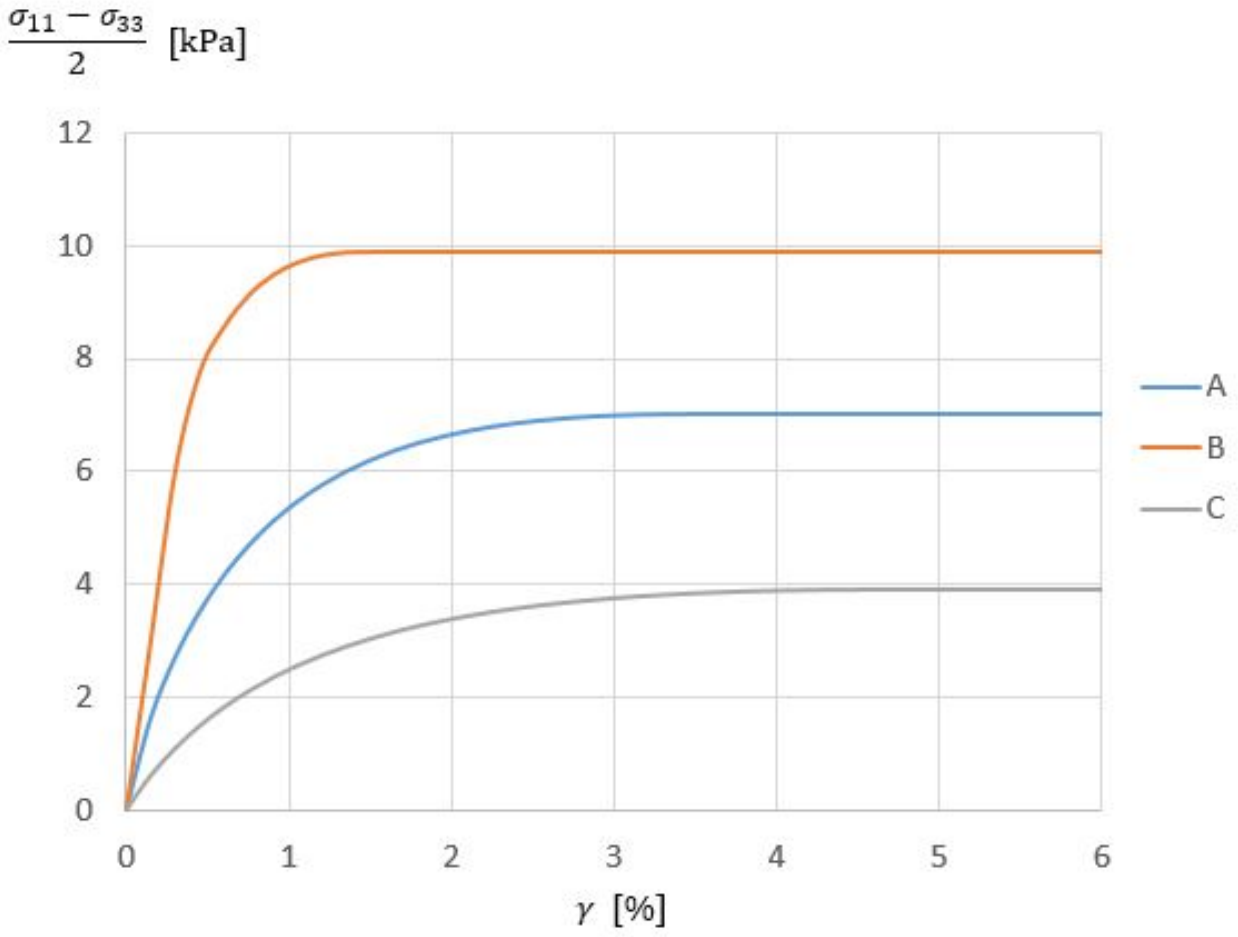

Figure 7.1: Triaxial test results UCCM-Average and NGI-ADP

In a triaxial stress state, UCCM-Average represents the mean response between the compression- and extension behavior defined by the NGI-ADP model, as seen in figure 7.1. The undrained shear strength of UCCM-Average is fully mobilized at an intermediate shear strain, as expected.

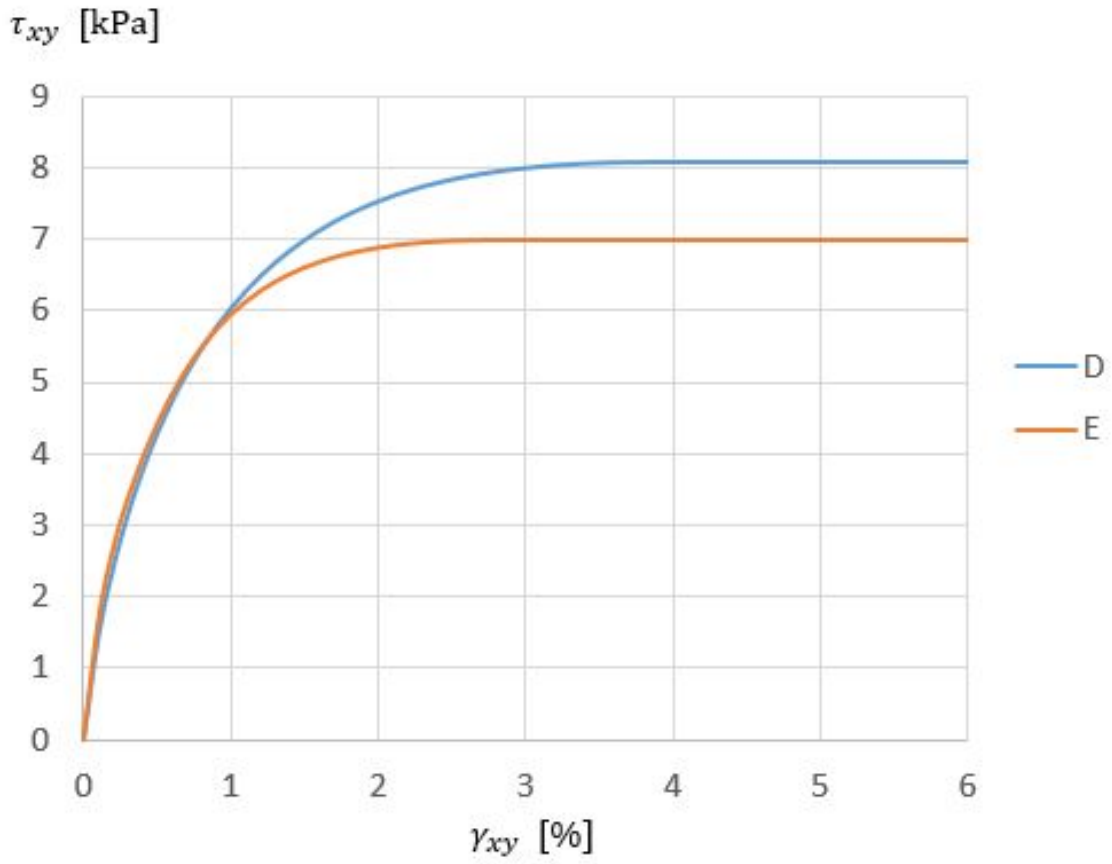

Figure 7.2: Direct Simple Shear test results UCCM-Average and NGI-ADP

Figure 7.2 illustrates the tendency of UCCM-Average to overestimate the DSS undrained shear strength in the general $3D$ formulation.

UCCM-Cyclic

Different soil tests have been simulated with UCCM-Cyclic. An overview of the soil tests are summarized in table 7.2. Figure 7.3 and 7.4 display the cyclic shear strain when subjected to a number of cycles (ΔN_{eq}) with specific cyclic shear stress (τ_{cy}).

Input Parameters:
$S_u = 10$ kPa, $t = 0.29$
$\tau_{cy,1}^{max} = 7$ kPa, $\tau_{cy,\infty}^{max} = 2$ kPa
$\gamma_{cy,1} = 0.9\%$, $\gamma_{cy,\infty} = 0.1\%$
$\beta_1 = 0.4$, $\beta_\infty = 0.2$

Type of Test	ΔN_{eq}	τ_a [kPa]	Curve
Triax	1	0	A
Triax	1	3	B
Triax	10^6	0	C
Triax	10^6	3	D
DSS	1	0	E
DSS	1	3	F
DSS	10^6	0	G
DSS	10^6	3	H

Table 7.2: Overview of soil tests with UCCM-Cyclic

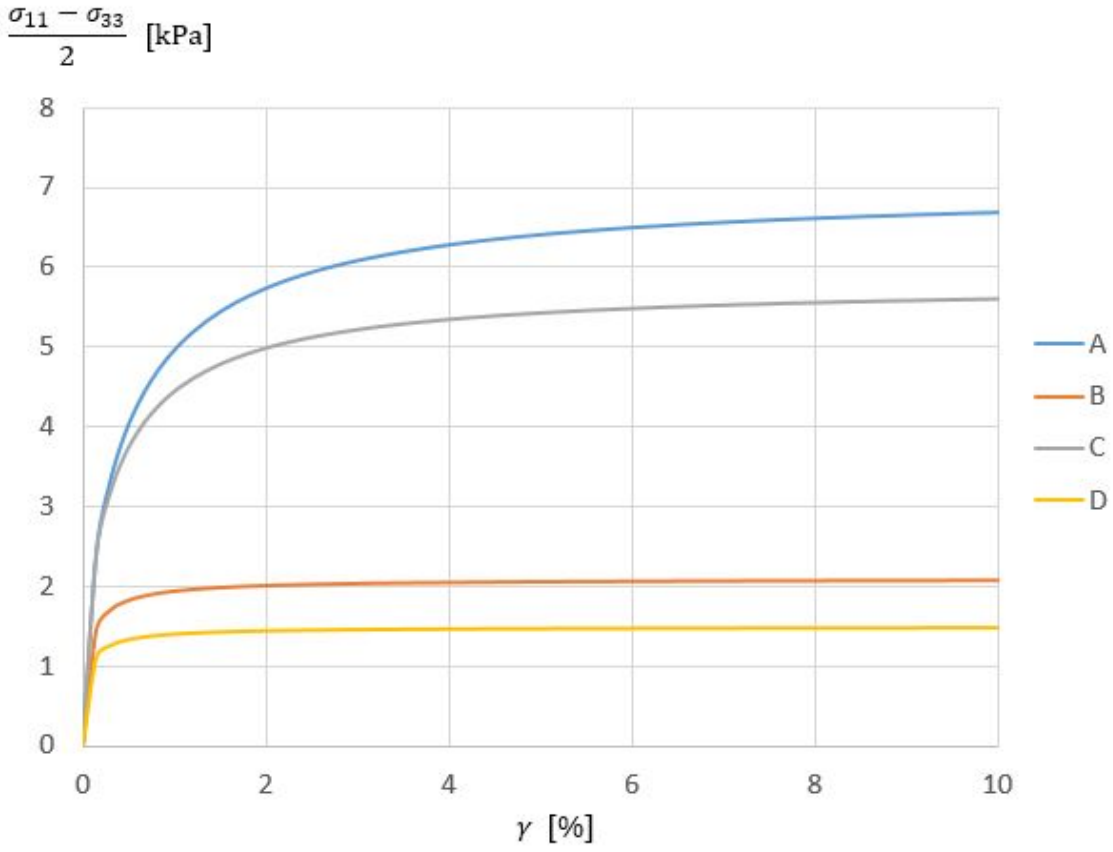

Figure 7.3: Cyclic triaxial test results with UCCM-Cyclic

The expected cyclic response according to figure 6.4 is illustrated in figure 7.3. The maximum cyclic shear stress is lower for a nonzero average shear stress, as the intention of the model formulation is to represent the mean response between triaxial compression- and extension stress states. The difference in maximum cyclic shear stress with respect to the average shear stress is controlled by the input parameters, $\beta_{\#}$.

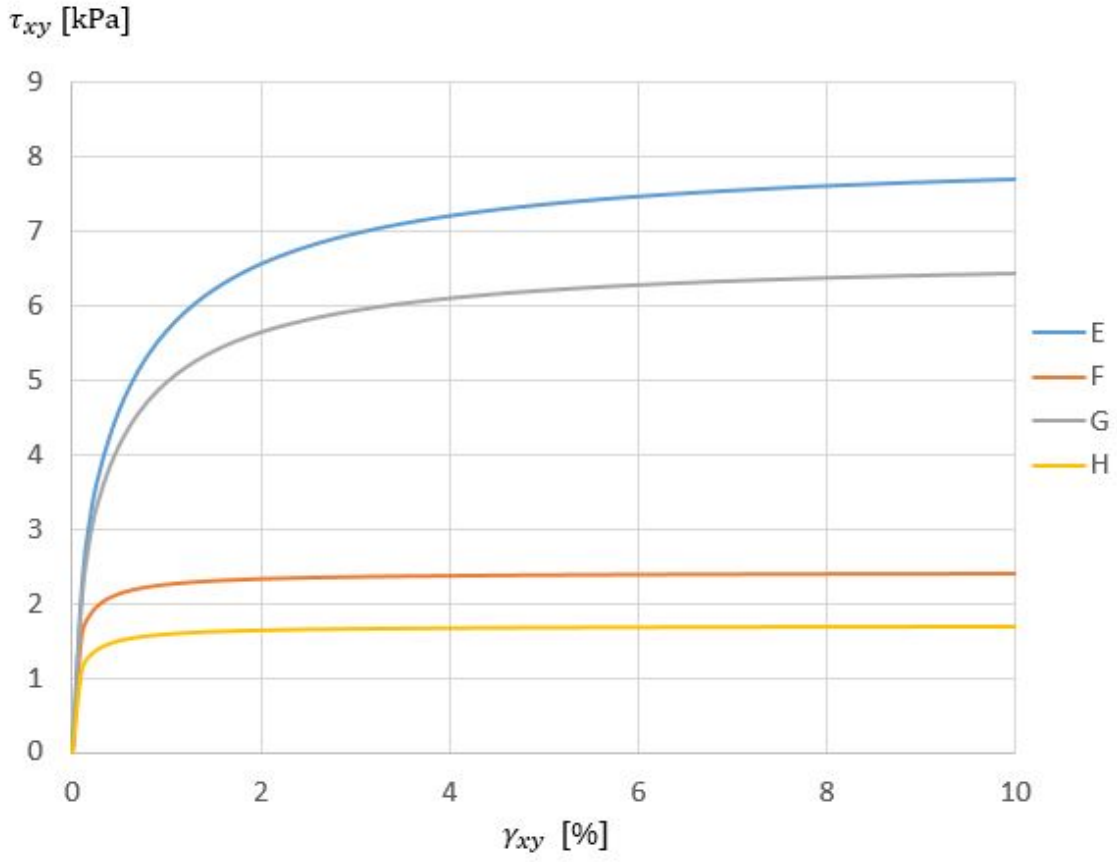

Figure 7.4: Cyclic Direct Simple Shear test results with UCCM-Cyclic

The maximum cyclic shear stress in a DSS type is more than the specified value. This is due to the von-Mises type formulation of the cyclic shear strain invariant. One can expect a DSS shear strength of $\frac{2}{\sqrt{3}}$ times the average shear strength in a triaxial stress state.

7.2 Bearing Capacity UCCM-Average

A bearing capacity model made in Plaxis 2D is used to check the behavior of UCCM-Average. The same model has been calculated with the use of NGI-ADP in order to verify the results.

UCCM-Average Input Parameters:
$S_u = 8,66$ kPa
$\gamma^p_{a,f} = 0.0203$
$G = 1500$ kPa
NGI-ADP Input Parameters:
$S^C_u = 15$ kPa, $S^E_u = 5$ kPa, $S^{DSS}_u = 10$ kPa
$\gamma_{fC} = 2.2\%$, $\gamma_{fE} = 3.2\%$, $\gamma_{fDSS} = 2.47\%$
$G = 1500$ kPa

Table 7.3: Input parameters for UCCM-Average and NGI-ADP

The parameters presented in table 7.3 are chosen to give similar bearing capacity for the two models. The calculations illustrate a similar failure surface for both models and the result from UCCM-Average is illustrated in figure 7.5.

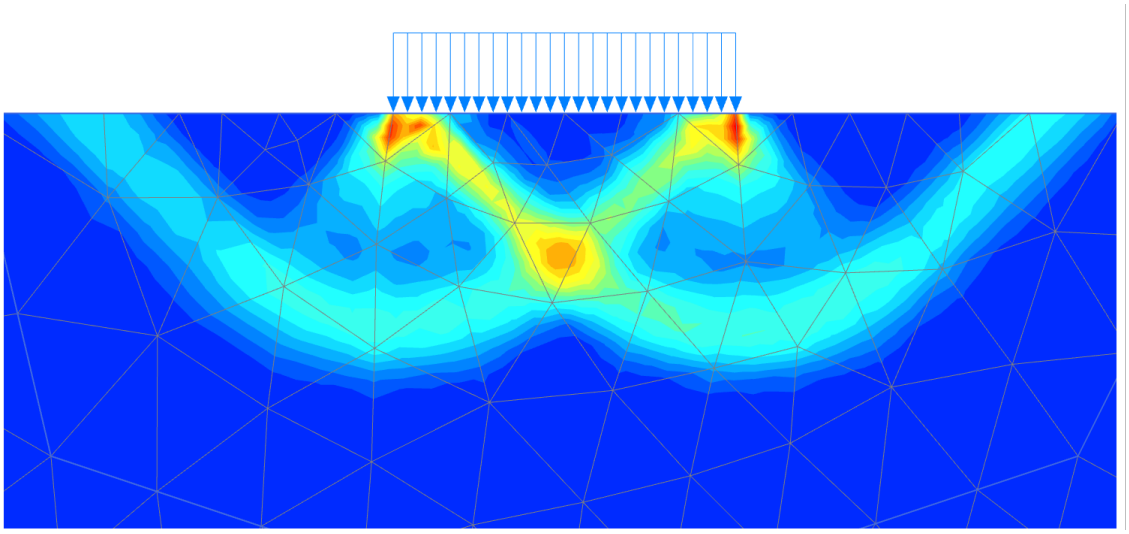

Figure 7.5: Shear strain at failure with UCCM-Average

A visualization of the shear stress, on the other hand, reveals two different shapes of stress distribution through the ground, as shown in figure 7.6 and 7.7. This can be due to the difference in shear strain at failure for Active, Passive and DSS stress states for NGI-ADP. This leads to a faster mobilization of the active strength compared to passive and DSS. Because of the strain compatibility, most of the stress is distributed to active soil elements right under the foundation. For UCCM-Average the shear strain until full mobilization is equal for all stress states, i.e. isotropic mobilization. The stress will therefore be equally distributed both vertically and horizontally.

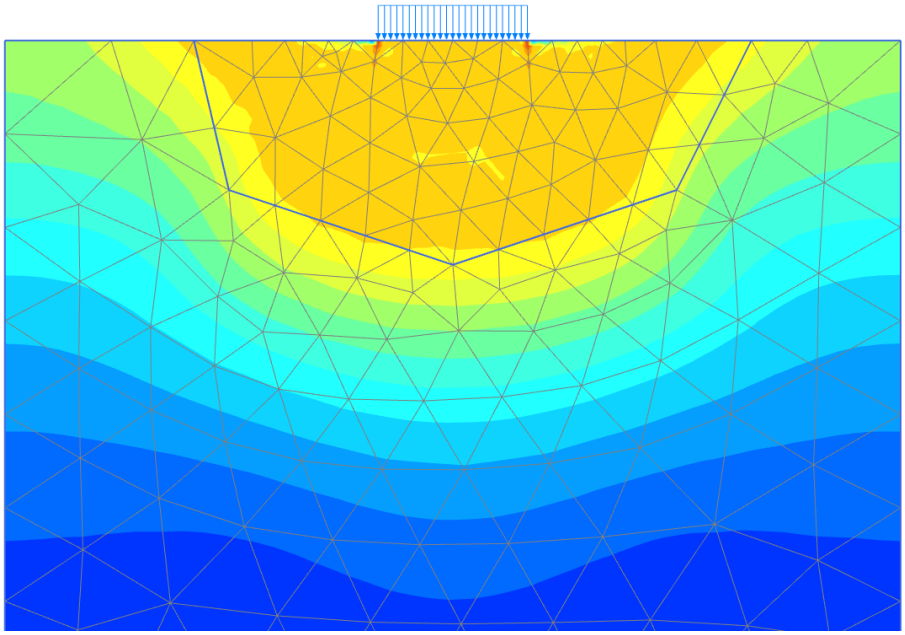

Figure 7.6: Shear stress distribution at failure UCCM-Average.

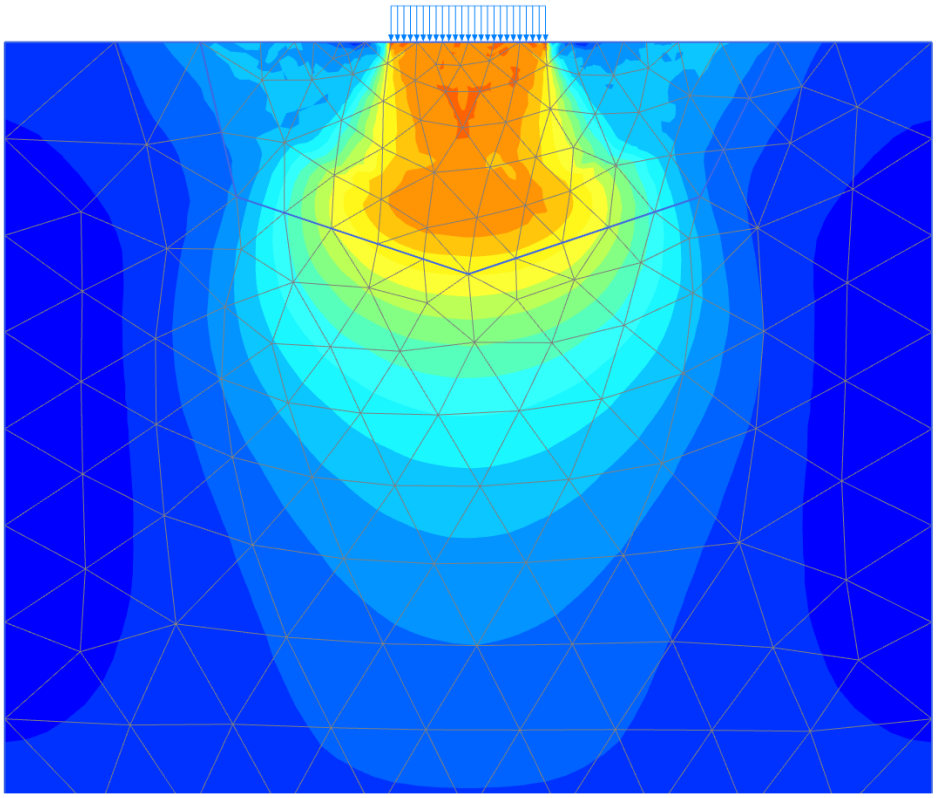

Figure 7.7: Shear stress distribution at failure NGI-ADP.

A load-strain curve for a node in a passive stress state at the failure surface is shown in figure 7.8. By using S_u^{2D} from section 6.1, a satisfying bearing capacity for UCCM-Average compared to NGI-ADP is achieved.

Figure 7.8 shows a difference in development of strains for the two models. This is likely due to the mobilization of the active shear strength at low shear strains. The strain is only expected to show the same behavior for a DSS stress state due to the difference in mobilization between the models.

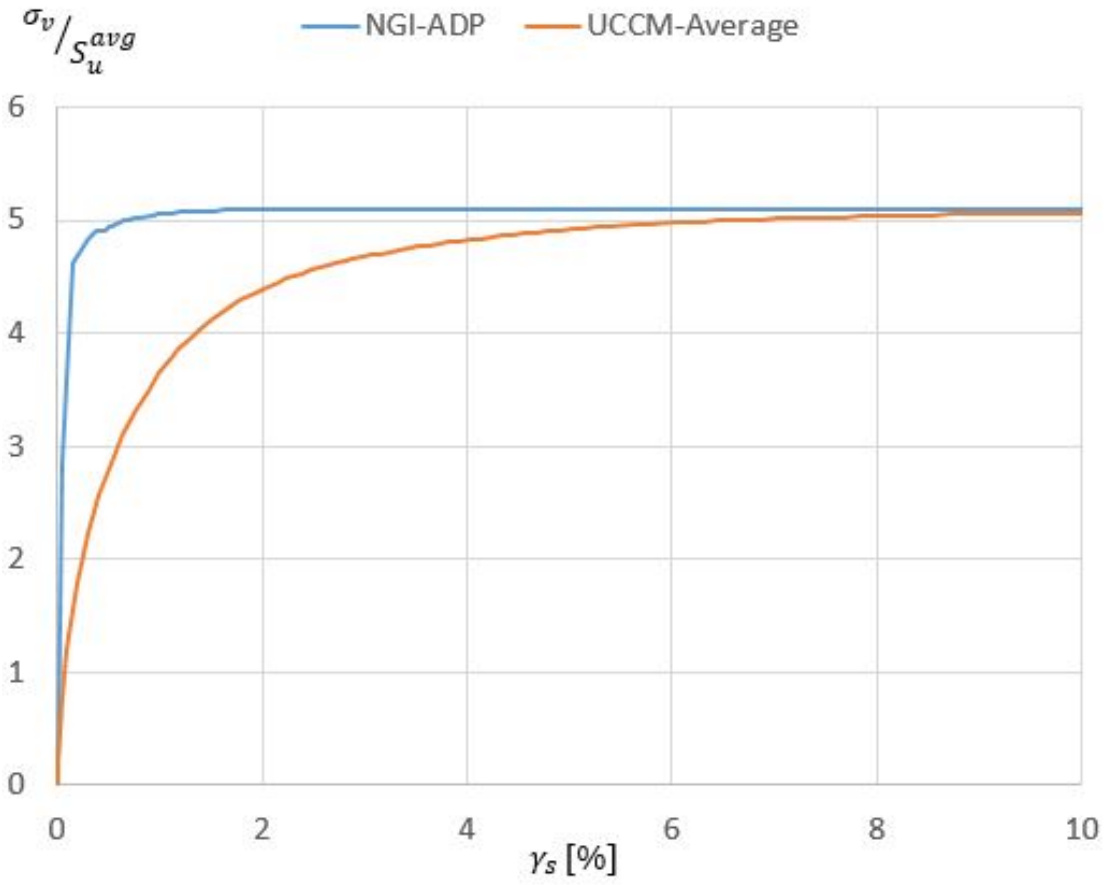

Figure 7.8: Load versus shear strain at failure surface

The results from the bearing capacity test seem to give satisfying behavior for UCCM-Average. The simulation fails at a loading equal to 51,55 kPa which is close to the theoretical value:

$$\sigma_v = 5.14 S_u^{avg} = 5.14 S_u^{2D} \frac{2}{\sqrt{3}} = 51.4 kPa \tag{7.1}$$

7.3 Direct Simple Shear Test UCCM

A DSS test with multiple calculation phases was constructed in Plaxis in order to check the behavior of UCCM compared to the soil model UDCAM, introduced in section 5.4. The geometry, input values and simulation results for UDCAM are found in Gustav Grimstad (2012). Input parameters and simulation results

for UCCM, with the same geometry and cyclic load history, are presented in table 7.4. The input parameters are deduced from DSS contour diagrams for NC Drammen Clay presented in Gustav Grimstad (2012).

UCCM-Average Input Parameters:

$$S_u = 6, \text{kPa}$$
$$\gamma^p_{a,f} = 0.04$$
$$G = 1500 \text{ kPa}$$

UCCM-Cyclic Input Parameters:

$$S_u^C = 10 \text{ kPa } S_u^{DSS} = 7 \text{ kPa } S_u = 6 \text{ kPa}, \; t = 0.29$$
$$\tau^{max}_{cy,1} = 7.9 \text{ kPa}, \; \tau^{max}_{cy,\infty} = 2.9 \text{ kPa}$$
$$\gamma_{cy,1} = 0.5\%, \; \gamma_{cy,\infty} = 0.08\%$$
$$\beta_1 = 0.15, \; \beta_\infty = 0$$

Table 7.4: Input parameters used in the DSS tests

Cyclic Coupling

The first DSS test was done with no average shear stress, and essentially the test is used to check the interaction between multiple cyclic phases. The load history and resulting equivalent number of cycles is shown in table 7.5.

Parcel	ΔN_{eq}	τ_{cy} [kPa]	N_{eq}^{UCCM}	N_{eq}^{UDCAM}
1	14	4.58	14	14
2	8	4.98	15	15
3	4	5.31	13	13
4	2	5.71	10	10
5	1	5.98	8	8

Table 7.5: Load history and simulation results from DSS test with UCCM and UDCAM

Results from the UCCM simulation show similar behavior as predicted by UDCAM. The final number of equivalent cycles, N_{eq}, is the same as UDCAM, and the final shear strain corresponds well (see figure 7.9). The stress-strain curve

from the UCCM simulation, shows a softer behavior in the start of the calculation and a stiffer behavior towards the end. The difference in behavior may be related to the formulation of UCCM.

The behavior of UDCAM depends on laboratory results organized in contour diagrams and the interpolation function defining the behavior for intermediate stress states. The contour diagrams are presented in Gustav Grimstad (2012) and are defined for $N = 1$, $N = 10$, $N = 100$ and $N = 1000$ number of cycles. The difference between the results for number of cycles greater than 10, may also be related to the interpolation between the two relatively nonadjacent contour diagrams, $N = 10$ and $N = 100$. UCCM predicts a higher final strain compared to the in-house NGI program Accumul which predicts a final strain of 2.3% (Gustav Grimstad, 2012).

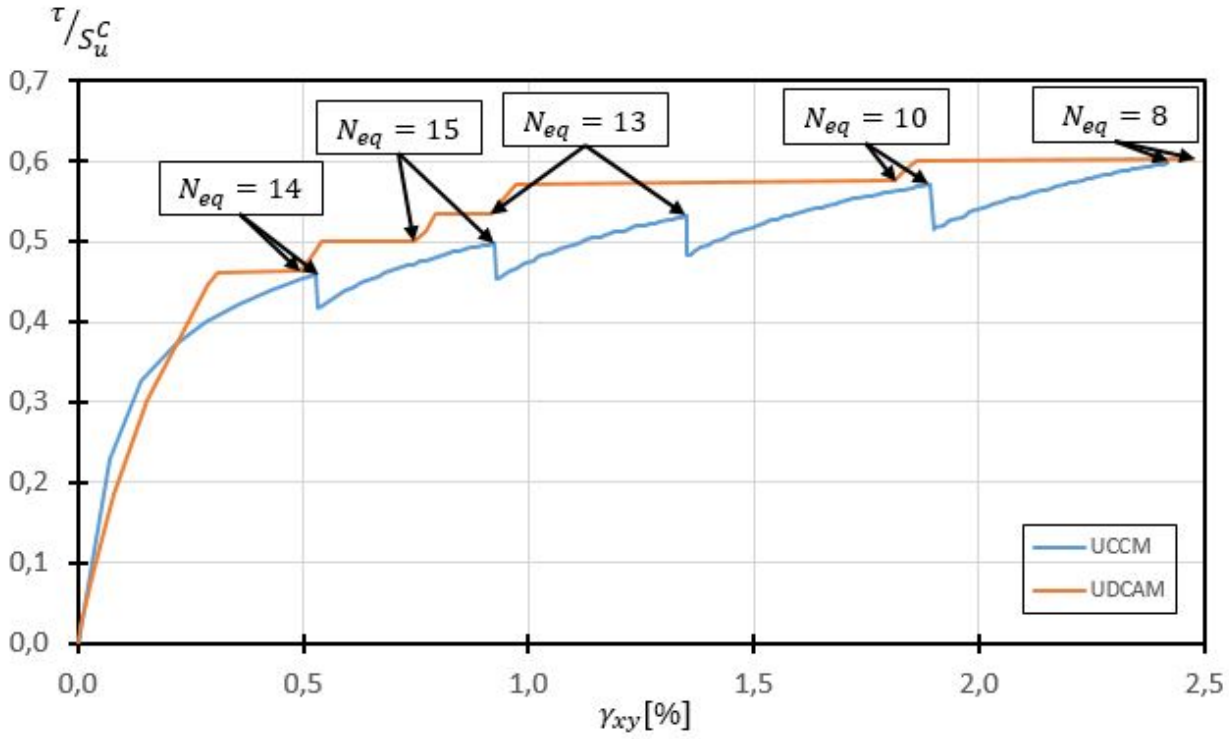

Figure 7.9: Stress-strain response for cyclic DSS simulation with UCCM

Average-Cyclic Coupling

A DSS test including nonzero average load was simulated with UCCM. The loading history and resulting N_{eq} is presented in table 7.6. The results achieved will

give some indication of how well the interaction between UCCM-Average and UCCM-Cyclic is working.

Input Parameters:

$S_u^C = 10$ kPa $S_u^{DSS} = 7$ kPa $S_u = 6$ kPa, $t = 0.29$
$\tau_{cy,1}^{max} = 7.9$ kPa, $\tau_{cy,\infty}^{max} = 2.9$ kPa
$\gamma_{cy,1} = 0.5\%$, $\gamma_{cy,\infty} = 0.08\%$
$\beta_1 = 0.15$, $\beta_\infty = 0$

Parcel	ΔN_{eq}	τ_{cy} [kPa]	τ_{av} [kPa]	N_{eq}
1	10	3	2	10
2	5	4	2	7
3	15	5	2	17

Table 7.6: Overview and simulation results from DSS test with UCCM with average loading

The results from the test i presented in figure 7.10. It can been seen that the cyclic phase is degrading the average material strength leading to development of strains. It can be concluded that the interaction seem to work satisfying.

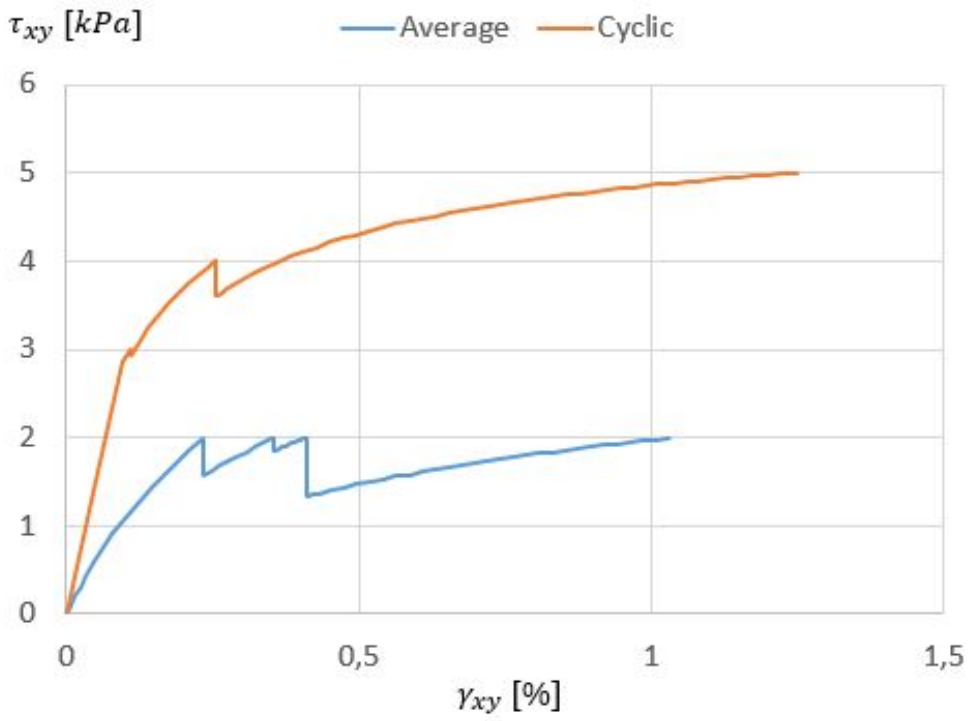

Figure 7.10: Stress-strain response for cyclic DSS simulation with UCCM

7.4 Gravity Base Foundation UCCM

A plane strain simulation of a gravity base foundation is used to further test the interaction between UCCM-Average and UCCM-Cyclic. The FE geometry is inspired by GBS model tests performed at NGI (see figure 7.11). The GBS model tests were subjected to cyclic and static actions representing an offshore environment (Dyvik et al., 1989). A FE analysis for direct comparison with the GBS model tests was reported by Gustav Grimstad (2012). The details of the plane strain geometry, used in the UCCM simulation, are summarized in table 7.7. The weight of the platform is modelled as a line load applied at the bottom of the GBS foundation as seen in figure 7.11. The frame of weightless and stiff plates are used to represent the gravity base structure.

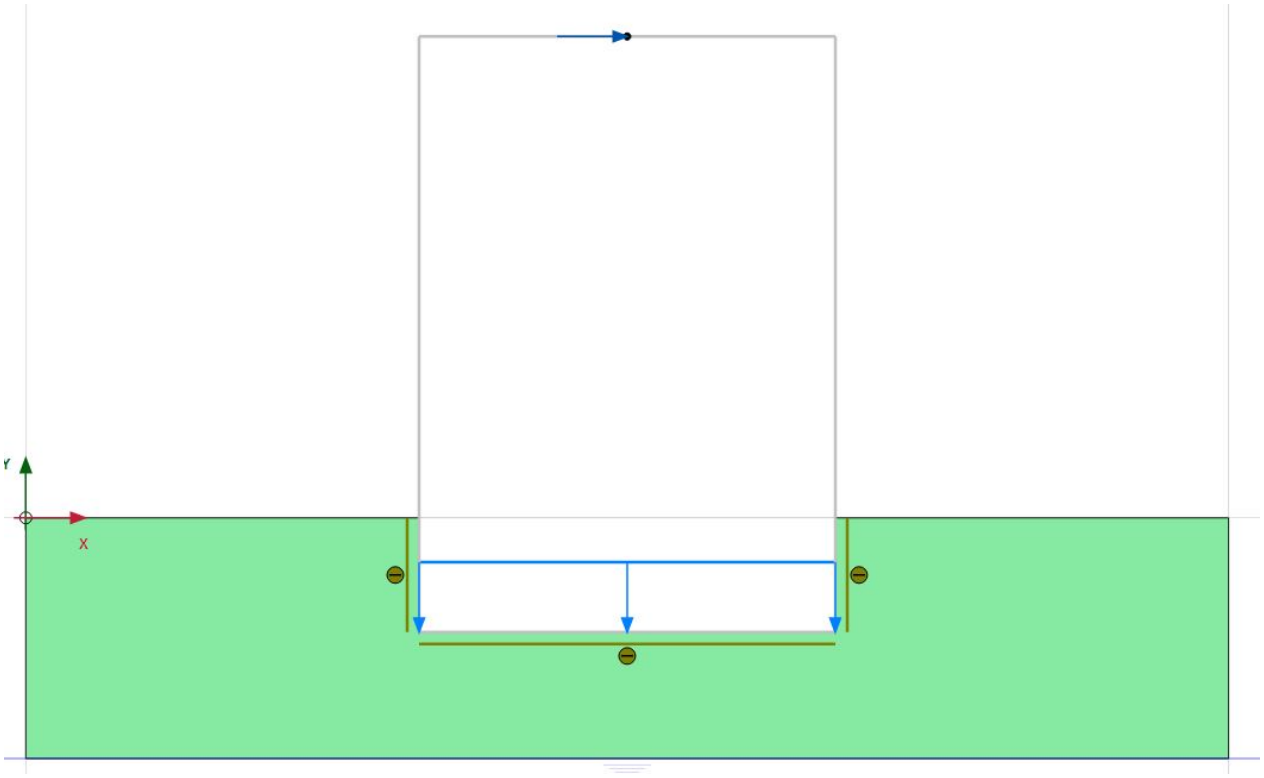

Figure 7.11: Finite element model for GBS simulation

Geometry:	
Foundation width (D):	0.346 [m]
Foundation height (H):	0.095 [m]
Depth of model (h):	0.2 [m]
Width of model (b):	1.0 [m]
Load point to surface (a):	0.4 [m]
Weight, line load (w):	22.44 [kPa]

Table 7.7: Geometry and weight used in the simulation of the GBS model test with UCCM

Static Test

The first test of the GBS design is a static test where a horizontal static load is applied at the top of the model (see figur 7.11). The input parameters of UCCM-Average are summarized in table 7.8.

UCCM-Average Input Parameters:
$S_u = 6.67$ kPa
$\gamma^p_{a,f} = 0.020$
$G = 3000$ kPa

Table 7.8: Input parameters of UCCM-Average in GBS simulation

The maximum static horizontal load in plane strain, using UCCM-Average for the chosen geometry and boundary conditions, is 2 kN. For the model test presented in Dyvik et al. (1989), a maximum static horizontal load of 1 kN was reached. It is not possible to compare results from the FE simulation with results from the model test directly. This is due to the difference in geometry and boundary conditions. The load-displacement curve for the FE-simulation is illustrated in figure 7.12. The failure surface illustrated in figure 7.13 is similar to one of the potential failure mechanisms suggested by Andersen et al. (1989).

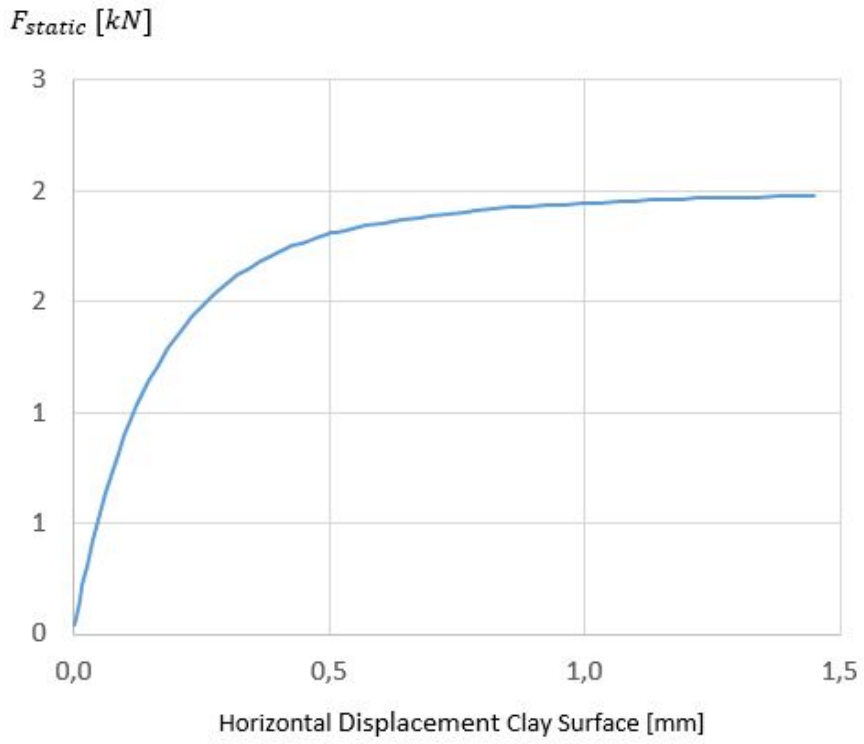

Figure 7.12: Load-displacement curve from static simulation with UCCM-Average

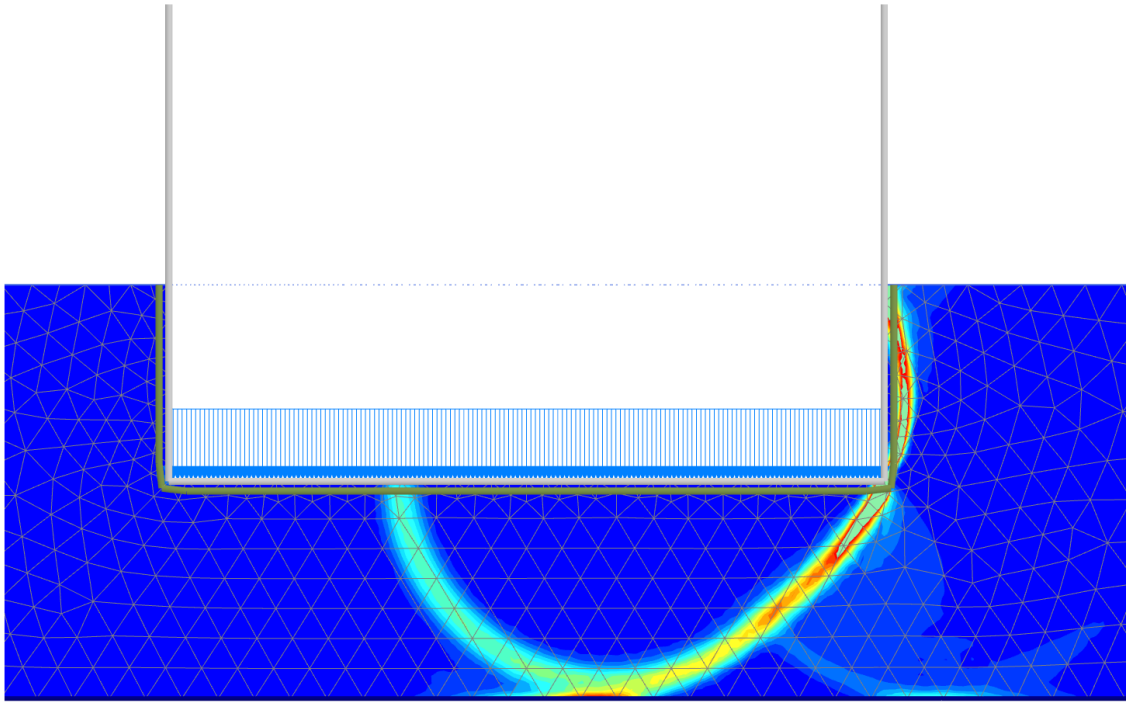

Figure 7.13: Failure surface for the static GBS simulation

Cyclic Test with $N_{eq} = 40$

A cyclic test of the plane strain FE model presented in figure 7.11 is simulated for an equivalent number of cycles, $N_{eq} = 40$, and a cyclic load of 1.75 kN. Andersen et al. (1989) found the critical state of the GBS model test presented in Dyvik et al. (1989) to be $N_{eq} = 38$ for a cyclic load of 0,72 kN. A finite element simulation of this model test was reported by Gustav Grimstad (2012) with a similar result.

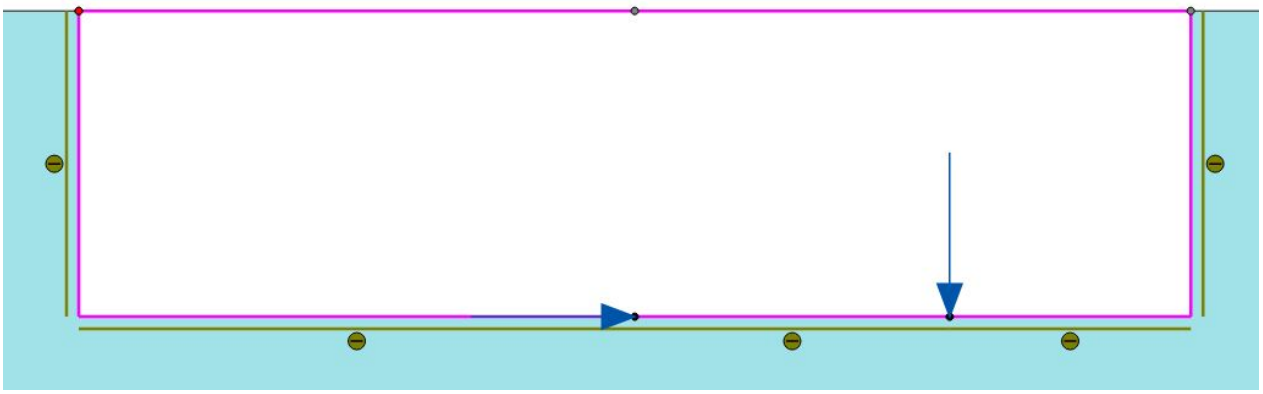

Figure 7.14: The alternative loading application for the cyclic phase

As for the static test, the UCCM results are not directly comparable for the strength and stiffness, but the overall behavior should have the same trend. For the UCCM test, the overturning moment was transferred to the soil as a horizontal and vertical force as seen in figure 7.14. It was introduced to transfer the stresses to the soil in a more correct manner for the cyclic phase, which lack the weight of the platform to prevent the foundation from overturning. The input parameters for UCCM-Cyclic are developed from DSS contour diagrams in Gustav Grimstad (2012) presented in table 7.9.

UCCM-Cyclic Input Parameters:
$S_u = 6.67$ kPa, $t = 0.28$
$\tau_{cy,1}^{max} = 10.48$ kPa, $\tau_{cy,\infty}^{max} = 2.94$ kPa,
$\gamma_{cy,1} = 0.6\%$, $\gamma_{cy,\infty} = 0.1\%$
$\beta_1 = 0.05$, $\beta_\infty = 0.0$, $\alpha = 0.2$

Table 7.9: Input parameters to UCCM for cyclic GBS simulation

Figure 7.15 illustrates the load-displacement curve in the cyclic phase for the plane strain simulation. The load displacement curve depends on the boundary values of the finite element model and how the loads are transferred to the soil volume. The development of the curve seems reasonable with a form that is similar to UDCAM. The GBS-soil system reaches a high horizontal load for a relatively small horizontal displacement of the clay surface.

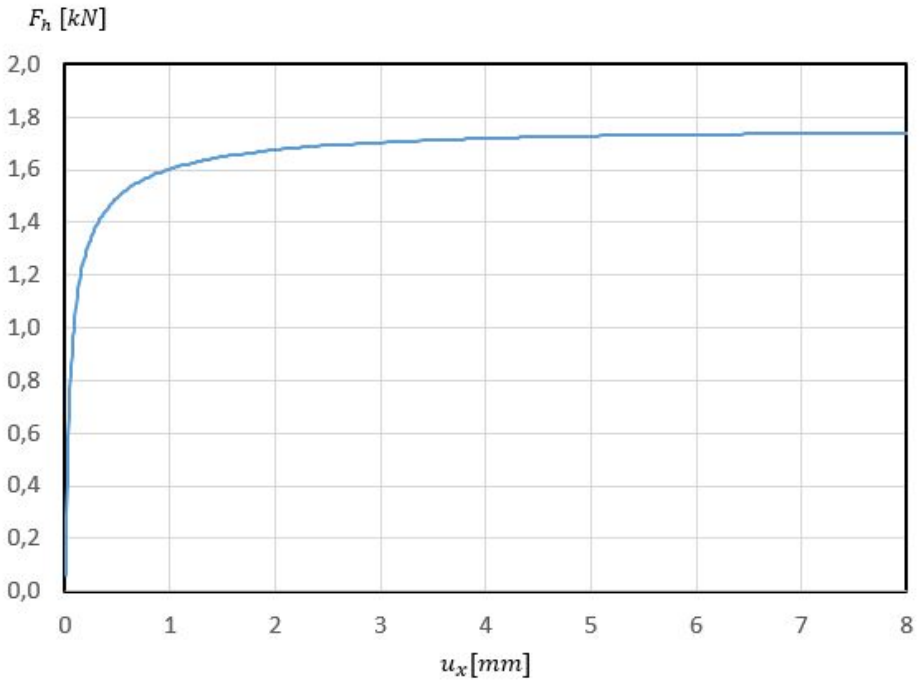

Figure 7.15: Cyclic load versus horizontal displacement of clay surface for cyclic GBS simulation with $N_{eq} = 40$

Two failure surfaces develop as seen in figure 7.16. The failure surface most similar to the GBS static test, appear to be critical. Bot failure mechanisms seem realistic and are suggested as potential failure surfaces by Andersen et al. (1989).

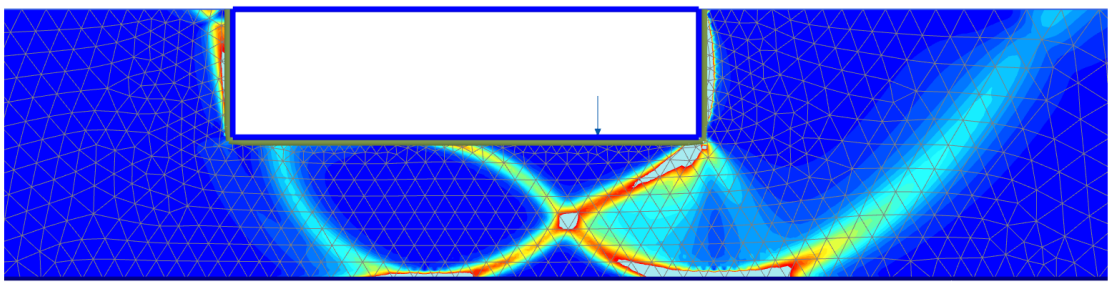

Figure 7.16: Failure surface for the cyclic GBS simulation with $N_{eq} = 40$

Cyclic Test

A cyclic GBS test is simulated using the cyclic load history presented in table 7.10. The test is simulated to investigate the behavior predicted by UCCM for a full cyclic FE simulation.

Parcel	ΔN	$F_{cy,h}$ [kN]	$F_{avg,v}$
1	15	0.582	w
2	10	1.163	w
3	7	1.236	w
4	4	1.302	w
5	3	1.394	w
6	20	1.457	w
7	10	1.600	w
8	7	1.719	w
9	4	1.844	w
10	1	1.959	w
11	20	1.743	w

Table 7.10: Cyclic- and average loads applied in GBS simulation, inspired by similar test from Gustav Grimstad (2012).

The cyclic test was not fully calculated and stopped after six parcels. The reason may be due to singularities for certain vulnerable soil clusters. Before the numerical difficulties were encountered, the results looked promising, as shown in figure 7.17. The numerical problems started in parcel 3, as seen in the figure.

Figure 7.17 shows that the response to the two first cyclic load histories are softer than the response predicted by the cyclic test with $N_{eq} = 40$. This is not expected and illustrates the uncertainties in the results. For parcels from 3 to 6, figure 7.17 shows that Plaxis must redistribute displacements to obtain equilibrium. The maximum redistribution takes place in the start of the ultimate phase, where the calculation finally stops.

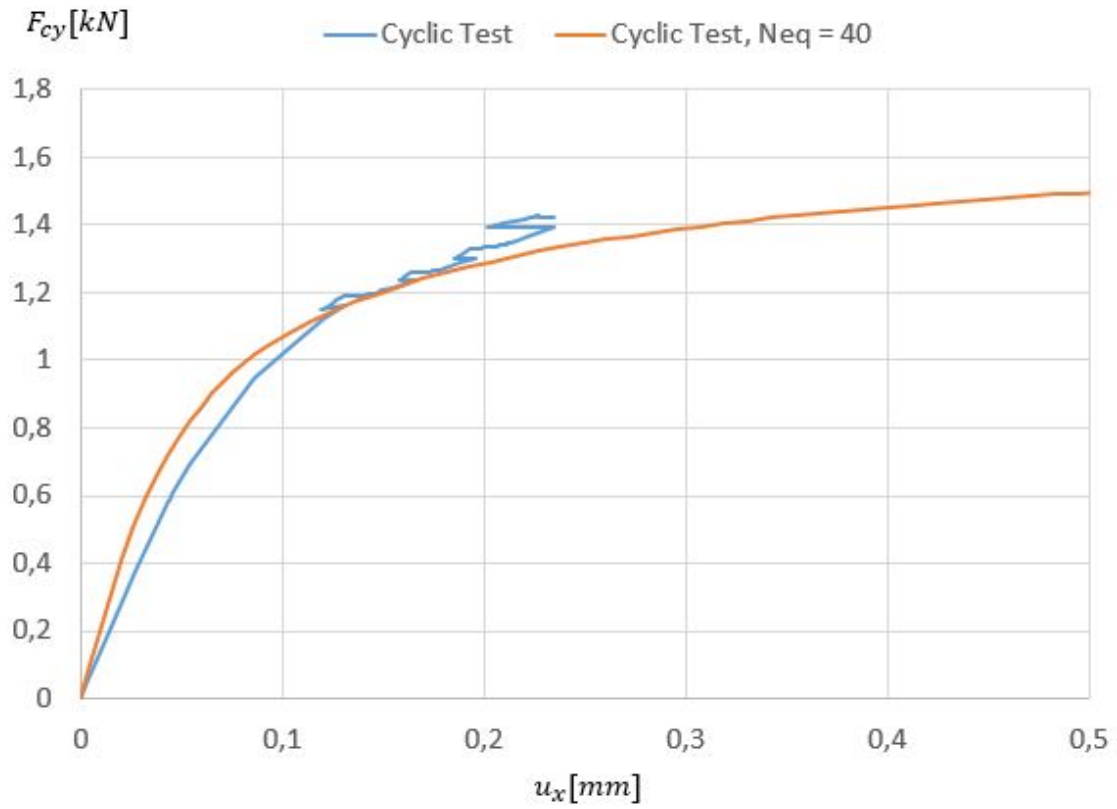

Figure 7.17: Load-displacement curve for cyclic test and cyclic test with $N_{eq} = 40$

A deviatoric shear strain plot from the phase, in which the calculation stops, is presented in figure 7.18. The figure demonstrates what is believed to be the start of a similar failure surface as seen in figure 7.16.

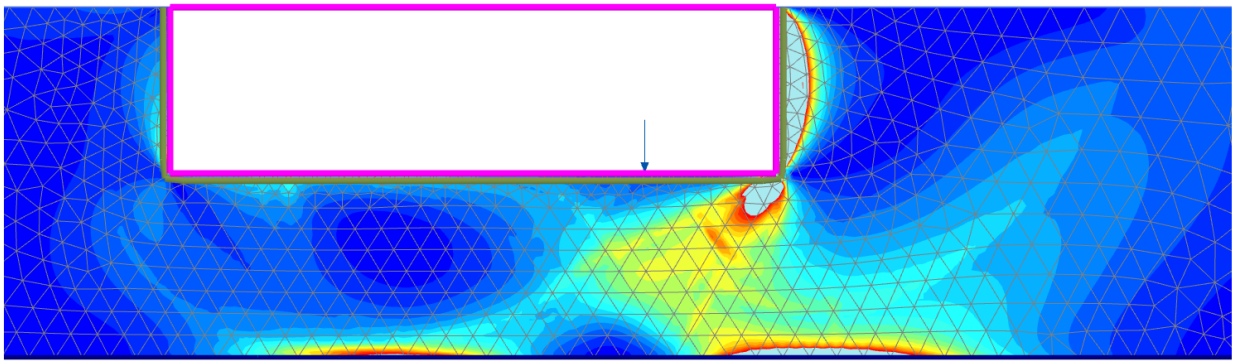

Figure 7.18: The total deviatoric shear strain accumulated up to the 6th cyclic parcel.

7.5 General Discussion

The overall result from UCCM seems satisfying. Especially the results of the simpler tests, where the model seems to be able to reproduce the desired behavior. Both UCCM-average and UCCM-Cyclic have proven to get reasonable results compared to already well established calculation methods. The interaction between UCCM-Cyclic and UCCM-Average also seem to be working well. The last DSS test clearly shows a degradation of the average strength due to the cyclic phase and thereby an accumulation of plastic shear strains.

The more complicated simulation of the GBS test, lacks verification as the geometry and boundary conditions play an important role in the general behavior of the system. With the limited amount of testing, it is hard to say what inflicts the problem for the full cyclic GBS calculation. The authors acknowledge the difficulty of the calibration of input parameters, as well as the design itself. There can also be problems connected to the interaction between UCCM-Average and UCCM-Cyclic. The authors believe the most likely explanation is a singularity problem related to stress distribution interaction between Plaxis and UCCM. Further investigation is needed to clarify and fix this problem. The GBS results are obtained using a high number of desired iterations. For further work it is recommended to try a strict equilibrium criterion and a high number of unloading steps in the simulation.

The UCCM formulation with two different phases for average and cyclic loading, entails a problem connected to the load application for certain designs. The GBS tests in this chapter are such a design. These type of problems need extra assessment in order to represent a realistic foundation-soil interaction. This requires a user which is familiar with the mechanical problem, and in general this makes UCCM less user-friendly.

Chapter 8

Summary and Recommendations for Further Work

8.1 Summary and Conclusions

A material model, based on total stresses, has been developed to represent the undrained cyclic behavior of clay for FE analyses. The material behavior is split into an average- and a cyclic part, formulated as two material models, UCCM-Average and UCCM-Cyclic. A coupling between these models is implemented such that the overall behavior of an element can be visualized as isotropic contour diagrams. The isotropic contour diagrams represent an explicit formulation for the undrained cyclic behavior, and the loads are therefore defined by a number of cycles with specific cyclic load magnitude. The cyclic loads are assumed to be defined in terms of forces and have a frequency within the "cyclic" range (≈ 0.1 Hz), which implies that mass and damping considerations can be omitted.

Degradation of the maximum average shear stress and the cyclic shear stiffness is accounted for using the mathematical expressions for the isotropic contour diagrams and the cyclic shear strain accumulation principle. The resulting accumulation of plastic shear strains is a byproduct of the degradation of maximum average shear stress.

The average model and the cyclic model are verified individually by Plaxis simulations with satisfactory results. A bearing capacity problem was simulated with

the average model and compared directly to a simulation with NGI-ADP. The average model exhibited the expected behavior and the authors believe it can be used in similar boundary value problems when used with care.

The cyclic model was used in a cyclic DSS simulation with no average shear stresses. The simulation result was compared directly to a similar calculation presented in Gustav Grimstad (2012) and can be concluded that the cyclic model is able to represent the undrained cyclic behavior in DSS.

A DSS model included average stress was calculated with UCCM to check the average-cyclic interaction. The results seem satisfying and it is therefore believed that the UCCM-Cyclic-Average coupling should be able to describe the total response for a cyclic loaded design adequately.

An objective was to compare the presented model directly to results from the GBS model test presented in Dyvik et al. (1989). Due to time limitations and the complexity of the problem, only a hypothetical analysis is undertaken. Results indicate further investigation is necessary to confirm the applicability of the soil model on gravity base structures.

8.2 Recommendations for Further Work

A new set of parameters is introduced in UCCM to define the isotropic contour diagrams. A further study of these parameters is recommended in order to use the material model in design. The cyclic model is based on a mathematical expression defined by a maximum cyclic shear stress at a high strain level and a curve fit parameter. It is recommended to replace the curve fit parameter by the maximum shear modulus, which is readily obtained from field- or laboratory tests. The fatigue shear stress should be investigated further and correlated to existing soil parameters e.g. remolded shear strength, S_r, if possible.

To investigate the coupling between the average- and cyclic model further, multiple cyclic DSS and triaxial tests should be simulated and compared directly to laboratory test result. A simplified expression for the degradation of the maximum average shear stress is used in the current formulation of the material model. This expression should be further investigated to obtain reliable results.

The average material model is formulated with a modified von-Mises yield surface. It is believed that a modified Tresca criterion with direct input of clay parameters from laboratory results represents the average behavior more accurately. It can therefore be recommended to implement this yield criterion as the average criterion. An extension into an anisotropic formulated model, similar to NGI-ADP, is yet another possibility to represent the soil behavior more accurate.

There should be an iteration process on phase level which ensures the correct solution. A platform which controls the iteration on phase level should therefore be developed. Implementation of a possibility to do calculations for strain-controlled designs will be a natural development.

Bibliography

Achmus, M., Kuo, Y.-S., and Abdel-Rahman, K. (2009). Behavior of monopile foundations under cyclic lateral load. *Computers and Geotechnics*, 36(5):725–735.

Amzallag, C., Gerey, J., Robert, J., and Bahuaud, J. (1994). Standardization of the rainflow counting method for fatigue analysis. *International journal of fatigue*, 16(4):287–293.

Andersen, K. and Lauritzsen, R. (1988). Bearing capacity for foundations with cyclic loads. *Journal of Geotechnical Engineering*, 114(5):540–555.

Andersen, K. H. (2015). *Cyclic soil parameters for offshore foundation design*, pages 5–82. CRC Press. doi:10.1201/b18442-4.

Andersen, K. H., Dyvik, R., Lauritzsen, R., Heien, D., Harvik, L., and Amundsen, T. (1989). Model tests of gravity platforms. ii: Interpretation. *Journal of Geotechnical Engineering*, 115(11):1550–1568.

Ansal, A. M. and Erken, A. (1989). Undrained behavior of clay under cyclic shear stresses. *Journal of Geotechnical Engineering*, 115(7):968–983.

API. Recommended practice for planning, designing and constructing fixed offshore platforms – working stress design: Api reommended practice 2a-wsd (rp2a-wsd). In *Twenty-2000*.

Billington, E. (1988). Generalized isotropic yield criterion for incompressible materials. *Acta mechanica*, 72(1-2):1–20.

Brinkgreve, R., Swolfs, W., and Engin, E. (2016). Plaxis 2d manual. *Delft University of Technology and PLAXIS bv The Netherlands*.

Cook, R. D. et al. (2007). *Concepts and applications of finite element analysis*. John Wiley & Sons.

Das, B. and Ramana, G. (2011). Principles of soil dynamics, 2nd edn. cengage learning.

Dyvik, R., Andersen, K. H., Madshus, C., and Amundsen, T. (1989). Model tests of gravity platforms. i: Description. *Journal of Geotechnical Engineering*, 115(11):1532–1549.

Grimstad, G., Andresen, L., and Jostad, H. P. (2012). Ngi-adp: Anisotropic shear strength model for clay. *International Journal for Numerical and Analytical Methods in Geomechanics*, 36(4):483–497.

Grimstad, G., Rønningen, J. R., and Nøst, H. A. (2014). *Use of IWAN models for modelling anisotropic and cyclic behavior of clays*, pages 49–54. CRC Press. doi:10.1201/b17017-11.

Gustav Grimstad, Hans Petter Jostad, K. H. M. (2012). User manual for equivalent cyclic adp model for undrained behavior-"udcam". Report, Norwegian Geotechical Institute.

Head, K. H. and Epps, R. (1986). *Manual of soil laboratory testing*, volume 3. Pentech Press London.

Hopperstad, O. and Børvik, T. (2014). *Lecture Notes - Materials Machanics - Part 1*. Structural IMpact Laboratory.

Huurman, M. (1996). Development of traffic induced permanent strain in concrete block pavements. *Heron*, 41(1):29–52. Cited By :17 Export Date: 19 November 2015.

Idriss, I. M., Dobry, R., and Sing, R. (1978). Nonlinear behavior of soft clays during cyclic loading. *Journal of Geotechnical and Geoenvironmental Engineering*, 104(ASCE 14265).

Iwan, W. D. (1966). A distributed-element model for hysteresis and its steady-state dynamic response. *Journal of Applied Mechanics*, 33(4):893–900. 10.1115/1.3625199.

Iwan, W. D. (1967). On a class of models for the yielding behavior of continuous and composite systems. *Journal of Applied Mechanics*, 34(3):612–617. 10.1115/1.3607751.

Jostad, H., Grimstad, G., Andersen, K., Saue, M., Shin, Y., and You, D. (2014). A fe procedure for foundation design of offshore structures–applied to study a potential owt monopile foundation in the korean western sea. *Geotechnical Engineering Journal of the SEAGS & AGSSEA*, 45(4).

Kramer, S. L. (1996). *Geotechnical earthquake engineering*. Pearson Education India.

Niemunis, A., Wichtmann, T., and Triantafyllidis, T. (2005). A high-cycle accumulation model for sand. *Computers and Geotechnics*, 32(4):245–263.

Nordal, S. (2014). *Geotechnical Engineering Advanced Course*. Kompendieforlaget.

Ottosen, N. S. and Petersson, H. (1992). *Introduction to the finite element method*. Prentice-Hall.

Ottosen, N. S. and Ristinmaa, M. (2005). *The mechanics of constitutive modeling*. Elsevier.

Terzaghi, K. (1925). *Erdbaumechanik auf bodenphysikalischer grundlage*. F. Deuticke, Leipzig u. Wien.

Thiers, G. and Seed, H. (1969). *Strength and stress-strain characteristics of clays subjected to seismic loading conditions*. ASTM International.

Vermeer, P. A. and De Borst, R. (1984). Non-associated plasticity for soils, concrete and rock. *HERON, 29 (3), 1984*.

Wood, D. M. (1990). *Soil behaviour and critical state soil mechanics*. Cambridge university press.

Yasuhara, K., Hirao, K., and Hyde, A. F. (1992). Effects of cyclic loading on undrained strength and compressibility of clay. *Soils and Foundations*, 32(1):100–116.

Åhnberg, H., Larsson, R., and Holmén, M. Degradation of clay due to cyclic loadings and deformations. In *Proceedings of the 18th international conference on soil mechanics and geotechnical engineering ICSMGE, Paris*.

List of Figures

List of Tables

Appendix A

Fortran Source Code

UCCM was written in FORTRAN using a programming environment called PLATO, and compiled to a Dynamic Link Library file. The soil model provides information to Plaxis structured into six different tasks which Plaxis calls IDTask. Start of the source code is presented below.

```
Subroutine User_Mod (IDTask,iMod,IsUndr,iStep,iTer,iEl,Int,X,Y,Z,Time0,dTime,Props,Sig0,Swp0,StVar0,dEps,D,&
        Bulk_W,Sig,Swp,StVar,ipl,nStat,NonSym,iStrsDep,iTimeDep,iTang,iPrjDir,iPrjLen,iAbort)

        implicit none

        ! Input Parameters:
        integer :: IDTask,iMod,IsUndr,iStep,iTer,iEl,Int
        double precision :: X,Y,Z,Time0,dTime,Swp0
        double precision, dimension(18) :: Props
        double precision, dimension(9) :: Sig0
        double precision, dimension(6) :: dEps

        ! Output Parameters
        double precision :: Bulk_W,Swp
        double precision, dimension(6,6) :: D
        double precision, dimension(6) :: Sig
        double precision, dimension(12) :: StVar
        integer :: ipl,nStat,NonSym,iStrsDep,iTimeDep,iTang,iPrjDir,iPrjLen,iAbort

        ! Input and output parameter:
        double precision, dimension(12) :: StVar0

        !Parameters used within this script:
        double precision sjekk

!=============================================================================
        !A part which let the program write and read from different files
        Character PrjDir*255, Dbg_Name*255, Dbg_Name2*255, Dbg_Name3*255, Dbg_Name4*255
        Dimension iPrjDir(*)
        integer iounit2, i, ios2
        Data iounit2 / 0 /
        Save iounit2

        !Creating a debugfile
        Logical IsOpen
        Data IsOpen / .FALSE. /
        Save IsOpen
```

Appendix B

Derivatives UCCM

The double derivative of the yield function with respect to the current stress state is omitted due to space limitations.

$$\left\{\frac{\partial F}{\partial \underline{\sigma}}\right\}_{n+1} = \frac{1}{2\sqrt{3J_2}} \begin{bmatrix} 2\sigma_{11} - \sigma_{22} - \sigma_{33} \\ 2\sigma_{22} - \sigma_{11} - \sigma_{33} \\ 2\sigma_{33} - \sigma_{22} - \sigma_{11} \\ 3\sigma_{12} \\ 3\sigma_{23} \\ 3\sigma_{31} \end{bmatrix} \tag{B.1}$$

$$\frac{d\kappa}{d\gamma_a^p} = \begin{cases} \dfrac{-\sqrt{\frac{\gamma_a^p}{\gamma_{a,f}^p}}\left(1-\frac{\gamma_a^p}{\gamma_{a,f}^p}\right)}{\left(1+\frac{\gamma_a^p}{\gamma_{a,f}^p}\right)^2 \gamma_{a,f}^p}, & \gamma_a^p < \gamma_{a,f}^p \\ 0, & \gamma_a^p \geq \gamma_{a,f}^p \end{cases} \tag{B.2}$$

$$\frac{d\gamma_a^p}{d\lambda} = \frac{3}{4} \tag{B.3}$$

$$\frac{dN_{eq}}{d\tau_{cy}} = -\frac{1}{t}\frac{(\tau_{cy,1} - \tau_{cy,\infty})^{\frac{1}{t}}}{(\tau_{cy} - \tau_{cy,\infty})^{\frac{1+t}{t}}} \tag{B.4}$$

$$\frac{dN_{eq}^{intm}}{d\tau_{cy}} = \frac{1}{t}\left(\frac{\tau_{cy,1}^{intm} - \tau_{cy,\infty}^{intm}}{\tau_{cy} - \tau_{cy,\infty}^{intm}}\right)^{\frac{1-t}{t}} \frac{du}{d\tau_{cy}} \tag{B.5}$$

$$\frac{du}{d\tau_{cy}} = \frac{g'h - gh'}{h^2} \tag{B.6}$$

$$\frac{dg}{d\tau_{cy}} = \frac{\tau_{cy,1}^{intm}}{d\tau_{cy}} - \frac{\tau_{cy,\infty}^{intm}}{d\tau_{cy}} \tag{B.7}$$

$$\frac{dh}{d\tau_{cy}} = 1 - \frac{\tau_{cy,\infty}^{intm}}{d\tau_{cy}} \tag{B.8}$$

$$\frac{d\tau_{cy,\#}^{intm}}{d\tau_{cy}} = \frac{d\tau_{cy,\#}^{intm}}{d\gamma_{cy}^{intm}} \frac{d\gamma_{cy}^{intm}}{d\tau_{cy}} \tag{B.9}$$

$$\frac{d\tau_{cy,\#}^{intm}}{d\gamma_{cy}^{intm}} = \frac{\tau_{cy,\#}^{max} \cdot \gamma_{cy,\#}}{2\sqrt{\gamma_{cy}^{intm}}\left(\gamma_{cy,\#} + \gamma_{cy}^{intm}\right)^{3/2}} \tag{B.10}$$

$$\frac{d\gamma_{cy}^{intm}}{d\tau_{cy}} = \frac{2\gamma_{cy,1} \cdot \tau_{cy} \cdot \left(\tau_{cy,1}^{max}\right)^2}{\left(\left(\tau_{cy,1}^{max}\right)^2 - \tau_{cy}^2\right)^2} \tag{B.11}$$